Synthesis and Evaluation of Peptides for Radiopharmaceutical Applications

2017

Jyotibon Dutta

Synthesis and evaluation of peptides for radiopharmaceutical applications

214581166

Jyotibon Dutta

2017

A thesis submitted to the School of Health Sciences, College of Health Science, University of KwaZulu-Natal, Westville, for the degree of Doctor of Philosophy in Pharmaceutical Chemistry.

This is the thesis in which the chapters are written as a set of discrete research publications that have followed the format of the European Journal of Medicinal Chemistry with an overall introduction and final summary. These chapters have either been published or submitted to internationally recognized, peer-reviewed journals.

This is to certify that the contents of this thesis is the original research work of Mr Jyotibon Dutta, carried out under our supervision at the Catalysis and Peptide Research Unit, Westville Campus, University of KwaZulu-Natal, Durban, South Africa.

Supervisor:

Signed: _____ Name: **Prof. T Govender** Date: _____

Co-Supervisor:

Signed: _____ Name: **Prof. T Naicker** Date: _____

Co-supervisor:

Signed: _____ Name: **Prof. HG Kruger** Date: _____

Abstract

Bacterial infection is considered as one of the major threats to human life as well as to the global economy; especially with the increasing number of new multidrug resistant strains. Timely as well as accurate diagnosis of these infections significantly affect the treatment strategies and the prognosis of the disease. Until now, isolation and culturing of the organism is considered to be the gold standard for bacterial infection diagnosis. Conversely, this method is time consuming and labor-intensive. However, with the exponential development in the area of radiopharmaceutics, new imaging probes for the diagnosis of bacterial infection are emerging. The aim of this study focuses particularly on the development of potential radiotracers for imaging of bacterial infection.

In this thesis, several topics related to bacterial infection imaging were explored. These topics can be categorized into sections namely; a review on the synthetic approaches of existing potential probes for bacterial imaging, novel on and off resin synthesis of a bifunctional chelator NODASA with a model peptide and lastly, an efficient method for the synthesis of LL37 and NODAGA-LL37 along with its evaluation for bacterial specificity.

The first concern about radio tracers is the requirement for an ideal radiopharmaceutical for direct imaging of bacteria. The prime aim of the first part of this thesis is to evaluate the current approaches used for the synthesis of radiolabelled probes for bacterial infection identification as it is clear that such a review will be timeous. In this regard, a review of published work was carried out on the clinical as well as preclinical available probes. Furthermore, existing radiolabelling procedures and suggested mechanisms of radio tracer uptake is also discussed. These molecular probes comprises of leukocytes, antibodies, small molecules, peptides, antibiotics, macrolides, vitamins, oligomers and siderophores.

Bifunctional chelators (BFCs) are one of the key elements of a successful radiotracer, which act as a linker between the tracer moiety and the radio isotope. One of the major aims of this study is to develop a method for the synthesis of bifunctional metal chelator NODASA, a potential chelator for radiolabelling. Herein, a facile economic on and off resin method for the synthesis of potential bifunctional chelator "NODASA" functionalized peptide is presented. The seven step synthesis was initiated with a Michael addition reaction between monomethyl fumarate and 1,4,7-triazacyclononane. The final product of NODASA functionalized peptide was obtained with an isolated yield of 84%.

A potential human antimicrobial peptide LL37 possesses impending therapeutic values due to its close association with the immune system. Efforts to synthesize LL37 efficiently is one of the

goals of this study. In this regard, a highly efficient and optimized methodology for the synthesis of LL37 on solid phase using microwave energy was developed. During this method development it was concluded that uronium coupling reagents along with standard conditions were inadequate for the synthesis of 20th amino acid residue onwards. Val and Ile amino acid coupling was revealed as the key problematic reaction in the segmentation approach of synthesizing the peptide. It was also found that DIC/OxymaPure in THF is a better combination of reagents for this coupling. The synthesized peptide was further verified for its antimicrobial activity.

In the last part of this study the aim was to explore the radiolabelling potential of LL37 and its usability as a radiotracer. For this purpose LL37 was functionalized with bifunctional chelator NODAGA. NODASA-LL37 was also labelled with cold/hot gallium successfully. This complex was further evaluated *in vitro* for its bacterial selectivity over mammalian cell line.

With the rapid development of bacterial resistance and the development of "super bugs" there is an urgent need for diagnostic tools which can provide a faster and efficient detection of pathogenic microorganisms. Radiopharmaceutics is an ideal candidate to solve this problem, especially due to its high selectivity, sensitivity and non-invasive nature. In this thesis, an effort was put forward to answer the critical questions regarding the development of synthetic methods, purification and characterization of the antimicrobial peptide LL37. Firstly, a combination of different coupling reagents were used for the optimization of the synthesis, from this study we were able to conclude that the DIC/OxymaPure is better than the HBTU/DIPEA and HATU/DIPEA systems. This method can now be utilized for the large scale production of LL37. In addition to this, a facile seven step method for the synthesis of the bifunctional chelator NODASA functionalized peptide was developed. In this study a NODASA functionalized peptide was conjugated with cold gallium which, demonstrating it as a potential PET agent for molecular imaging. This route offers a simple and inexpensive alternative to commercially available NODASA and can be coupled with various other peptides. Finally, LL37 was also functionalized with the chelator, NODAGA, and subsequently labelled with ^{nat}Ga. This complex showed significant affinity towards bacterial cells in comparison with mammalian cells and providing evidence that NODAGA-LL37 could be a potential radiotracer for bacterial infection imaging.

Abbreviations: NODAGA: 1,4,7-triazacyclononane,1-glutaric acid-4,7-acetic acid; NODASA: 1,4,7-Triazacyclononane-1-succinic acid-4,7-diacetic acid

Declaration 1- Plagiarism

I, Jyotibon Dutta declare that

1. The research report in this thesis, except where otherwise indicated, is my original work.
2. This thesis has not been submitted for any degree or examination at any other university.
3. This thesis does not contain other person's data, pictures, graphs or other information, unless specifically acknowledged as being sourced from other persons.
4. This thesis does not contain other person's writing, unless specifically acknowledged as being sourced from other researchers. Where other written sources have been quoted, then:
    a. Their words have been re-written but the general information attributed to them has been referenced.
    b. Where their exact words have been used, then their writing has been placed in italics and inside quotation marks, and referenced.
5. This thesis does not contain text, graphics or tables copied and pasted from the internet, unless specifically acknowledged, and the source being detailed in the thesis and in the references sections.

Signed

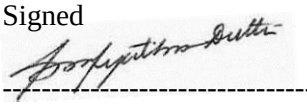

Declaration 2- Publication

List of publications originated from this Thesis

[1] **J. Dutta,** T. Naicker, T. Ebenhan, H.G. Kruger, P.I. Arvidsson, T. Govender, Synthetic Approaches to Radiochemical Probes for Imaging of Bacterial Infections, Eur J Med Chem., (2017) *Submitted*

J. Dutta contributed to the design and wrote the paper.
T. Ebenhan contributed towards adding valuable information into the paper.
The remaining authors are supervisors.

[2] **J. Dutta,** P.K. Chinthakindi, P.I. Arvidsson, G. Beatriz, H.G. Kruger, T. Govender, T. Naicker, F. Albericio, A Facile Synthesis of NODASA-Functionalized Peptide, Synlett., 27 (2016) 1685-1688. *Published*

J. Dutta contributed to the design of the project, synthesized and characterized all compounds, performed the testing of the compounds and wrote the paper.
P.K. Chinthakindi contributed towards writing the paper.
The remaining authors are supervisors.

[3] **J. Dutta,** S. Ramesh, S.M. Radebe, A.M. Somboro, G. Beatriz, H.G. Kruger, S.Y. Essack, F. Albericio, T. Govender, Optimized Microwave Assisted Synthesis of LL37, a Cathelicidin Human Antimicrobial Peptide, Int J Pept Res Ther., 21 (2015) 13-20. *Published*

J. Dutta contributed to the design of the project, synthesized and characterized all compounds, performed the testing of the compounds and wrote the paper.
S. Ramesh and S.M. Radebe contributed towards the synthesis.
A.M. Somboro contributed towards microbiological work.
The remaining authors are supervisors.

[4] **J. Dutta,** S. Baijnath, A.M. Somboro, S. Nagiah, F. Albericio, G.d.l.T. Beatriz, B. Marjanovic-Painter, J.R. Zeevaart, M. Sathekge, H.G. Kruger, A. Chuturgoon, T. Naicker, T. Ebenhan, T. Govender, Synthesis, in vitro evaluation and ^{68}Ga-radiolabeling of CDP1 towards PET/CT imaging of bacterial infection, Chem Biol Drug Des., (2016), *Submitted*

J. Dutta contributed to the design of the project, synthesized and characterized all compounds, performed the testing of the compounds and wrote the paper.
S. Baijnath contributed towards LC-HRMS part of the project.
A.M. Somboro contributed towards microbiological work.

S. Nagiah contributed towards cell culture work.

The remaining authors are supervisors.

Publications for non-degree purposes

[1] R. Azumah, **J. Dutta,** A.M. Somboro, M. Ramtahal, L. Chonco, R. Parboosing, L.A. Bester, H.G. Kruger, T. Naicker, S.Y. Essack, In vitro evaluation of metal chelators as potential metallo-β-lactamase inhibitors, J Appl Microbiol., 120 (2016) 860–867.

J. Dutta contributed towards synthesis and characterized few of the compounds utilized in the project; and also wrote the synthesis part.

Acknowledgement

I would like to express my most sincere words of gratitude to:

- My supervisors, Prof Thavendran Govendor, Dr Tricia Naicker and Prof Gert Kruger, for their remarkable guidance, support and motivation throughout my studies. They have provided me with the ideal platform to hone my research capabilities, while helping me to personally develop.

- Prof Fernando Albericio, Prof Glenn Maguire and Prof Beatriz Garcia de la Torre, for the interesting discussions and support during this research.

- My role model, Dr Sanil Singh, for constant motivation and personal support during some of the most trying times in my life and career. For always believing in me and pushing me to go further.

- My lifelong friend, Sooraj Baijnath, for professional, emotional and personal support. We met as strangers and will be friends for life.

- Dr Byron Peters, Dr Yahya ElSayed Jad and the CPRU group 2015/2016 for their professionalism, eagerness to assist and each having the ability to be a team player.

- My father Mr Haresh Dutta, my mother Mrs Kunjalata Hatiboruah, my father in law Late Mr Hiranmay Bhattacharyya, my mother in law Mrs Renu Devi, my wife Dr Neelakshi Bhattacharyya, my younger brother Mr Angshuman Dutta and my little brother Mr Priyam Dutta, for tolerating me and putting up with all the stress that I put them through during the recent years and for continuing to motivating me and for believing in my abilities.

- National Research Foundation (NRF, SA), AspenPharmacare and the University of KwaZulu-Natal (College of Health Sciences), for financial support.

- Lastly, to my little girl, Adrita Dutta, for her warm presence. A real inspiration and a constant source of motivation for me to achieve anything. This is for you my Baby!

Table of Contents

Chapter 1

Introduction

1. Preamble

Biological processes can be visualized, characterized and measured *in vivo* with the aid of molecular imaging [1]. This exponentially growing technique is utilized to monitor molecules or cellular processes for the diagnosis and/or management of diseases and disorders. Some of these imaging procedures include positron emission tomography (PET) and single-photon emission computed tomography (SPECT) that acquire images by detecting signals from radiolabelled tracers that have to be injected into the test subjects. However, endogenous molecules or exogenous molecular probes are generally considered in some modalities like optical imaging and magnetic resonance imaging (MRI) to monitor disease progression. Due to its critical role in medical diagnostics, the design and development of radiotracers are becoming a focal area in molecular imaging research [2]. Characteristically, a radiotracer is equipped with a targeting moiety, a signaling radioisotope and a linker connecting these components.

2. Bifunctional chelators in radiopharmaceutics.

Radio-metals carry promise as a tool towards the diagnosis, as well as for monitoring the progression of many diseases. These isotopes have to be impounded by metal chelators in order for use in a biological system. Based on the compatibility, these organic compounds are able to make stable complexation products with a particular radio-metal. An ideal chelator binds to the radio-metal well enough so that it can be delivered to the desired site without trans-chelation thereby improving therapy or *in vivo* diagnosis [3]. In radiopharmaceutics, typically utilised ligands for metal binding are mostly bifunctional chelators (BFCs). These are distinctive chelators with a functional group to form a covalent bond with the tracer molecules, such as, but not limited to antibodies, nucleotides and peptides. Such functional groups can be carboxylic acids/activated esters, isothiocyanates or maleimides for amide, thiourea and thiol coupling agents, respectively [4, 5]. Moreover, click chemistry based reactions which are either copper-free (Diels-Alder and strain-promoted azide-alkyne cycloadditions click reactions) or copper catalyzed (azide-alkyne Huisgen 1,3-dipolar cycloaddition “click” reactions) are also gaining popularity in bio-conjugate chemistry [6]. Chelators play a major role in the pharmacokinetics of the radiochemical; it has been noted that by only changing the ligand the biodistribution of peptide-conjugates are affected [7]. A simple synthetic strategy which avoids diastereospecific/ non-enantio and stereoisomer reactions are always desirable for BFC synthesis. In addition, it should have a maximum number of modularity possibilities for assigning a variety of

tracers/moieties to impact biodistribution by altering charge and polarity [3]. Broadly, BFCs are categorized into macrocyclic and acyclic chelators. However, macrocyclic chelators have an advantage over its counterpart acyclic ligands as it inherits a pre-organized binding pocket for metal ions which minimizes the entropic loss during radio-isotope coordination. Conversely, acyclic chelators change their physical orientation and geometry drastically for the positioning of the donor atoms to form the conjugate product with the metal ion. This phenomenon leads to a substantial drop in entropy as compared to macrocyclic chelators [8]. A few popular macrocyclic chelators are 1,4,7,10-tetraazacyclododecane-1,4,7,10-tetraacetic acid (DOTA), 1,4,8,11-tetraazacyclotetradecane-1,4,8,11-tetraacetic acid (TETA), diamsar, 1,4,7-triazacyclononane-1,4,7-triacetic acid (NOTA), 1,4,7,10,13,16-hexaaza-cyclohexadecane *N′,N″,N‴, N⁗,N⁗′,N⁗″*-hexaacetic acid (HEHA), 1,4,7,10,13-pentaazacyclopentadecane-*N′,N″,N‴, N⁗,N⁗′*-pentaacetic acid (PEPA) (Figure 1) and their derivatives; on the other hand diethylenetriaminepentaacetic acid (DTPA), N,N0-bis(2-hydroxybenzyl)-ethylenediamine-N,N-diacetic acid (HBED), N,N-(methylenephosphonate)-N,N0-[6-(methoxycarbonyl)pyridin-2-yl]-methyl-1,2-diaminoethane (H_6phospa), bipyridine-chelator (BPCA), desferrioxamine B (DFO) and CP256 (Figure 2) are some examples of widely studied acyclic BFCs [3]. Alongside the chelating moiety, there are a variety of options to choose with regards to the radio-nucleoid which includes ^{18}F, $^{67/68}$Ga, ^{99m}Tc, ^{111}In, ^{177}Lu, ^{64}Cu, ^{44}Sc, ^{86}Y and ^{89}Zr [3]. These ligands have been widely studied in diagnostic imaging of carcinomas, inflammations and infections.

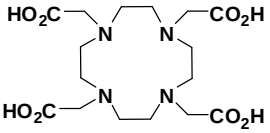

DOTA, 1,4,7,10-tetraazacyclododecane-1,4,7,10-tetraacetic acid

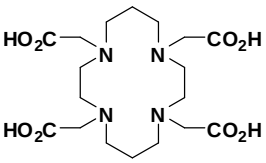

TETA, 1,4,8,11-tetraazacyclotetradecane-1,4,8,11-tetraacetic acid

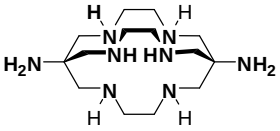

Diamsar

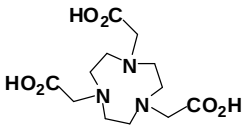

NOTA, 1,4,7-triazacyclononane-1,4,7-triacetic acid

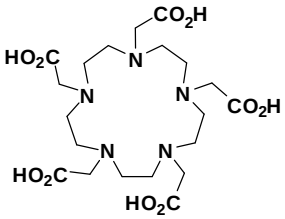

PEPA, 1,4,7,10,13-pentaazacyclopentadecane -N$^{/}$,N$^{//}$,N$^{///}$,N$^{////}$,N$^{/////}$-pentaacetic acid

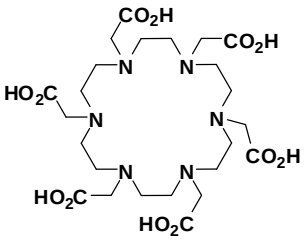

HEHA, 1,4,7,10,13,16-hexaaza-cyclohexadecane N$^{/}$,N$^{//}$,N$^{///}$, N$^{////}$,N$^{/////}$,N$^{//////}$-hexaacetic acid

Figure 1 Macrocyclic chelators commonly used for radioisotope conjugation

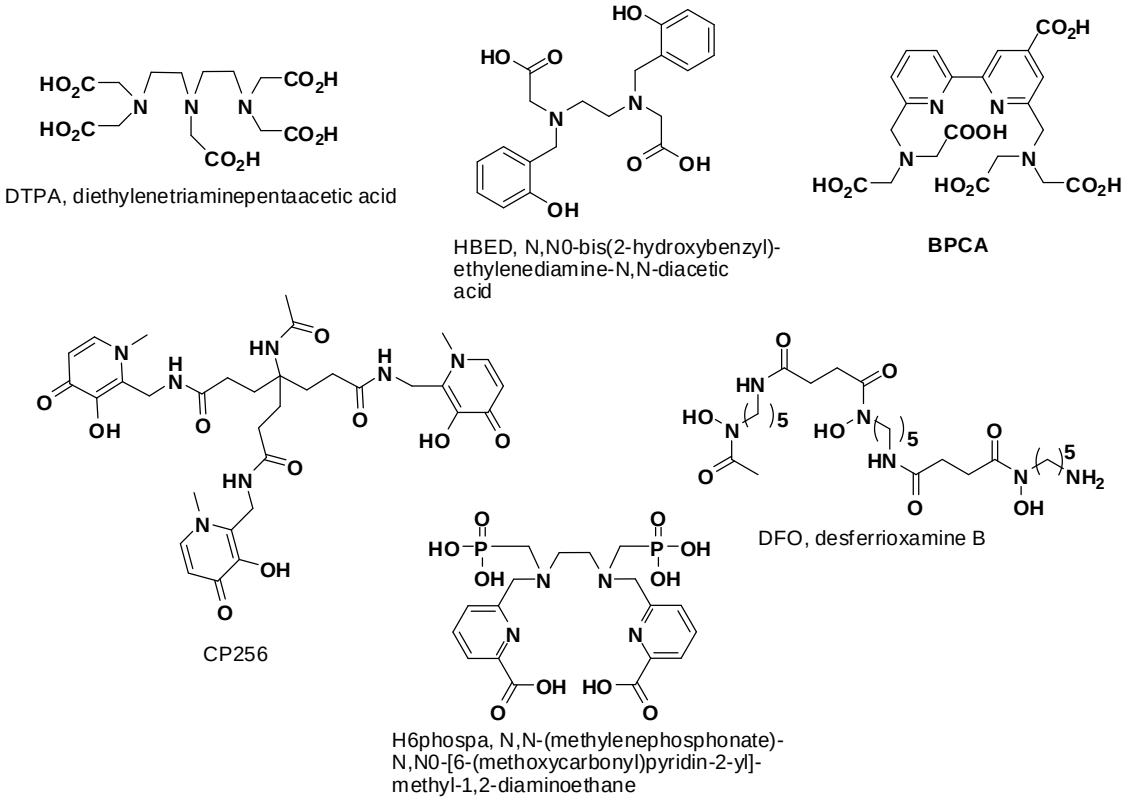

Figure 2. Acyclic chelators commonly used for radioisotope conjugation

3. Radio imaging a need for bacterial infection

Bacterial infection is a major threat to human health; and is still recognized as one of the most vicious causes of mortality and morbidity worldwide [9]. Because of its heterogeneous nature, infectious diseases are associated with a variety of different clinical signs and symptoms. They may be systemic or localized in one foci and often reoccurs; in many cases these infections require long term treatment [10]. Therefore, in a clinical set up it is difficult to distinguish between infection and aseptic inflammation in addition to its size and distribution throughout the body. This in turn affects the treatment strategies that are employed [11]. In general, the diagnosis of infectious diseases is carried out by using clinical history, physical inspection, pathogen identification in suspected sample and by imaging approaches. Though the application of imaging techniques has advantages due to its non-invasive nature, but there is a significant difference between the uses of non-radionuclide medicine and radionuclide imaging. Imaging techniques such as ultrasound, plain radiography and computed tomography are based on anatomical changes, which arise in the advanced stages of infectious diseases [12]. This highlights the need to develop radio nuclear approaches for the early and precise identification of infectious lesions. Due to the knowledge gained and better understanding, we now have in pathophysiology a number of new promising radiopharmaceuticals have been developed for

imaging bacterial infections [13-15]. This development in radiopharmaceutics is feeding the clinician with invaluable information regarding the infection, thereby giving an opportunity to commence with the best therapeutic strategies for the patients. Up till now, various molecules have been taken into consideration as radio-labelled tracers to detect infection foci; this includes leukocytes, antibiotics, antibodies, peptides, siderophores, bacteriophages, vitamins, carbohydrates and aptamers [16-19]. However, very few from this have been clinically approved for human use; that taken into account includes ^{111}In-oxine-Leukocyte-SPECT, ^{99m}Tc-HMPAO-Leukocyte-SPECT, ^{99m}Tc-Sn-Colloid "LLK"-SPECT, ^{99m}Tc-Besilesomab-SPECT, ^{99m}Tc-Sulesomab-SPECT, ^{18}F-FDG-PET and ^{67}Ga-citrate-SPECT [20-24].

4. Peptides as radiotracers

Recently, attention has been drawn to antimicrobial peptides (AMPs) for use as a guiding molecule for the radio-isotope and in PET tracer development [25]. Evolutionarily, AMPs are the ancient ordinance of the immune system. They are widely spread amongst the animal species, as well as in the plant kingdom; this suggests the involvement of AMPs in the evolution of multicellular organisms. These peptides are still an effective and integral part of the primary host defense system regardless of its ancient lineage [26]. They are of greater interest because of the fact that peptides show low toxicity and immunogenicity with high specificity and binding capability towards its desired target [27, 28]. The mechanism of action of AMPs are based on differences in the basic design of the cellular membrane of multicellular organisms and microbes. The outermost bilayer of bacteria is composed of heavily condensed negatively charged lipids, whereas the outer layer of the animal and plant cells are populated mainly with neutral lipids [29]. This feature gives the AMPs specificity towards bacterial cells and accumulation at the infectious site; making them promising PET and SPECT tracers, for imaging bacterial infections [30]. Even though the use of AMPs in radiopharmaceutics is not a new concept [31, 32]; only a few members of this group have been evaluated so far [33]. Some of the AMPs studied so far include ubiquicidin, human neutrophil peptide, neutrophil elastase inhibitor peptide, human-β-defensin and human lactoferrin-derived peptide. In addition to the aforementioned peptides, human cathelecidin antimicrobial peptide LL37 is also extensively involved with the innate immune system and can be useful in radiopharmaceutics. This antimicrobial peptide is found in various cell lines (human squamous epithelia, granulocytes and neutrophil) and other bodily fluids [34]. LL37 is involved in neutralizing biologically active molecules, which are present in the bacterial cell wall and also acts as growth inhibitor [35, 36]. Moreover, this antimicrobial peptide also contributes towards chemotaxis, cell migration, cytokine production, angiogenesis and histamine release [34]. Due to its association with the human defense system; it can be evaluated as a potential PET radiotracer for infection imaging.

5. LC-MS as a means for peptide/protein quantification

In the current era, peptide and protein quantification is quickly gaining momentum due to the increasing demand for them to be evaluated as diagnostic and therapeutic molecule. Moreover, there is a shift in the trend of drug discovery towards a target oriented approach and therefore a need for the precise and accurate quantification of these molecules [37]. In that context, liquid chromatography–mass spectrometry (LC-MS) which is considered as the gold standard for small molecule quantification is now showing great potential towards larger molecules (such as peptide and protein) determination, due to its inherent advantages [38, 39]. The advantages of this technique over immune based assays include a shorter method development time, lack of antibody requirement, high specificity as well as sensitivity (up to ng/ml or pg/ml concentrations) and its ability to monitor product degradation. Based on the size of the peptide/protein, LC-MS quantification can be broadly categorized into 1) a bottom up approach where the molecule (usually >10-15 kDa), is digested with an enzyme and is followed by the liquid chromatography–mass spectrometry/mass spectrometry (LC-MS/MS) analysis; and 2) a top down approach where the native molecule (usually <10-15 kDa) is analyzed directly, either by liquid chromatography–high resolution mass spectrometry (LC-HRMS) or LC-MS/MS (Figure 3). A variety of sample preparation methods such as solid phase extraction, protein precipitation, immuno-capture enrichment and depletion of high-abundant proteins can be integrated into the LC-MS workflow based on the nature of the analyte and to increase sensitivity of the method [37].

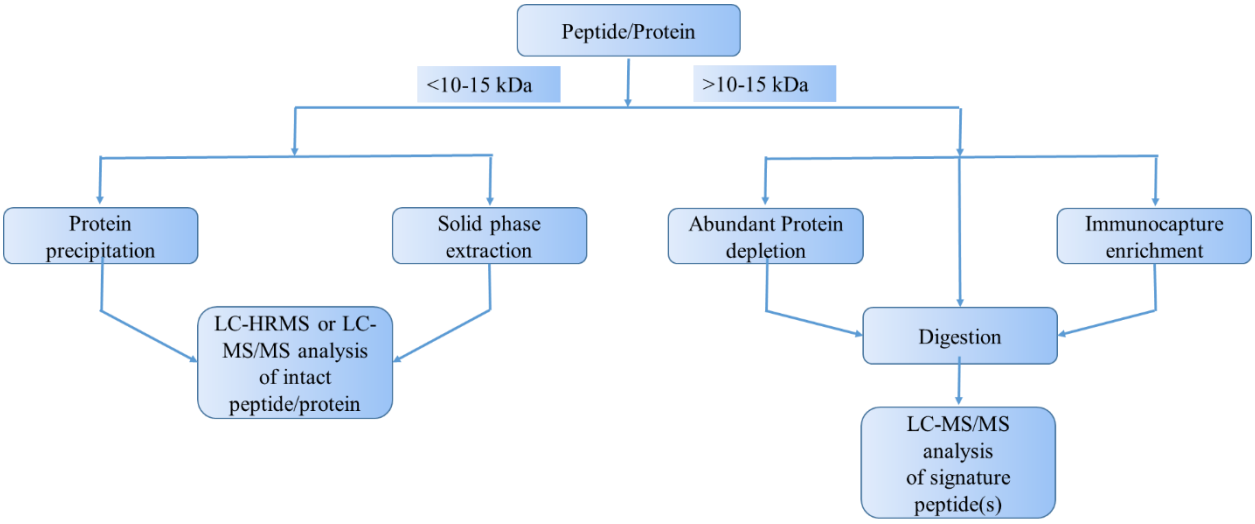

Figure 3. Generalized workflow of peptide/protein quantification by LC-MS

6. Research Aims and Objectives

1. What are the current approaches used for the synthesis of radiolabelled probes for bacterial infection identification?

Objective: To assess the currently available radiotracers and evaluate them for imaging of bacterial infections and their synthetic approaches.

2. Till date, there is no method developed for on and off resin synthesis of bifunctional metal chelator 1,4,7-Triazacyclononane-1-succinic acid-4,7-diacetic acid (NODASA); is it possible to synthesize NODASA economically using solid phase synthesis?

Objective: To develop a facile method for the synthesis of NODASA.

3. LL37 is a human antimicrobial peptide, can it be produced efficiently by solid phase peptide synthesis?

Objective: To develop an efficient synthetic route for the production of LL37 by solid phase peptide synthesis.

4. Literature reveals that antimicrobial peptides bears the potential to be used as radiotracer for bacterial infection imaging, can LL37 be radiolabelled and utilized for this purpose?

Objective: To synthesize 1,4,7-triazacyclononane,1-glutaric acid-4,7-acetic acid-LL37 (NODAGA-LL37), investigate its complexation with $^{nat/68}$Ga and evaluate cellular uptake of ^{nat}Ga-NODAGA-LL37.

7. Thesis outline

A brief review on radiotracers having potential for bacterial infection imaging will be presented in Chapter 2. A facile approach for the synthesis of bifunctional chelator NODASA will be presented in Chapter 3. The synthesis of antimicrobial peptide LL37 will be discussed in Chapter 4. The synthesis and the evaluation of $^{nat/68}$Ga complexed NODAGA-LL37 will be discussed in Chapter 5. Finally, in chapter 6 the overview of the results is put into perspective.

Reference

[1] R. Weissleder, U. Mahmood, Molecular Imaging, Radiology, 219 (2001) 316-333.

[2] T.F. Massoud, S.S. Gambhir, Molecular imaging in living subjects: seeing fundamental biological processes in a new light, Genes Dev., 17 (2003) 545-580.

[3] E.W. Price, C. Orvig, Matching chelators to radiometals for radiopharmaceuticals, Chem. Soc. Rev., 43 (2014) 260-290.

[4] C.F. Ramogida, C. Orvig, Tumour targeting with radiometals for diagnosis and therapy, Chem. Commun., 49 (2013) 4720-4739.

[5] B.M. Zeglis, J.S. Lewis, A practical guide to the construction of radiometallated bioconjugates for positron emission tomography, Dalton Trans., 40 (2011) 6168-6195.

[6] D. Zeng, B.M. Zeglis, J.S. Lewis, C.J. Anderson, The growing impact of bioorthogonal click chemistry on the development of radiopharmaceuticals, J. Nucl. Med., 54 (2013) 829-832.

[7] M. Lin, M.J. Welch, S.E. Lapi, Effects of Chelator Modifications on 68Ga-Labeled [Tyr3] Octreotide Conjugates, Mol. Imaging Biol., 15 (2013) 606-613.

[8] R.D. Hancock, Chelate ring size and metal ion selection. The basis of selectivity for metal ions in open-chain ligands and macrocycles, J. Chem. Educ, 69 (1992) 615-621.

[9] S. Auletta, F. Galli, C. Lauri, D. Martinelli, I. Santino, A. Signore, Imaging bacteria with radiolabelled quinolones, cephalosporins and siderophores for imaging infection: a systematic review, Clin Transl Imaging, 4 (2016) 229-252.

[10] A. Signore, A.W. Glaudemans, The molecular imaging approach to image infections and inflammation by nuclear medicine techniques, Ann. Nucl. Med., 25 (2011) 681-700.

[11] A. Signore, A.W. Glaudemans, F. Galli, F. Rouzet, Imaging infection and inflammation, BioMed Res. Int., 2015 (2015) 615150.

[12] A. Signore, C. D'Alessandria, E. Lazzeri, R. Dierckx, Can we produce an image of bacteria with radiopharmaceuticals?, Eur. J. Nucl. Med. Mol. Imaging, 35 (2008) 1051-1055.

[13] V. Kumar, D.K. Boddeti, 68Ga-radiopharmaceuticals for PET imaging of infection and inflammation, in: Theranostics, Gallium-68, and Other Radionuclides, Springer, 2013, pp. 189-219.

[14] A. Glaudemans, F. Galli, M. Pacilio, A. Signore, Leukocyte and bacteria imaging in prosthetic joint infection, Eur. Cell. Mater., 25 (2013) 61-77.

[15] A.W. Glaudemans, E.F. de Vries, F. Galli, R.A. Dierckx, R.H. Slart, A. Signore, The Use of F-FDG-PET/CT for Diagnosis and Treatment Monitoring of Inflammatory and Infectious Diseases, Clin. Dev. Immunol., 2013 (2013) 623036.

[16] C. Tsopelas, Radiotracers used for the scintigraphic detection of infection and inflammation, Scientific World J., 2015 (2015) 676719.

[17] E. Lazzeri, P. Erba, M. Perri, R. Doria, C. Tascini, G. Mariani, Clinical impact of SPECT/CT with In-111 biotin on the management of patients with suspected spine infection, Clin. Nucl. Med., 35 (2010) 12-17.

[18] C. A Dougherty, W. Cai, H. Hong, Applications of aptamers in targeted imaging: state of the art, Curr. Top. Med. Chem., 15 (2015) 1138-1152.

[19] M. Rusckowski, S. Gupta, G. Liu, S. Dou, D.J. Hnatowich, Investigations of a 99mTc-labeled bacteriophage as a potential infection-specific imaging agent, J. Nucl. Med., 45 (2004) 1201-1208.

[20] D.K. Hughes, Nuclear medicine and infection detection: the relative effectiveness of imaging with 111In-oxine-, 99mTc-HMPAO-, and 99mTc-stannous fluoride colloid-labeled leukocytes and with 67Ga-citrate, J. Nucl. Med. Technol., 31 (2003) 196-201.

[21] W.S. Richter, V. Ivancevic, J. Meller, O. Lang, D. Le Guludec, I. Szilvazi, H. Amthauer, F. Chossat, A. Dahmane, C. Schwenke, 99mTc-besilesomab (Scintimun®) in peripheral osteomyelitis: comparison with 99mTc-labelled white blood cells, Eur. J. Nucl. Med. Mol. Imaging, 38 (2011) 899-910.

[22] R. Sousa, M. Massada, A. Pereira, F. Fontes, I. Amorim, A. Oliveira, Diagnostic accuracy of combined 99mTc-sulesomab and 99mTc-nanocolloid bone marrow imaging in detecting prosthetic joint infection, Nucl. Med. Commun., 32 (2011) 834-839.

[23] H. Zhuang, Q.Y. Jian, A. Alavi, Applications of fluorodeoxyglucose-PET imaging in the detection of infection and inflammation and other benign disorders, Radiol. Clin. North Am., 43 (2005) 121-134.

[24] M. Bester, P. Van Heerden, J. Klopper, H. Wasserman, S. Rubow, F. De Klerk, Imaging infection and inflammation in an African environment: Comparison of 99Tcm-HMPAO-labelled leukocytes and 67Ga-citrate, Nucl. Med. Commun., 16 (1995) 599-607.

[25] M. Sathekge, The potential role of 68Ga-labeled peptides in PET imaging of infection, Nucl. Med. Commun., 29 (2008) 663-665.

[26] M. Zasloff, Antimicrobial peptides of multicellular organisms, Nature, 415 (2002) 389-395.

[27] K. Chen, X. Chen, Design and development of molecular imaging probes, Curr. Top. Med. Chem., 10 (2010) 1227-1236.

[28] T. Ebenhan, N. Chadwick, M.M. Sathekge, P. Govender, T. Govender, H.G. Kruger, B. Marjanovic-Painter, J.R. Zeevaart, Peptide synthesis, characterization and 68 Ga-radiolabeling of NOTA-conjugated ubiquicidin fragments for prospective infection imaging with PET/CT, Nucl. Med. Biol., 41 (2014) 390-400.

[29] K. Matsuzaki, Why and how are peptide–lipid interactions utilized for self-defense? Magainins and tachyplesins as archetypes, Biochim. Biophys. Acta, Biomembr., 1462 (1999) 1-10.

[30] S.M. Okarvi, Peptide-based radiopharmaceuticals: future tools for diagnostic imaging of cancers and other diseases, Med. Res. Rev., 24 (2004) 357-397.

[31] A. Lupetti, P.H. Nibbering, M.M. Welling, E.K. Pauwels, Radiopharmaceuticals: new antimicrobial agents, Trends Biotechnol., 21 (2003) 70-73.

[32] C.J. Palestro, Radionuclide imaging of infection: in search of the grail, J. Nucl. Med., 50 (2009) 671-673.

[33] M.S. Akhtar, M.B. Imran, M.A. Nadeem, A. Shahid, Antimicrobial peptides as infection imaging agents: better than radiolabeled antibiotics, Int J Pept, 2012 (2012) 965238.

[34] J. Dutta, S. Ramesh, S.M. Radebe, A.M. Somboro, G. Beatriz, H.G. Kruger, S.Y. Essack, F. Albericio, T. Govender, Optimized Microwave Assisted Synthesis of LL37, a Cathelicidin Human Antimicrobial Peptide, Int. J. Peptide Res. Therapeut., 21 (2015) 13-20.

[35] D.A. Devine, Antimicrobial peptides in defence of the oral and respiratory tracts, Mol. Immunol., 40 (2003) 431-443.

[36] M.J. Nell, G.S. Tjabringa, A.R. Wafelman, R. Verrijk, P.S. Hiemstra, J.W. Drijfhout, J.J. Grote, Development of novel LL-37 derived antimicrobial peptides with LPS and LTA neutralizing and antimicrobial activities for therapeutic application, Peptides, 27 (2006) 649-660.

[37] S.W. Zhang, W. Jian, Recent advances in absolute quantification of peptides and proteins using LC-MS, Rev. Anal. Chem., 33 (2014) 31-47.

[38] E. Ciccimaro, I.A. Blair, Stable-isotope dilution LC-MS for quantitative biomarker analysis, Bioanalysis, 2 (2010) 311-341.

[39] F. Li, D. Fast, S. Michael, Absolute quantitation of protein therapeutics in biological matrices by enzymatic digestion and LC-MS, Bioanalysis, 3 (2011) 2459-2480.

Chapter 2

Synthetic Approaches to Radiochemical Probes for Imaging of Bacterial Infections

Jyotibon Dutta[1], Tricia Naicker[1], Thomas Ebenhan[2], Hendrik G. Kruger[1], Per I. Arvidsson[1,3] and Thavendran Govender[1*]

[1]Catalysis and Peptide Research Unit, School of Health Sciences and School of Chemistry and Physics, University of KwaZulu-Natal, Durban 4001, South Africa
[2]University of Pretoria & Steve Biko Academic Hospital, Crn Malherbe and Steve Biko Rd, Pretoria, 0001, South Africa.
[3]Science for Life Laboratory, Drug Discovery and Development Platform and Division of Translational Medicine and Chemical Biology, Department of Medical Biochemistry and Biophysics, Karolinska Institutet SE-171 77 Stockholm, Sweden

** Corresponding author. E-mail address: govenderthav@ukzn.ac.za (Thavendran Govender)*

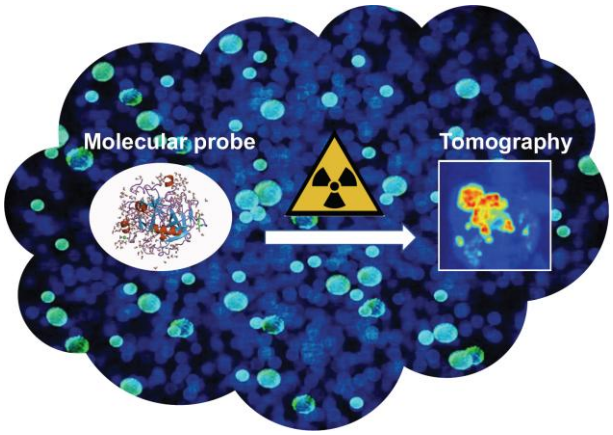

Abstract

This present review provides an account on the available synthetic strategies employed to radiolabel commercial and potential bacteria-selective probes for tomographic imaging. These molecular probes encompass leukocytes, antibodies, small molecules, peptides, antibiotics, macrolides, vitamins, oligomers and siderophores. Although this technique has shown to be a valuable tool for non-invasive infection imaging, more development is required to create easy-to-radiolabel kit solutions/procedures for the preparation of the probes.

Contents

1. Introduction

Throughout the world, bacterial infections remain a major cause for human morbidity and mortality [1]. Infectious diseases are one of the oldest challengers for humans; and can be ranked with war and famine [2]. In this current era, the growing incident of infection and the development of drug resistance have a huge impact on the global economy and human health [2]. Early detection of bacterial infection is crucial for the prognosis of the disease but insignificant progress has been done in this field. Conventional ways for bacterial diagnosis are based on either or combination of biochemical, physical and bacterial cultures where the bacterial culturing can be considered as the gold standard method [3]. However, bacterial culture methods do not provide *in vivo* localization of the infection or reservoirs. With the advancement of modern day technology, various diagnostic tools bear the potential for locating the site of infection. Radiological techniques such as computed tomography (CT) can be advantageous for imaging bacterial infections but it is only useful when there is a significant anatomical change in potentially infected tissues. Likewise, magnetic resonance imaging (MRI) can be applied for bacterial imaging aided by specific probes but it is limited to patients without claustrophobia or implanted medical devices. Nuclear medicine techniques such as single photon emission computed tomography (SPECT) and positron emission tomography (PET) stand out as potential candidates because these techniques are able to locate the site of infection with the help of a radiolabeled biomolecule/probe [4]. Available SPECT- or PET-based probes consist of *in vitro* or *in vivo* (for example) radiolabeled leukocytes. There are recurring comprehensive reports on the clinical use of commercially available radiotracers targeting infection and inflammation [5, 6]. The radiolabeled probes under current studies showed the potential for targeting molecular components of bacteria or its metabolites resulting in specific identification of the infection site in contrast to the sterile inflammation [7-10]. This field of study is also positively influenced and expanding due to the hybridization of imaging techniques such as PET(SPECT)/CT or PET(SPECT)/MRI [11].

Herein, we aim to provide a concise guide to the synthetic approaches of molecular radiotracers with focus on bacterial imaging aimed at medicinal chemists. This review is divided into commercially available and novel probes as followed: i) clinical/preclinical availability, ii) probe functionalizing via suggested radiolabeling procedures and iii) probe distribution and suggested mechanisms of the probe uptake, internalization and signal amplification. At the end of each class of radiolabeled probe, is a table summary of the transformations that provides information on the non-radiolabeled core, radioisotope, disease target, labeling efficiency and technique used for detection of the radiotracer.

2. Commercially available infection imaging probes:

Most of the clinically used radiotracers for infection detection are based on leukocytes due to the fact that there is an influx of leukocytes during inflammation. A few of these radiopharmaceuticals are Food and Drug Administration (FDA) approved. These commercially available radiotracers can be divided broadly into i) radiolabeled leukocytes (^{111}In-oxine-leukocyte, ^{99m}Tc-HMPAO-leukocute and ^{99m}Tc-Stannous Colloid), ii) radiolabeled anti-granulocyte antibodies (^{99m}Tc-Besilesomab and ^{99m}Tc-Sulesomab), iii) unspecific biomolecules such as *2*-deoxy-*2*-(^{18}F)*fluoro*-D-glucose (^{18}F-FDG) and $^{67/68}$Ga-citrate.

2.1. ^{111}In-oxine-Leukocyte

The current "gold standard" tomographic imaging technique targeting infection is considered to be direct leukocyte labeling with radio metals [12]. Efficient labeling of leukocytes and its imaging can be obtained with ^{111}In-oxine because of its long half-life [13]. Detection and localization of the infectious site is the prime area of interest for ^{111}In-oxine-leukocyte which included various clinical presentations such as pulmonary infection including tuberculosis, endocarditis, neurological infections, fever of unknown origin, diabetic foot, inflammatory bowel disease, infected central venous catheters or other devices; infected joint and vascular prosthesis, postoperative abscesses and osteomyelitis of the appendicle skeleton [14-16]. Roca *et al.* described a method of radiolabeling necessitating at least 2 x 10^8 leukocytes for good labeling efficiencies [14]. A whole-blood sample was collected from the patient in acid-citrate-dextrose (ACD) anticoagulant solution containing vial, at a blood /ACD ratio of 1:5.6. Out of that, 15 ml of the mixture was centrifuged at 2000 g for 10 min at room temperature to separate the blood cells from the cell free plasma (CFP) and the latter was used as re-suspending medium after labeling in the subsequent steps. Leukocyte isolation was initiated by separating the erythrocytes with 10% 2-hydroxyethyl starch (HES) (molecular weight 200/0.5 or 200/0.6) by sedimentation. Recommended blood-ACD solution to HES ratio was 10:1 and the leukocyte-rich plasma (LRP) was collected with a 20G lumbar needle without disturbing the erythrocyte layer which was followed by centrifugation at 150 g for 5 min. Platelet-rich plasma (PRP) was removed and the mixed leukocyte pellet was gently re-suspended. An optional PBD/saline wash was advised to reduce the number of platelets. For radiolabeling, 20 MBq of ^{111}In-oxine was incubated with the isolated mixed leukocyte cell suspension for 10 min at room temperature with gentle periodic swirling. The authors recommended working with HEPES buffer (about 6 mg/ml final concentration) if ^{111}In-oxine has to be used without the buffer provided by the manufacturer. After incubation, at least 3 ml (up to a maximum of 10 ml) of PBS/saline was added to the solution and centrifuged at 150 g for 5 min. The supernatant containing the unbound ^{111}In-oxine

was removed and used to calculate the labeling efficiency. Radioactivity was measured in the leukocyte pellet and subsequently dissolved in 3-5 ml of previously extracted CFP [14].
During the process of leukocyte labeling with ^{111}In-oxine, it diffused through the lipid bilayer of the cell because of its neutral and lipophilic nature. Upon internalization, the ^{111}In-complexes (i.e. the radioisotope) irreversibly associate with intercellular and nucleus components and free oxine may experience cellular efflux.

2.2. ^{99m}Tc-HMPAO-Leukocyte:

Technetium-99m (^{99m}Tc) can be chelated with hexamethylpropyleneamine oxine (HMPAO) and has been used as a non-invasive diagnosis tool for numerous physiological abnormalities [17]. The SPECT radioisotope ^{99m}Tc- can be chelated with HMPAO, which facilitates the uptake into cells [18]. Leukocyte labeling with ^{99m}Tc-HMPAO follows a similar technique to using ^{111}In-oxine; i.e. it needs the separation of WBC from the whole blood. Once inside the cell, ^{99m}Tc-HMPAO changes its lipophilic character to non-diffusible hydrophilic complexes and becomes trapped [19]. This compound has a half-life of 6 h and emits 140-keV γ-rays which can be detected by a SPECT camera [20]. The normal probe bio-distribution can be seen mainly in the kidney, liver and spleen with notable activity in the gastrointestinal tract and bone marrow. Hence, imaging of hepatic and splenic infections using ^{99m}Tc-HMPAO-Leukocyte SPECT may lead to suboptimal image interpretation [20].

2.3. ^{99m}Tc-Stannous Colloid

^{99m}Tc-labled stannous colloids (^{99m}Tc-SnC) is a radiolabeling technique to label neutrophils and monocytes for imaging of inflammation and spatial localization of infection for gram-positive as well as gram-negative bacteria [21-26]. The radiolabeling of leukocytes does not require its separation from the whole blood as ^{99m}Tc-SnC can selectively bind to the target immune cells in the infection site which make it simpler and less expensive compared to other labeling agents [21, 27, 28]. The ^{99m}Tc-SnC has a shelf-life of up to 6 h [29]. Colloid incubation with a heparinized patient whole blood sample (up to 20 mL) comprises of a 1 h syringe rotation followed by a brief centrifugation step to part cells and plasma supernatant prior to cell re-suspension and re-administration into the patient. It should be noted that ^{99m}Tc-SnC labeled blood cells cannot distinguish between sterile inflammation and infection [30]. It has unanimously been reported that its labeling efficiency is more than 95% using whole blood samples [27, 28, 31-33]. The detailed mechanism of action concerning ^{99m}Tc-SnC-labeling leukocytes may not be entirely understood [21, 22, 27, 34-36]; it is hypothesized that phagocytosis of the colloidal compounds and/or its reversible binding of the leukocyte to cell membranes may occur.

2.4. ^{99m}Tc-Besilesomab

Besilesomab, a murine derived monoclonal antibody of the IgG1 κ isotype with a molecular weight of 150 kDa, targets the NCA-95 epitope of granulocyte or granulocyte precursors. After injection of ^{99m}Tc-Besilesomab to the recipient, 10% of the compound binds to neutrophils whereas 20% of them freely circulate and localize in infected sites through a non-specific mechanism [37, 38]. ^{99m}Tc-Besilesomab can be used for the diagnosis of pyrexia of unknown origin, appendicitis, acute myocarditis and diabetic pedal osteomyelitis but it showed variable results in the case of joint infection and inflammatory bowel disease [39-43]. Radiopharmaceutical preparation of ^{99m}Tc-Besilesomab is marketed under the trade name Scintimun® and the kit contains Besilesomab with pre-reduced disulfide bonds. Generator-eluted ^{99m}Tc-sodium pertechnetate is reduced by the stannous chloride (provided as a kit vial component) yielding ^{99m}Tc(IV), which in turn binds to the free thiol groups of the reduced Besilesomab [44]. The usage of Scintimun® might be challenged by: the risk of the pattern of human anti-mouse antibodies (HAMA) response, i.e. eliminates repeated probe administrations, a delayed probe accumulation at the infected site due to the high molecular weight of the antibody, and significant unspecific probe uptake in the liver and bone marrow [45]. ^{99m}Tc-Besilesomab-SPECT imaging is unspecific for infection.

2.5. ^{99m}Tc-Sulesomab

^{99m}Tc-Sulesimab is a sensitive probe primarily used to detect musculoskeletal infections. It also showed to be useful in the case of diagnosing pyrexia of unknown origin as well as infection in soft tissues [46]. Sulesomab is a murine originated fragment antigen binding (Fab) portion of an IgG_1 and can couple to ^{99m}Tc through its thiol groups. This fragment is 50 kDa and can bind to leukocytes through the normal cross-reactive antigen-90 (NCA-90) [38]. After infusion, 34% of ^{99m}Tc-sulesomab can be detected in the blood after 1 h and at 4 h the radioactivity starts to wash out with only 7% of the injected dose remaining in the body after 24 h. This tracer shows higher affinity towards the activated rather than latent granulocytes, thus *in vivo* radiolabeling is likely to occur at the inflammation site rather than to circulating granulocytes [46]. The commercially available sulesimab (LeukoScan®) kit comprises of sulesomab, stannous chloride dihydrate, potassium sodium tartrate tetrahydrate, sodium acetate trihydrate, sodium chloride, glacial acetic acid (trace), hydrochloric acid (trace) and sucrose under the nitrogen. These lyophilized components are reconstituted in a solution of sodium chloride before adding the radioactivity with a simple 10 min incubation at room temperature is needed to achieve ^{99m}Tc-Sulesimab [47]. The final formulation has pH values of 4.5-5.5 with the shelf-life of the probe being 4 h.

2.6. ^{18}F-FDG-PET

Aside from mainly imaging oncologic abnormalities, ^{18}F-FDG-PET is also a technique to image infection and inflammation [48]. The mechanism of ^{18}F-FDG-PET for infection imaging is due to an elevated glucose demand by mononuclear and granulocyte cells during their metabolic eruption when activated [49-53]. Moreover, glucose is also utilized by proliferating fibroblasts [54] but again, this technique cannot distinguish between infection and sterile inflammation. Hamacher *et al.* described a nucleophilic substitution of ^{18}F-fluoride for the synthesis of ^{18}F-FDG where they used 1,3,4,6-tetra-*O*-acetyl-2-*O*-trifluoromethanesulfonyl-d-manno-pyranose as a precursor (Scheme 1) [55]. The major drawback of this method is the activation of the ^{18}F-fluoride for the nucleophilic substitution reaction which needs an azeotropic drying step [56].

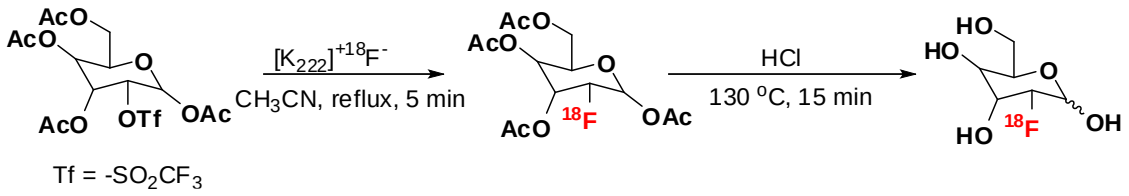

Scheme 1. Synthesis of *2*-deoxy-*2*-(^{18}F)*fluoro*-D-glucose

2.7. $^{67/68}$Ga-Citrate

The former gold standard of infection imaging, gallium-67 (^{67}Ga) or gallium-68 (^{68}Ga)-labeled citrate has been in use as a probe for the last five decades [57]. However, the mechanism of uptake of $^{67/68}$Ga-citrate is still not entirely clear. There are several factors which can affect the accumulation of this compound around the infection site; this includes direct leukocyte binding, complexation to siderophores, or binding to lactoferrin and transferrin [58]. With the advent of germanium-68 (^{68}Ge)/Ga/^{68}Ga-generators, ^{68}Gallium-citrate gained momentum as a PET radiotracer as it is a more advanced technique than ^{67}Ga-citrate-SPECT. Rizzello *et. al.* described a method for the preparation of ^{68}Ga-citrate for regular clinical use with a commercial semi-automatic labeling module (Eckert & Ziegler F-CON Pharmaitalia) [59]. Ayuob *et. al*. described the synthesis where $^{68}GaCl_3$ (3-5 mCi in 150µl) in 0.6 M HCl was heated to dryness. A sodium citrate solution was added to the dried $^{68}GaCl_3$ and incubated at 50 ˚C for 10-15 min followed by filtration through a 0.22 micron membrane (Scheme 2). The final pH of the solution was adjusted to 5.5-7 [60]. There is also a kit-based ^{68}Ga-radiolabeling procedure available using ACD as a precursor [61].

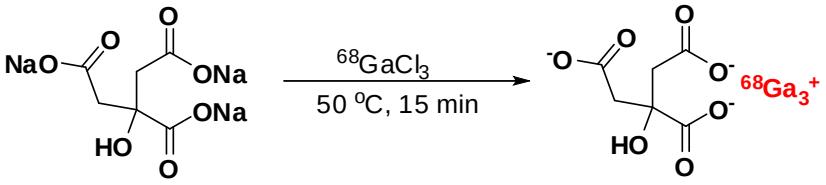

Scheme 2. Synthesis of ^{68}Ga-Citrate

Table 1 Commercially available probes for infection imaging

Radiotracer class	Probe name	Targets	Labelling efficiency	Method	Reference
Radiolabeled leukocytes	^{111}In-oxine-leukocyte[#]	Endocarditis, neurological infections, fever of unknown origin, diabetic foot, inflammatory bowel disease	72.5 ± 5.5%	SPECT	[62]
	^{99m}Tc-HMPAO-leukocyte[#]	Imaging of infection and inflammation (diabetic foot prosthetic graft infection, abdominal sepsis, osteomyelitis)	44 ± 13%	SPECT	
	^{99m}Tc-Stannous colloids	Spatial localization of infection for gram-positive and gram negative bacteria	>95%	SPECT	[27, 28, 31-33]
Radiolabeled antigranulocyte antibodies	^{99m}Tc-Besilesomab	Pyrexia of unknown origin, appendicitis, acute myocarditis and diabetic pedal osteomyelitis	--	SPECT	[44]
	^{99m}Tc-Sulesomab	Pyrexia of unknown origin and infection in soft tissues	4.5%	SPECT	[46]
Biomolecules	^{18}F-FDG[#]	Oncologic or cardiac indications, imaging infection and inflammation	50%	PET	[55]
	^{67}Ga-citrate[#]	Detection of some acute infections and inflammation	--	SPECT	[63-65]

[#]) FDA approved

3. Novel imaging probes for direct, more specific imaging of bacterial infection

Compounds having affinity towards a specific pathogen can be utilized for its direct *in vivo* imaging after being radiolabeled with a compatible radioisotope. In 2016, Auletta *et al*. systematically discussed the potential of quinolones, cephalosporins and siderophores as promising imaging agents for infection [66]. In a 2015 review, Tsopelos elaborated on compounds bearing potential towards scintigraphic detection of infection and inflammation [5]. Moreover, a few promising tracers show affinity towards bacteria such as ^{11}In-DPC11870, ^{11}In-DTPA-IgG(^{14}C), ^{111}In/^{99m}Tc -DTPA-hpc-IgG, ^{18}F-DPA-714, ^{99m}Tc-PEG-liposomes, ^{99m}Tc-HAS, labelled fMLFKs and labelled interleukins was explained by Tsopelos, however, these molecules fall out of the scope of this review. Furthermore, ^{99m}Tc labelled bacteriophages were also omitted from this discussion. The following text highlights selected compound clusters that bear the largest potential to accomplish bacteria-selective tomographic imaging: i) antimicrobial peptides and ii) biomimetics.

3.1. Antimicrobial peptides as bacteria-selective imaging probes

Peptides are short chains of amino acids linked by amide bonds. These naturally occurring biomolecules are logical options for development as possible targeting vectors for PET tracers as they have unique characteristics such as; high target specificity and binding ability, low toxicity and immunogenicity and easy scale up production in the laboratory [67, 68]. Generally, peptides containing less than 50 amino acids are considered for imaging tracers due to their molecular weight. These peptides are relatively small in size, facilitates rapid accumulation at the target site as well as lead to faster clearance from the recipient which would make them desirable candidates for PET molecular imaging probes [67].

In general, naturally occurring peptides are most suited for designing peptide-based PET tracers; as they play a vital role in certain physiological conditions by mediating via their high-affinity, specific and massively overexpressed receptors [69]. However, various plasma-containing proteases and peptidases lead to rapid degradation of some of these compounds resulting in a shorter pharmacological half-life and decreased target availability. Thus, to increase the *in vivo* stability of naturally occurring peptides, these compounds require molecular engineering at the amino acid residues that are involved in degradation without compromising the most desired biological activity. Till date, a number of researchers have described various approaches to modify amino acid residues to increase the efficiency and stability of peptides. These approaches include peptide bond substitution, N- and C-terminus acetylation, side-chain and unnatural amino acid introduction, suitable D-amino acid incorporation and amino alcohol utilization. In addition,

suitable hydrophilic and/or lipophilic amino acids can also be introduced to modify the permeability of the peptide without compromising the binding efficiency [70-72].

The success of PET probes development is based on identification of its molecular target and characterization of its biological role. Some of the targets best studied for the development of peptide-based PET probes are integrin, somatostatin and gastrin-releasing peptide receptors [73-81]. Moreover, antimicrobial peptides (AMP) are also trending for developing PET tracers for infection imaging because of their direct involvement in the innate immune system and their ability to bind selectively to pathogenic bacteria or yeast [7, 68]. AMPs are synthesized by various cells; however, regardless of the origin, these peptides share a few common characteristics as they are membrane active, positively charged and amphipathic [82]. Due to their cationic properties, it is believed that AMPs have strong electrostatic affinity towards the negatively charged bacterial cell wall while having relatively lower attraction to mammalian cells which are less negatively charged [7, 83]. Peptides are becoming popular as infection imaging probes because of their ability to accumulate at infection foci as well as a lack of cytotoxicity in the recipient [84]. Even though, peptides have been studied extensively as radiotracers for various physiological conditions; there is only a handful of AMPs evaluated for infection imaging [85].

3.1.1. Ubiquicidin (UBI)

Ubiquicidin is a 6.7 kDa polypeptide comprising of 59 amino acid residues. This peptide was first identified from a macrophage cell line of mouse and has antibacterial effects on *Salmonella typhimurium* and *Lysteria monocytogenes*. Subsequently it was also isolated from numerous organisms, including human. This peptide has a structure that is homologous to the murine ribosomal subunit S30 [86]. Brouwer *et al*., in 2006, synthesized several fragments of the ^{99m}Tc labeled UBI and studied the *in vitro* bacterial sensitivity as well as selectivity. They also found sufficient accumulation of the fragments ^{99m}Tc-KVAKQEKKKKKTGRAKRR (UBI-18-35) and ^{99m}Tc-TGRAKRRMQYNRR (UBI29-41) around the infected site in mouse models for SPECT imaging [87]. These peptides were synthesized on solid phase *via* 9-fluorenylmethoxycarbonyl (Fmoc) chemistry. PyBOP was employed as the coupling reagent along with the base 4-methylmorpholine (NMM) in NMP for the coupling [87]. Direct radiolabeling was carried out by adding $SnCl_2$ and sodium pyrophosphate in saline to a stock solution of the peptide. Thereafter, KBH_4 in 0.1 M NaOH and ^{99m}Tc-sodium pertechnetate solutions were added to the mixture respectively. The reaction was carried out for 1 hr at room temperature (Scheme 3) [87].

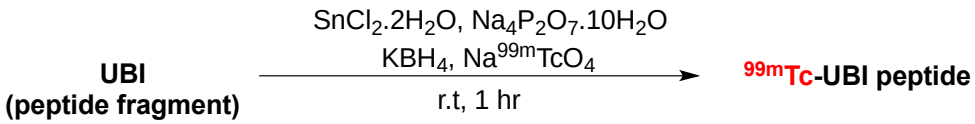

Scheme 3. Synthesis of ^{99m}Tc labeled UBI fragment

Over the years ^{99m}Tc-UBI(29-41) fragments were found to be specific as well as selective towards both gram positive and gram negative bacteria along with the multidrug resistant strains [88, 89] [90, 91] [92]. ^{99m}Tc-UBI (29-41) may attach the radioisotope at Lys and Arg residues of the peptide. This did not allow for the peptide to retain its natural configuration [93, 94]. The radiolabeled UBI fragment ^{99m}Tc-UBI(29-41) was first administered in human subjects in 2004 for studying its pharmacokinetic properties in a clinical trial on patients with soft-tissue, prosthesis or suspected bone infections. The results revealed high specificity, selectivity and accuracy without any significant adverse effects [95]. Recently, fluorine-18 was used to radiolabel UBI(29-41) for the purpose of PET imaging. However in this study, the ^{18}F-UBI(29-41) did not confirm specificity towards *S. aureus in vivo* [96] and there was also significant defluorination. Concerning the radiosynthesis, to a mixture of Kryptofix and $K_2CO_3/K_2C_2O_4$, fluorine-18 was added followed by evaporation under vacuum in the reactor. Thereafter, reduction of the compound was carried out by ethyl 4-(trimethylammonium)benzoate trifluoromethanesulfonate in DMSO. The reaction was heated at 95 °C for 6 min followed by the distillation of the product in a 0.5M NaOH solution. The product was again hydrolysed for 2 min at 50 °C in the reactor after rinsing it with 5% acetic acid and water. 0.5M HCl was then added to make the product 4-^{18}F-fluorobenzoic acid which was eluted through a Lichrolut EN cartridge. A purified solution of this product was mixed with 4-(dimethylamino)-pyridine (DMAP) and dried in the reactor. Subsequently, *N,N'*-disuccinimidylcarbonate (DSC, in acetonitrile) was added and heated at 95 °C for 7 min followed by cooling to 35 °C. This crude *N*-succinimidyl-4-[^{18}F]fluorobenzoate was eluted through a Lichrolut EN cartridge followed by HPLC purification and again eluted through a Lichrolut EN cartridge. Finally, the *N*-succinimidyl-4-[^{18}F]fluorobenzoate (in DMF) was mixed with UBI 29-41 in 0.1M boraxbuffer (pH 8.5) and left to react for 10 min at room temperature in a ultrasound bath. The radiolabeled 4-[^{18}F]fluoro-benzoyl-ubiquicidin 29-41 (^{18}F-UBI29-41) was HPLC purified followed by elution through a C18 cartridge (Scheme 4) [97].

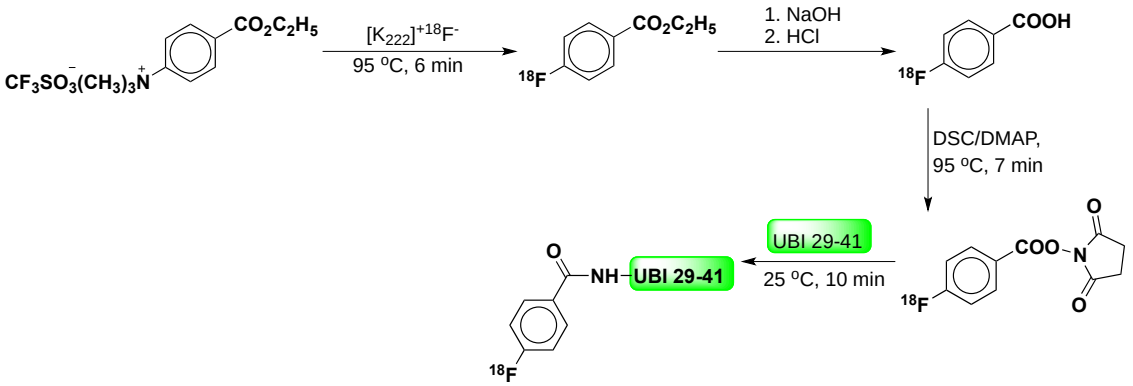

Scheme 4. Synthesis of [18F]UBI 29–41

^{68}Ga-NOTA-UBI(29-41) showed specificity towards *S. aureus* in a rabbit model and was able to distinguish infection from sterile inflammation [98]. For the design of the UBI containing the ^{68}Ga radiotracer, a chelator was envisaged. In this case the peptide was synthesized on resin and conjugated with 1,4,7-triazacyclononane-1,4,7-triacetic acid (NOTA). The NOTA conjugation was carried out by functionalizing the amino terminus of the peptide with bromoacetic acid and diisopropylcarbodiimide (DIC) in dichloromethane. The bromine was then displaced with excess 1,4,7-triazacyclononane and trimethylamine (TEA) in acetonitrile. *tert*-Butyl 2-bromoacetate was added to the remaining secondary amines of triazacyclononane ring [98] followed by full deprotection and cleavage from the resin (Scheme 5).

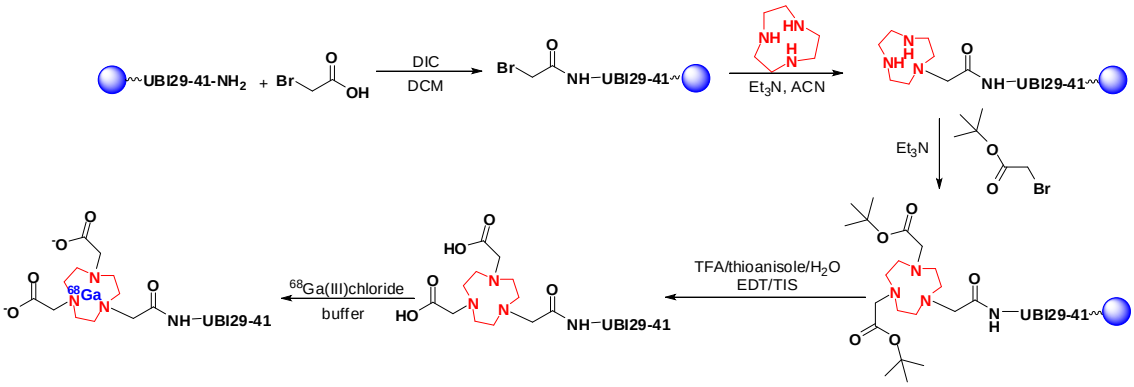

Scheme 5. Synthesis of ^{68}Ga-NOTA-UBI29-41 complex

3.1.2. Human neutrophil peptide (HNP)

Neutrophils are integral components of the immune system and play a vital role in protecting the host from microbial infections by producing neutrophil peptides. These cationic single chain peptides are rich in arginine and cysteine. Neutrophil peptides are of about 3.5 kDa and designated as defensins [99]. HNP-1, HNP-2, HNP-3 and HNP-4 are the four neutrophil peptides identified in human [100, 101]. HNP-1, HNP-2 and HNP-3 comprise of 29 common amino acid

residues which represents 99% sequence homology while HNP-4 shares only 32% homology with the others [101, 102]. HNP-1 is one of the more extensively studied antimicrobial peptides found in the defensin family. It is postulated that defensin interact with deoxyribonucleic acids, which in turn leads to cell death [103]. Mouse infection model studies revealed the potential use of HNP-1 as a therapeutic agent for bacteria including *M. tuberculosis* [104]. Biodistribution and potential antimicrobial evaluation of ^{99m}Tc labelled HNP-1 in *K. pneumoniae* and *S. aureus* infected (peritoneal and intramuscular infections) swiss mice confirms the accumulation of this tracer in the infection sites [105]. In this study, Welling *et. al.* isolated HNP-1 from human neutrophil, which was then purified by HPLC [105]. HNP-1 in sodium phosphate buffer (Na-PB) was then mixed with a sterile solution of stannous pyrophosphate and immediately reduced with KBH_4 dissolved in a NaOH solution. Finally, the solution was stirred for 30 min with ^{99m}Tc-sodium pertechnetate solution to yield radiolabelled HNP-1 [105-107]. Raj *et. al.*, in 2000, described a method for the solid phase synthesis of HNP-1 on Wang resin using Fmoc protected amino acids [108]. DIC in the presence of HOBt was used as the coupling reagent where a mixture of DCM and DMF (50% v/v) served as the solvents. Fmoc deprotection was carried out using 25% solution of piperidine in DMF and the peptide was cleaved from the resin using 90% TFA in DCM containing dimethyl sulphide (2.5%) and thioanisole (2.5%) [108].

3.1.3. Neutrophil elastase inhibitor peptide

The protease, neutrophil elastase is secreted by the activated neutrophils when triggered due to inflammation at the infection foci. This 29 kDa antimicrobial peptide is released upon internalization [109] and rapidly inhibited by α-1 trypsin inhibitor [110]. A peptide library was constructed based on wild-type bovine pancreatic trypsin inhibitors with the help of phage display technology. Screening of these peptides on immobilized human neutrophil elastase, revealed EPI-HNE-2 as the most potent and specific inhibitor [111, 112]. EPI-HNE-2 radiolabeled with ^{99m}Tc was studied in monkeys for inflammation/infection imaging. Based on the outcome, the bacterial specificity of the tracer was not clear, however, it did accumulate within areas with inflammations and infections [113]. EPI-HNE-2 can be radiolabeled with ^{99m}Tc using the bifunctional chelator molecule NHS-MAG3. Peptide-NHS-MAG3 conjugation was carried out by a dropwise chelator addition (in DMF) to a solution of EPI-HNE-2 in 0.1 M HEPES buffer (pH 8.0). The solution was then left for 1 h undisturbed and finally the conjugated peptide was purified on a P-4 column (Bio-Rad, Melville, NY). To the purified conjugated peptide in 0.25 M ammonium acetate buffer, sodium tartrate (in 0.5 M sodium bicarbonate), ammonium acetate and ammonium hydroxide was added followed by a solution of stannous chloride (in 10 mM HCl). Finally, ^{99m}Tc-pertechnetate was mixed in and incubated for 1 hr at

room temperature for the completion of the reaction (Scheme 6). The pH was adjusted to 7.6 and purified on a P-4 column [114].

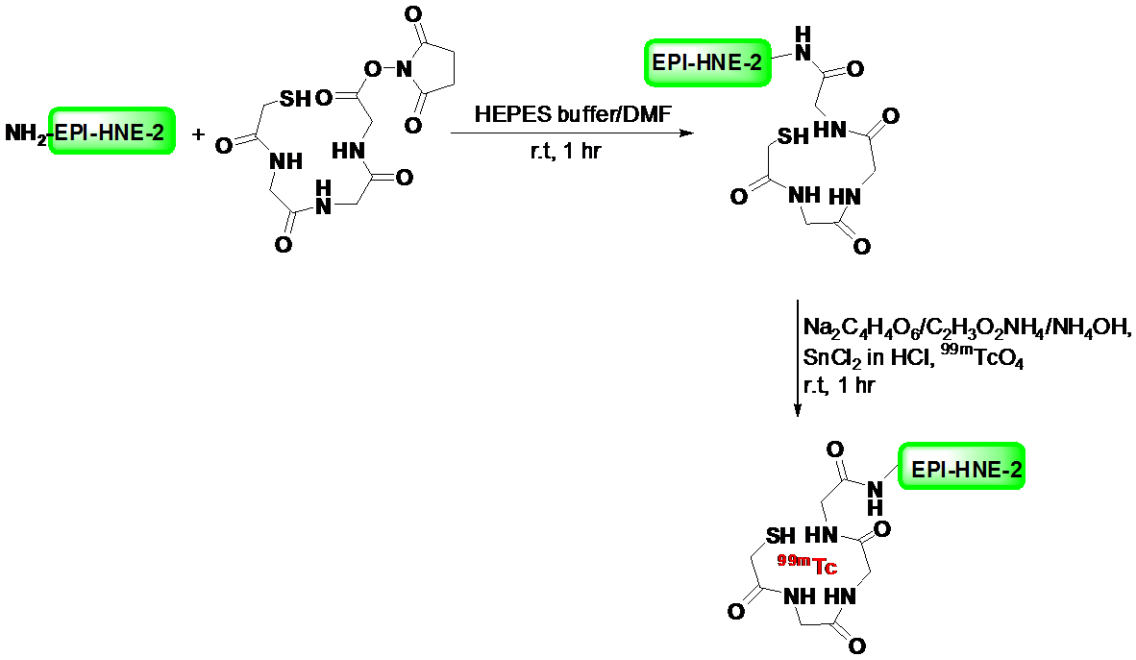

Scheme 6. Synthesis of ^{99m}Tc-MAG3-EPI-HNP2

3.1.4. Human β-defensin (HBD)

Defensins are the first line of the defense mechanism of the human immune system and the β defensins are one class that are of epithelial tissue origin [115, 116]. A 4 kDa peptide, human β defensin-3 (HBD-3), shows a broad range of antimicrobial activity including for both gram-positive and -negative bacteria [117-119]. HBD-3 was successfully radiolabeled with ^{99m}Tc and was able to distinguish between infection and sterile inflammation in a mouse model previously infected with *S. aureus* [115]. A cationic complex $[^{99m}Tc\ (H_2O)_3(CO)_3]^+$ was used to label the recombinant HBD-3 [115]. $[^{99m}Tc\ (H_2O)_3(CO)_3]^+$ can be synthesized through the reduction of $[^{99m}TcO_4]^-$ in saline (0.9% NaCl/H_2O) by $NaBH_4$. This reaction required heating at 75 °C and flashed with carbon monoxide [120]. The solution was cooled and adjusted to pH 8.0 with HCl. The peptide, dissolved in water, was added to the solution containing $[^{99m}Tc\ (H_2O)_3\ (CO)_3]^+$ and left for 60 min to react at room temperature (Scheme 7). The radiolabeled HBD-3 was finally purified by gel chromatography using a Sephadex G-2 column [115].

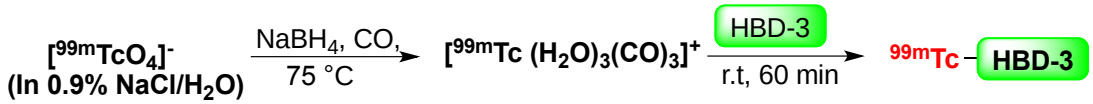

Scheme 7. Synthesis of ^{99m}Tc-HBD-3

3.1.5. Human lactoferrin-derived peptide (hLF)

Lactoferrin, a member of the transferrin family, is an 80 kDa iron-binding protein [121, 122]. This glycoprotein is secreted by mammalian mucosal epithelial cells including those of human [122]. Lactoferrin is found in milk, urine, bile, nasal and bronchial secretions, gastrointestinal fluids, semen, vaginal fluids, tears and saliva [123-125]. The defensive properties of this peptide includes antimicrobial (including antibiotic-resistant bacteria), anti-inflammatory and anticancer properties due to immune modulator activities [122, 126]. An eleven amino acid containing cation-rich sequence (1-11: GRRRRSVQWCA) from the N-terminus of human lactoferrin was reported to be active against bacteria and also showed immune modulatory compound behaviour [126, 127]. Welling *et. al.* in 2000, studied various fragments of UBI and hLF for their bacterial specificity and selectivity; concluding that the former is more favourable for infection detection [92]. For this study the peptide sequences were synthesized on solid phase employing Fmoc chemistry with PyBOP/NMM in NMP as coupling conditions with Fmoc deprotection using piperidine [128]. For radiolabelling, the synthesized peptide solutions (in 0.01 M of acetic acid pH 4) were mixed with stannous pyrophosphate followed by immediate addition of KBH_4 (in 0.1 M NaOH). Finally a ^{99m}Tc-sodium pertechnetate solution obtained from a ^{99m}Tc generator was added and the pH was adjusted to between 5-6. One hour of gentle stirring was carried out for completion of the reaction (Scheme 8) [92].

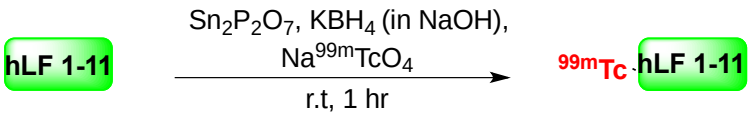

Scheme 8. Synthesis of ^{99m}Tc-hLF 1-11

Table 2 Antimicrobial peptides for bacterial imaging

Antimicrobial peptide name*	**Radioisotope**	**Targeted microorganism(s)^**	**T/NT [a] ratio**	**Labelling efficiency**	**Method**	**Reference**
UBI29-41	^{99m}Tc, ^{18}F, ^{68}Ga	*S. aureus, E. coli, C. albicans and A. fumigatus*	2.2-4.6	>95% - 99.2%	Scintigraphy, PET,	[89, 96, 98]
HNP-1	^{99m}Tc	*K. pneumonia, S. aureus, M. tuberculosis*	1.5-3.5	88%	Scintigraphy	[105]
EPI-HNE-2	^{99m}Tc	--	0.3-2	54%	Scintigraphy	[113, 114]
HBD-3	^{99m}Tc	*S. aureus, K. pneumoniae and E. coli*	3	40% - 50%	Scintigraphy	[115]
hLF	^{99m}Tc	*K. pneumonia, S. aureus*	>2.4	92%	Scintigraphy.	[92]

*) UBI29-41:ubiquicidin peptide fragment 29-41 ;HNP-1: human neutrophil peptide 1; EPI-HNE-2: Neutrophil elastase inhibitor peptide 2; HBD-3: human β defensin-3; hLF: human lactoferrin-derived peptide 1-11

^) *S. aureus*: *Staphylococcus aureus*; *E. coli*: *Escherichia coli*; *C. albicans*: *Candida albicans*; *A. fumigatus*: *Aspergillus fumigatus*; *K. pneumonia*: *Klebsiella pneumonia*; *M. tuberculosis*: *Mycobacterium tuberculosis*

[a]) T/NT = Target/Non Target

3.2. Biomimetics

Biomimetics are a group of compounds that are deliberate to exploit unique bacterial targets. These compounds are trapped upon internalization either because of their interaction with the cellular macromolecules or by acting as a substrate for the enzyme of the pathogen. This intracellular mechanism in turn promises for signal amplification and allows for imaging of the pathogen.

3.2.1. Antibiotics/Antimicrobial drugs

Antibiotics are potential candidates for tomographic imaging because of their characteristic specificity towards bacteria. ^{99m}Tc-ciprofloxacin is the first and most widely studied radiolabeled antibiotic [129-132]. ^{99m}Tc-fluoroquinolones (^{99m}Tc-norofloxacin, ^{99m}Tc-sparfloxacin) were subsequently explored as a second line of antibiotic based radiotracer. Evidently, the potential of other antibiotics has been investigated as imaging agents; for example, intracellular targets (^{99m}Tc-kanamycin, ^{99m}Tc-cefuroxineaxetil, ^{99m}Tc-cefoperazone, ^{99m}Tc, -ceftizoxine), cell wall (^{99m}Tc-vancomycin, ^{99m}Tc-alafosfalin, ^{99m}Tc-ceftizoxine) and specific mycobacterial targets (^{11}C/^{99m}Tc-rifampicin, ^{11}C/^{18}F/^{99m}Tc-isoniazid and ^{99m}Tc-ethambutol).

3.2.1.1. Aminoglycoside

Aminoglycosides are polycationic entities which manifests its effect by ribosomal blockade, misreading in translation, membrane damage, and irreversible uptake of the antibiotic [133, 134]. Labelling of kanamycin, streptomycin and gentamicin can be achieved with the reducing agent $SnCl_2(2.H_2O)$. A solution of $SnCl_2$ was added to a solution of kanamycin/streptomycin/gentamicin and the pH adjusted. To that mixture, $^{99m}TcO_4^-$ was added and the reaction was carried out at room temperature (Scheme 9) [135-137]. For the labeling of tobramycin, the same reducing agent was utilised but with the exception that the $SnCl_2(2.H_2O)$ was dissolved in HCl and then mixed with a solution of $NaOH:NaHCO_3$ and $Na^{99m}TcO_4$ under a blanket of nitrogen gas [138].

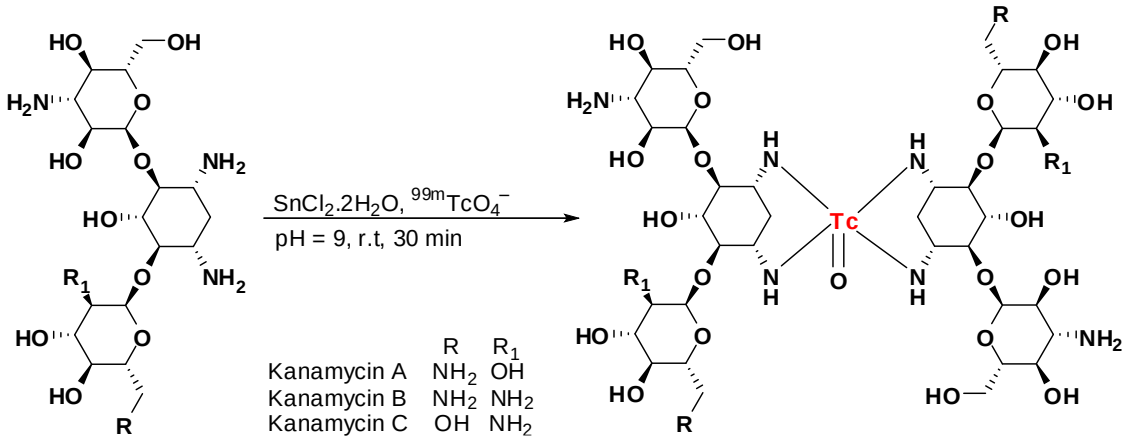

Scheme 9. Synthesis of ^{99m}Tc-Kanamycin

3.2.1.2. Amino-penicillin 3rd generation

As a member of the amino-penicillin group of drugs, amoxicillin acts against gram-positive and gram negative bacteria by interfering with the cell wall muco-peptide biosynthesis [139]. ^{99m}Tc-amoxicillin has demonstrated to be taken up by *E. coli* infected and inflamed thigh muscles in an animal model [140]. Amoxicillin was radiolabeled with ^{99m}Tc by Ozdemir *et. al.* in 2015 [140]. They demonstrated the use of both the reducing agent and antioxidant for labeling amoxicillin. Amoxicillin was mixed with stannous chloride under an atmosphere of nitrogen and radiolabeling was initiated by adding freshly eluted ^{99m}Tc. The improvement of labeling efficiency and stability of the complex was judged by addition of the antioxidant (ascorbic acid) to the solution. (Scheme 10) [140].

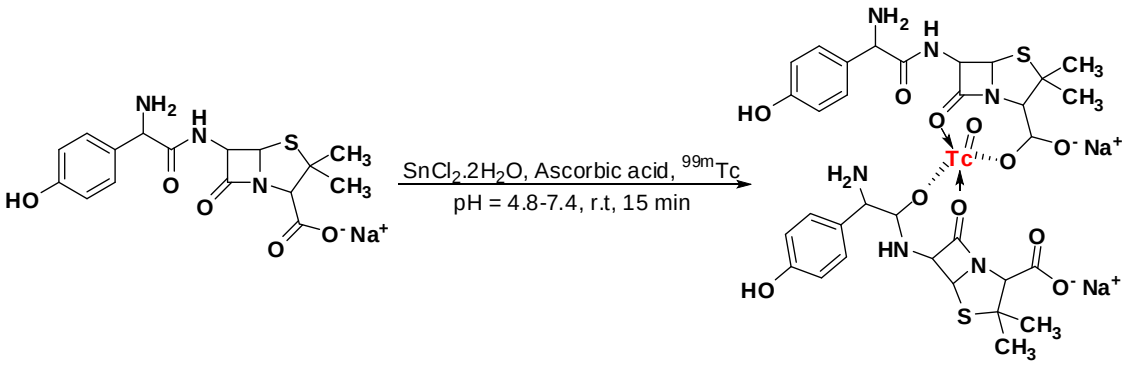

Scheme 10. Synthesis of ^{99m}Tc- amoxicillin

3.2.1.3. Cephalosporins

The β-lactam group of antibiotics compromises the bacterial cell wall integrity by hampering the peptidoglycan layer synthesis [5]. A few of the cephalosporins that have been radiolabeled so far are cefuroxine, ceftizoxine, ceftriaxone, cefotaxime, cefoperazone and cefepime. These antibiotics complexed with ^{99m}Tc showed potential advantages in distinguishing infection (*S. aureus* and/or *E. coli*) from aseptic inflammation foci in various animal models [141-146].

Cephalosporins such as cefuroxine axetil, ceftriaxone and cefepime were radiolabelled in the presence of the reducing agent stannous chloride. The compound was dissolved in sterile water, mixed with a solution of $SnCl_2(2.H_2O)$ and the pH was adjusted. Finally $Na^{99m}TcO_4$ was added to the solution and incubated at room temperature [141-143]. However in the case of ceftriaxone, the mixture was refluxed before incubation at room temperature (Scheme 11) [142].

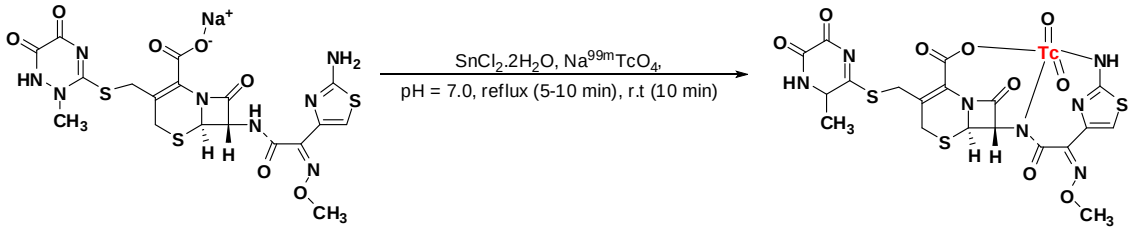

Scheme 11. Synthesis of 99mTc-ceftriaxone

For radiolabeling ceftizoxima and cefotaxime, the compounds were dissolved in water and sodium dithionate (dissolved in 0.5% $NaHCO_3$) was added followed by ^{99m}Tc-pertechnetate. The solutions were heated to 100 °C before maintaining it at room temperature [144, 145].

In the case of cefoperazone, the antibiotic was mixed with a tin(II) solution and the pH was adjusted. Finally, freshly eluted ^{99m}Tc-activity was added to the mixture and incubated at room temperature with vigorous shaking until completion of the reaction [146].

3.2.1.4. Glycopeptides

Teicoplanin and vancomycin fall under the glycopeptide group of antibiotics with their mode of action by interfering with the peptidoglycan layer synthesis [147]. Radiolabeled ^{99m}Tc-teicoplanin was shown to accumulate in high concentration (in 2 h) at the site of *S. aureus* in infected mice [148]. In another study, ^{99m}Tc-vancomycin also showed similar affinity towards *S. aureus* infection foci [149]. Glycopeptides, vancomycin and teicoplanin, were radiolabeled in the presence of $SnCl_2.H_2O$. Briefly, the glycopeptide was mixed with $SnCl_2.H_2O$ and the pH was adjusted. The solution was incubated at room temperature after addition of a freshly prepared solution of $^{99m}TcO_4^-$ [148, 149].

3.2.1.5. Lincosamide

Lincosamide binds to the 50S subunit of bacterial ribosomes and blocks the exit of the newly formed peptide [150]. The lincosamide group of antibiotics, namely clindamycin and lincomycin, were radiolabeled in the similar way as described above. ^{99m}Tc-lincomycin was studied in a rabbit model, which showed significant accumulation of this labeled antibiotic in *S. aureus* infected thigh [151]. In another study ^{99m}Tc-clindamycin showed its potential to distinguish infection from sterile inflammation in both rat as well as in rabbit models [152].

Antibiotics were mixed with $SnCl_2.2H_2O$ and the pH was adjusted. Ascorbic acid was added to the reaction mixture as a stabilizer followed by freshly eluted $^{99m}TcO_4^-$ [151, 152].

3.2.1.6. Macrolides

Macrolides, though structurally different from lincosamide antibiotics share the same mechanism of action by also binding to the 50S subunit of the bacterial ribosome [150]. Erythromycin, clarithromycin and azithromycin, as the group-representing compounds, were successfully radiolabeled with ^{99m}Tc. These probes were subsequently studied in a mouse model to evaluate their potential as radiopharmaceutics. In these studies, radiolabeled ^{99m}Tc-clarithromycin and ^{99m}Tc-azithromycin significantly accumulated in the *S. aureus* infected thigh compared to the uninfected contralateral thigh. Solutions of the macrolide class of antibiotics (erythromycin, clarithromycin and azithromycin) were mixed with $SnCl_2.2H_2O$ and pH was adjusted with HCl. $^{99m}TcO_4^-$ was added to the mixture and the reaction was carried out at room temperature [153-155].

3.2.1.7. Nitrofurans

The mode of action for nitrofurans is by targeting and damaging the *deoxyribonucleic acid* (DNA) of the pathogen in its reduced form. Nitrofuran is reduced by the flavoproteins of the pathogen into reactive intermediates which in turn affects the pyruvate metabolism, respiration and ribosomal DNA [156]. Nitrofurantoin was successfully radiolabeled with ^{99m}Tc for potential imaging of *E. coli*. It was labeled with sodium pertechnetate in the presence of stannous chloride (Scheme 12) [157].

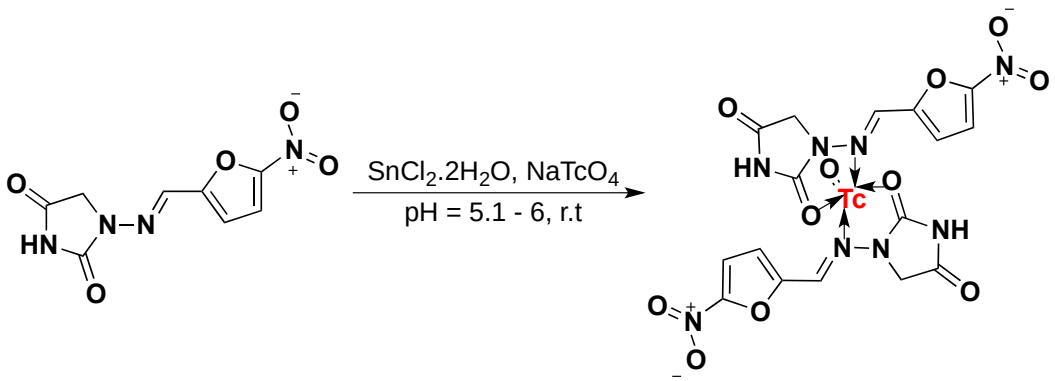

Scheme 12. Synthesis of ^{99m}Tc-Nitrofurantoin

3.2.1.8. Oxazolidinones

Linezolid is an oxazolidinone-type antibiotic that inhibits the bacterial protein synthesis initiation and shows activity against gram-positive microorganisms [158]. Iodine-131-(^{131}I)-linezolid was proven to be used for imaging *S. aureus* in a rat model. In the bacterial infected foci, the accumulation of this labeled antibiotic was five times more compared to the sterile inflammation

sites in 30 min. In order to radiolabel linezolid with ^{131}I, to an iodogen coated vial, a linezolid solution was added followed by $Na^{131}I$ and incubation at room temperature. Finally, Na_2SO_3 was added to the mixture to complete the reaction (Scheme 13) [159].

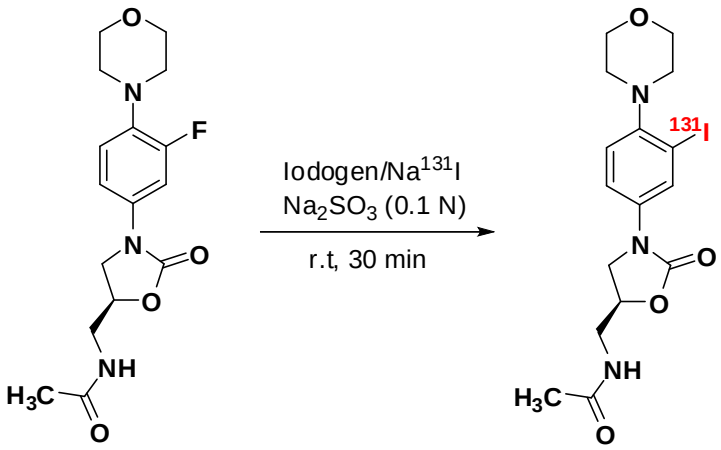

Scheme 13. Synthesis of ^{131}I-Linezolid

3.2.1.9. Fluoroquinolones

Fluoro-quinolones prevent the DNA synthesis of bacteria by interacting with the DNA gyrase which eventually restricts uncoiling of DNA [5]. A large number of compounds in this group of antibiotics were radiolabeled with ^{99m}Tc, ^{18}F and ^{68}Ga for radiopharmaceutical studies. As recently reviewed, PET or SPECT imaging using radiolabeled quinolones distinguished between infection and inflammation in various infected animal models as well as in human subjects. Radiolabeling procedures with ^{99m}Tc were used to study the potential of fluoroquinolones as imaging probes and included ciprofloxacin, enrofloxacin, difloxacin, perfloxacin, lomefloxacin, ofloxacin, rufloxacin (Scheme 14), norfloxacin, danoflaoxacin, sparfloxacin, levofloxacin, moxifloxacin (Scheme 15), gemifloxacin (Scheme 16), garenoxacin (Scheme 17), clinafloxacin (Scheme 18), gatifloxacin and trovafloxacin [131, 143, 157, 160-172]. Radiolabeling for these antibiotics was carried out with $SnCl_2(2.H_2O)$ and $^{99}TcO_4^-$ with the exception for enrofloxacin where stanous tartrate was used. However, in case of levofloxacin and gemifloxacin (Scheme 16) sodium pertechnetate was used in place of $^{99}TcO_4^-$. The antibiotics ciprofloxacin, fleroxacin and trovafloxacin were also radiolabeled with ^{18}F. For the synthesis of ^{18}F-fleroxacin; 6,7,8-trifluoro-1,4-dihydro-1-(2-hydroxyethyl)-4-oxo-3-quinolinecarboxylic acid ethyl ester was produced by alkylating 6,7,8- trifluoro-4-hydroxyquinoline-3-carboxylic acid ethyl ester by 2-bromoethanol. This was followed by condensation with 1-methyl-piperazine which yielded 6,8-difluoro-1,4-dihydro-1-(2-hydroxyethyl)-7-(4-methyl-1-piperazinyl)-4-oxo-3-quinolinecarboxylic acid ethyl ester. The reaction was followed by the addition of methanesulfonyl chloride which resulted in the mesylate precursor of fleroxacin. The anionic

form of ^{18}F, in the presence of Kryptofix, substituted the mesylate followed by basic hydrolysis resulting in the synthesis of ^{18}F-fleroxacin [173]. In the case of trodoxacin labeling; ^{18}F was dried in the presence of K_2CO_3 and Kryptofix. To this mixture trodoxacin in DMSO was added and heated to yield the radiolabeled product [172].

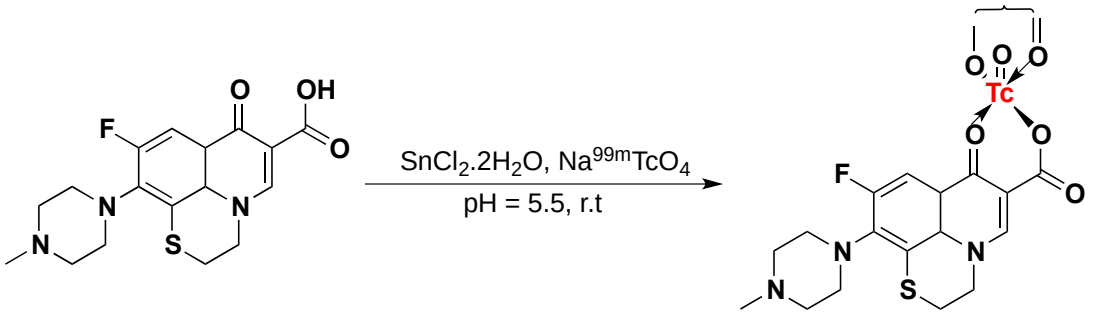

Scheme 14. Synthesis of ^{99m}Tc-Rufloxacin

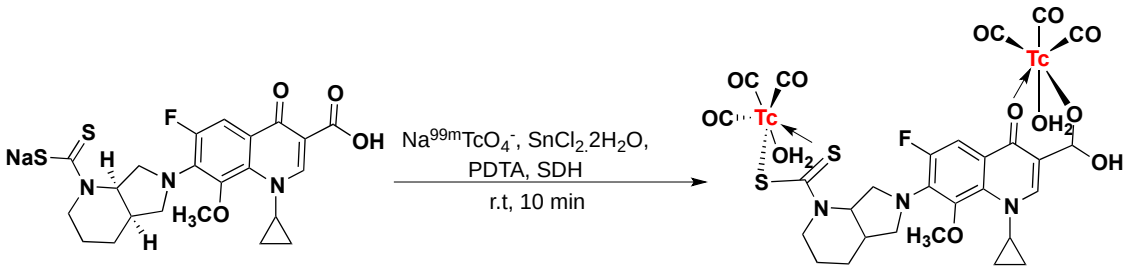

Scheme 15. Synthesis of ^{99m}Tc-Moxifloxacin

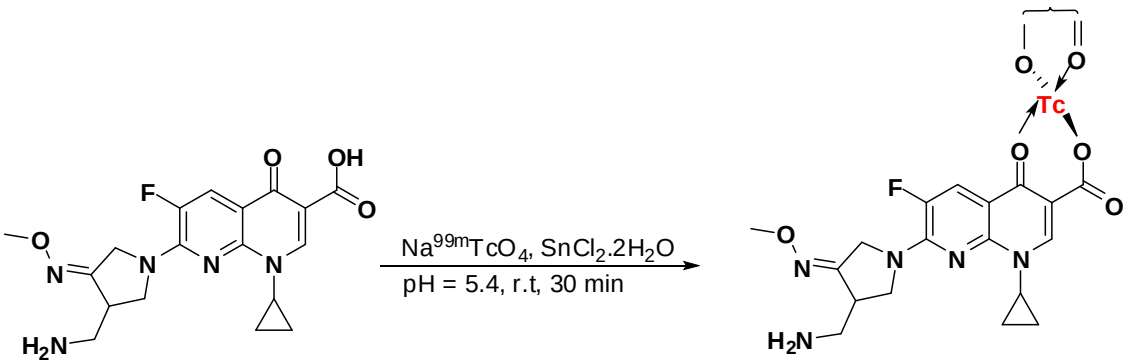

Scheme 16. Synthesis of 99mTc-Gemifloxacin

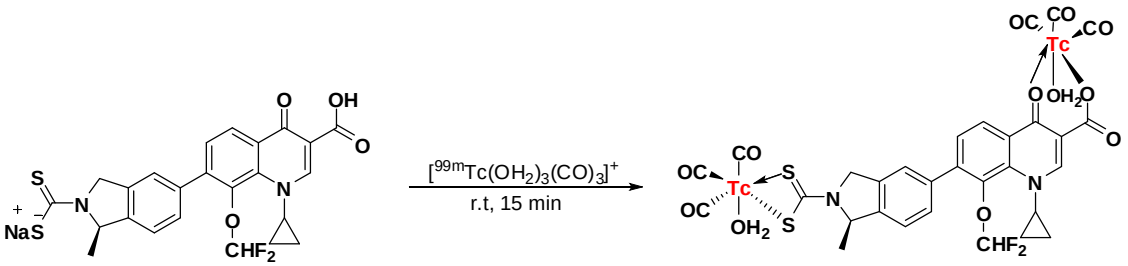

Scheme 17. Synthesis of ^{99m}Tc(CO)$_3$-Garenoxacin dithocarbamate

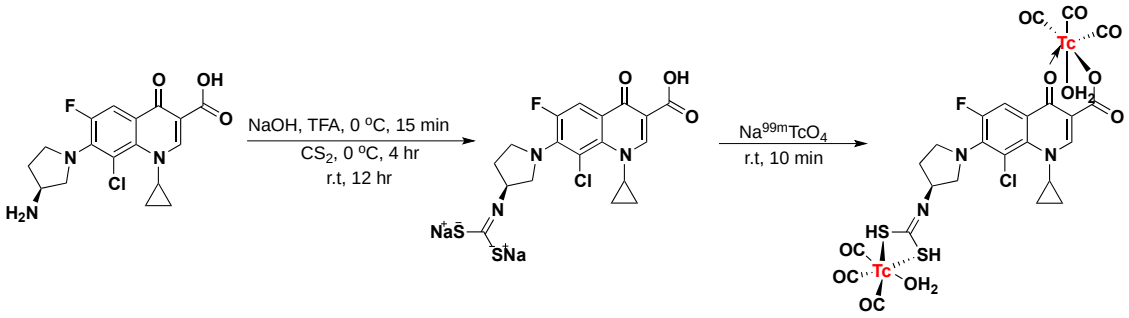

Scheme 18. Synthesis of $^{99m}Tc(CO)_3$-Clinafloxacin

Ciprofloxacin was also successfully radiolabeled with ^{68}Ga. Ciprofloxacin propyl amine was reacted with *p*-SCN-Bz-DOTA or *p*-SCN-Bz-NOTA to produce the DOTA- and NOTA-conjugates of ciprofloxacin, respectively. Radiolabeling was conducted by incubating ^{68}Ga with DOTA- or NOTA-ciprofloxacin at 70 °C or room temperature, respectively (Scheme 19) [174].

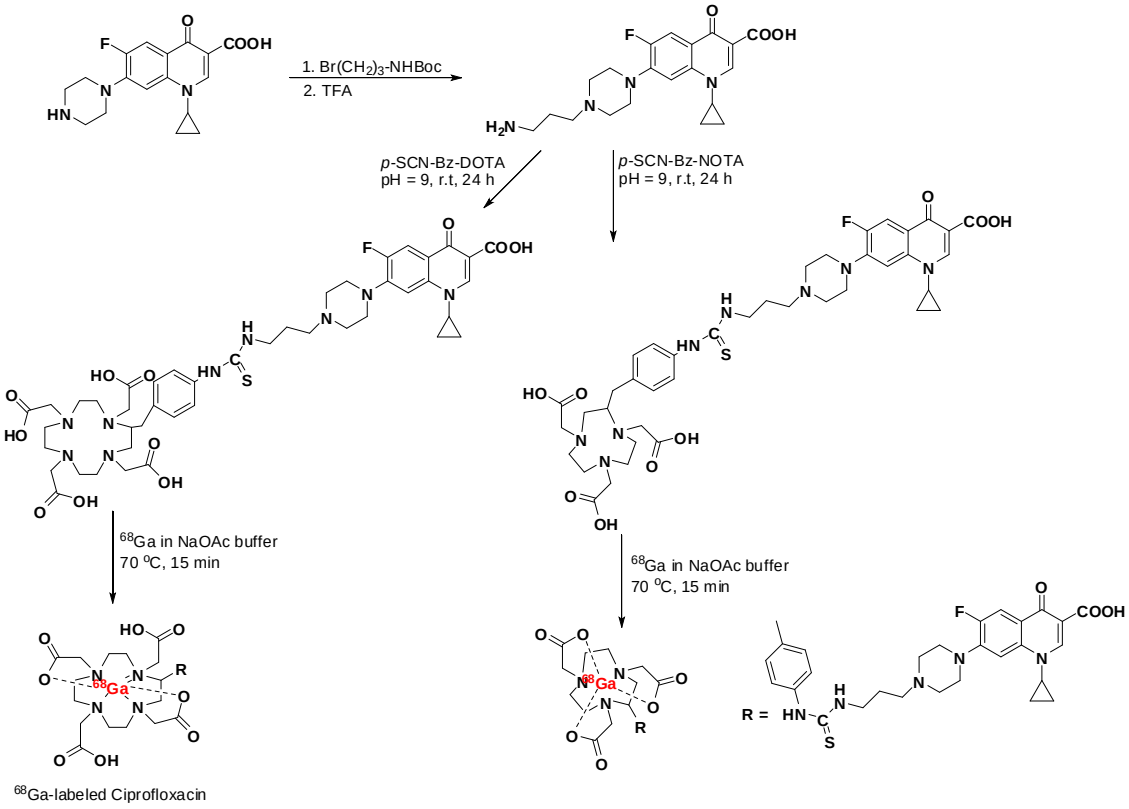

Scheme 19. Synthesis of ^{68}Ga-DOTA-Ciprofloxacin and ^{68}Ga-NOTA-Ciprofloxacin

3.2.1.10. Anti-mycobacteria

Rifampicin (Scheme 20) and ethambutol (Scheme 21) were radiolabeled with $^{99m}TcO_4^-$ in the presence of $SnCl_2(2.H_2O)$ or stannous tartrate, respectively [175, 176]; however, ^{99m}Tc–isoniazid was synthesized by utilizing co-ligands tricine and ethylenediamine-*N*,*N'*-diacetic acid (EDDA) with stannous chloride (Scheme 22) [177]. In addition,

carbon-11 (^{11}C)-radiolabeling procedures are reported for rifampicin and pyrazinamide. The rifampicin piperazine moiety was radiolabelled with $^{11}CCH_3I$ in the presence of potassium carbonate as the base in a mixture of DMSO and ACN as solvents (Scheme 23) [178]. The synthesis of ^{11}C-isoniazid and ^{11}C-pyrazinamide were initiated by reacting iodopyridine and 2-iodopyrazine with ^{11}C-HCN respectively in the presence of the catalyst tetrakis(triphenylphosphine)palladium (0). In case of isoniazid, cyanide was hydrolyzed by hydrazine and the subsequent imine was hydrolyzed by water (Scheme 24). However, in case of pyrazinamide, the cyano-group of the product ^{11}C-cyanopyrazine was hydrolyzed by hydrogen peroxide under basic conditions to yield [^{11}C]-pyrazinamide (Scheme 25) [178].

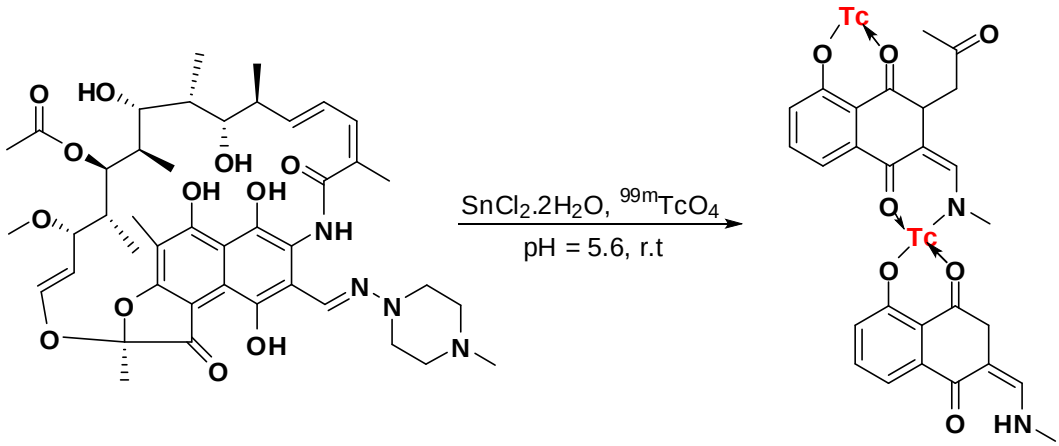

Scheme 20. Synthesis of ^{99m}Tc- rifampicin

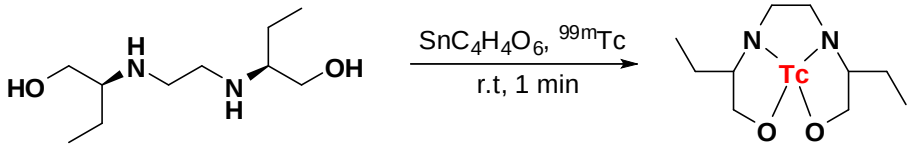

Scheme 21. Synthesis of ^{99m}Tc-ethambutol

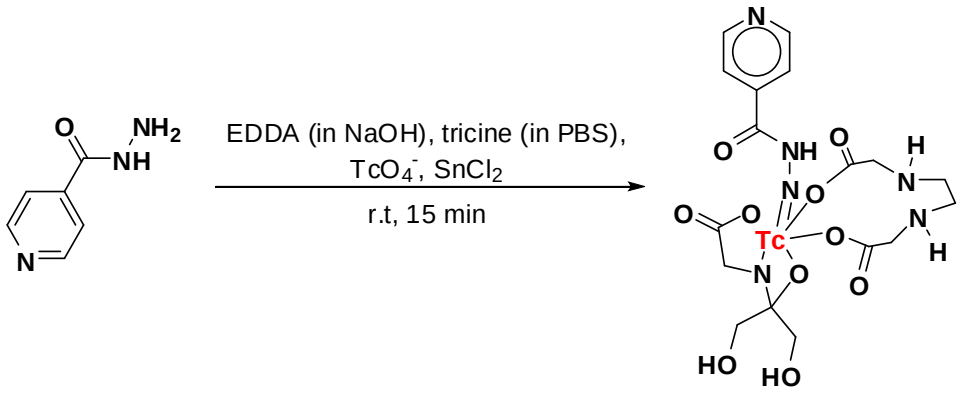

Scheme 22. Synthesis of ^{99m}Tc-isoniazid

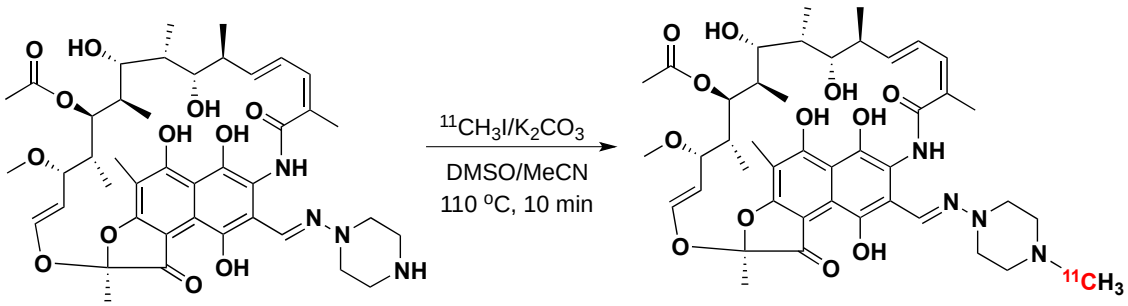

Scheme 23. Synthesis of ^{11}C-rifampicin

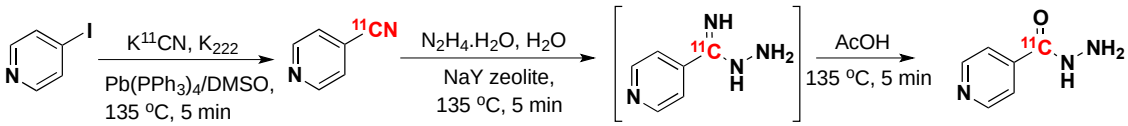

Scheme 24. Synthesis of ^{11}C-Isoniazid

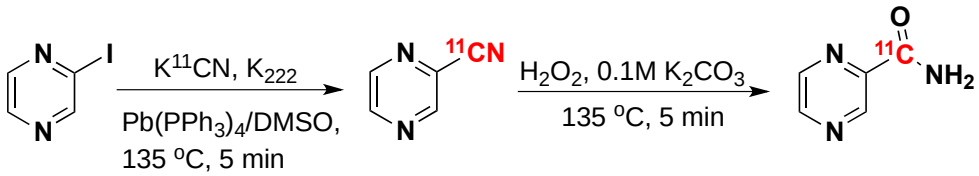

Scheme 25. Synthesis of ^{11}C-pyrazinamide

3.2.1.11. Tetracyclines

The mode of action with tetracycline antibiotics prevents the binding of the aminoacyl-tRNA to the ribosomal acceptor (A) site thereby inhibiting the protein synthesis [179]. One of the radiolabeled antibiotics from this group, ^{99m}Tc-doxycycline was explored in an *E. coli*-infected rat model. The study revealed a rapid accumulation of this radiotracer in the infected site and could easily be distinguished from the soft tissue. Doxycycline was radiolabeled with ^{99m}Tc in the presence of stannous tartrate and ascorbic acid carried out at room temperature [180].

Table 3 Antibiotics-based probes for infection imaging

Antibiotics class	Antibiotic name	Radioisotope	Targeted microorganism(s) [a)]	T/NT [b)] ratio	Labelling efficiency	Detection	Reference
Aminoglycoside	Kanamycin	^{99m}Tc	Some Gram-negative bacteria, *Staphylococci and M. tuberculosis*	2.5	95.0%	--	[136]
	Tobramycin	^{99m}Tc		-	--	Gamma camera	[138]
	Gentamicin	^{99m}Tc		-	96.9%	Gamma counter	[137]
	Streptomycin	^{99m}Tc		2.4	98.0%	SPECT	[135]
Amino-penicillin	Amoxicillin	^{99m}Tc	Susceptible Gram-positive and Gram-negative bacteria	4.2	>90%	Dual head gamma camera	[140]
Anti-mycobacteria	Isoniazid	^{99m}Tc and ^{18}F	Mainly *M. tuberculosis* and a few Gram-positive bacteria	1.3	--	PET/CT	[181]
	Ethambutol	^{99m}Tc		-	>85.0%	SPECT	[175]
	Rifampicin	^{99m}Tc and ^{11}C		7.3		Gamma camera, PET	[178]
	Pyrazinamide	^{11}C		-	99.0%	PET	[178]
Cephalosporins	Cefuroxine	^{99m}Tc	Susceptible Gram-positive and -negative bacteria	2.5	98.0%	Cd(Te) detector	[141]
	Ceftizoxine	^{99m}Tc	Susceptible enteric Gram-positive and -negative bacteria incl. *H. influenza*	3.2	94.9%	Gamma camera	[144, 182]
	Ceftriaxone	^{99m}Tc		5.6	96.0%	Gamma camera	[142, 183]
	Cefotaxime	^{99m}Tc		3.0	92.0%	Planar scintigraphy	[145]
	Cefoperazone	^{99m}Tc		4.5	97.9%	γ-scintillation counter	[146]
	Cefepime	^{99m}Tc	Extended spectrum of Gram-positive and -negative bacteria	8.4	98 ± 1.4 %	--	[143]
(Fluoro)-Quinolones	Ciprofloxacin	^{68}Ga, ^{18}F and ^{99m}Tc	Susceptible Gram-positive and -negative bacteria and fungi	1.8-5.5	85.0-90.0% / 81±4%	PET, Scintigraphy	[131, 160, 174, 184, 185]
	Difloxacin	^{99m}Tc		5.5	95.6 %	NaI(Tl) detector	[162]
	Perfloxacin	^{99m}Tc		4.9	98.1%	NaI(Tl) detector	[162]
	Lomefloxacin	^{99m}Tc		6.5	93.6%	γ-scintillation counter	[163]
	Ofloxacin	^{99m}Tc		4.3	96.6%	γ-scintillation counter	[163]

	Rufloxacin	^{99m}Tc		6.0	98.10 ± 0.18%	Well counter interface with scalar count rate meter (WCSCR)	[164]
	Norfloxacin	^{99m}Tc		6.9	95.4%	Scintigraphy	[165, 186]
	Danoflaoxacin	^{99m}Tc		7.2	90 ± 2%	Well-type c-scintillation detector	[166]
	Sparfloxacin	^{99m}Tc	Many Gram-positive and Gram-negative bacteria	5.9	>95%	Gamma camera	[167]
	Levofloxacin	^{99m}Tc		7.2	99.74%	Scintigraphy	[168]
	Fleroxacin	^{18}F		1.3	5-8%	PET	[173]
	Moxifloxacin	^{99m}Tc	Susceptible Gram-positive and Gram-negative bacteria incl. Methicillin-resistant *S. aureus* (MRSA) and Penicillin-resistant Streptococci stains (PRSC)	6.8	--	WCSCR	[169]
	Gemifloxacin	^{99m}Tc		4.9	--	Single well counter interface with scalar count rate meter	[187]
	Clinafloxacin	^{99m}Tc		5.0	--	Single well counter fitted with a scalar count rate meter	[170]
	Garenoxacin	^{99m}Tc		5.4	98.25 ± 0.22%	WCSCR	[171]
	Gatifloxacin	^{99m}Tc		4.5	90 ± 1.8%	--	[143]
	Trovafloxacin	^{18}F and ^{99m}Tc		6.0	15-30%	PET	[172]
Glycopeptide	Vancomycin	^{99m}Tc	Susceptible Gram-positive bacteria incl. Methicillin-resistant *S. aureus* (MRSA) and *E. faecalis*	5.0	> 95%	Gamma counter	[8]
	Teicoplanin	^{99m}Tc		4.3	87.7 ± 1.3%	Scintigraphy	[148, 188]
Lincosamide	Clindamycin	^{99m}Tc	Susceptible Gram-positive and Gram-negative bacteria	3.1	> 95%	Scintigraphy 85	[152]
	Lincomycin	^{99m}Tc		3.0	> 98%	Scintigraphy 86	[151]
Macrolides	Azithromycin	^{99m}Tc	Gram-positive-, some Gram-negative- and atypical bacteria.	6.2	97.5 ± 0.9%	--	[153]
	Erytmocytin	^{99m}Tc		2.4	>98%	Scintigraphy	[155]
	Clarithromycin	^{99m}Tc		7.3	98 ± 0.2%	well-type NaI scintillation γ-ray counter	[154]

Nitrofurans (DNA inhibitors)	Nitrofuratoin	^{99m}Tc	Susceptible Gram-positive and Gram-negative bacteria	7.3	97.50 ± 0.16%	Scintigraphy	[157]
Oxaolidinones	Linezolid	^{131}I	Susceptible Gram-positive and Gram-negative bacteria	77.48	85 ± 1%	Cd(Te) detector	[159]
Tetracyclines	Doxycycline	^{99m}Tc	All medically relevant aerobic and anaerobic bacteria (Gram-positive, Gram-negative and atypical)	2.24 ± 0.84	--	Scintigraphy	[180]

a) Bacteria targeted based on the antibiotics class preferences (not the radiolabeled equivalent), some candidates may divert slightly in their sensitivity or specificity towards single types of bacteria.

b) T /NT: target to non-target

3.2.2. Vitamins

3.2.2.1. Biotin (Vitamin H)

Biotin is an essential growth factor for some bacteria and is required for the metabolism of amino acids and fats. It also is involved in the production of fatty acids [189]. ^{111}In-labeled biotin demonstrated avid uptake in cultures of *S. aureus* [190]. Radiolabeled biotin also showed selectivity and specificity towards spinal infections in patients [191]. Biotin radiolabeling has been reported using the bifunctional chelator molecule diethylenetriaminepentaacetic acid (DTPA). Commercially available DTPA-Biotin was incubated with ^{111}In-chloride at room temperature for optimal radiolabeling [190, 191]. DOTA-functionalized biotin was also successfully labeled with ^{68}Ga (buffered with HEPES). ^{68}Ga-complexations were conducted at both at room and elevated (90 °C) temperatures (Scheme 26) [192].

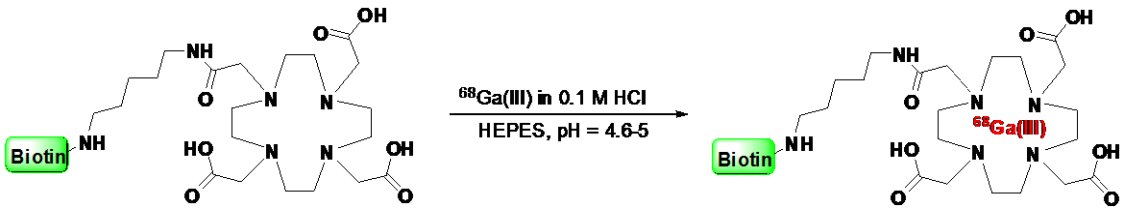

Scheme 26. Radiosynthesis of ^{68}Ga-DOTA-Biotin

3.2.2.2. Cyano-cobalamin (CBL)

Cyano-cobalamins are transported by cobalamin transport proteins. These proteins have antagonistic effects against bacterial growth and colonization; and are found in salivary glands and secondary granules of granulocytes [193]. Baldoni *et. al.* reported on the rapid *in vitro* specificity of the CBL derivative ^{99m}Tc-PAMA(4)-CBL towards *S. aureus* and *E. coli* [194]. Waibel *et. al.* demonstrated the synthesis and radiolabeling of ^{99m}Tc-PAMA-CBL [195]; Cbl-b-acid (obtained by the controlled acid hydrolysis of cyano-cobalamin in 0.1 mol/L HCl) was coupled with Boc-deprotected PAMA using coupling reagents, either 1-(3-dimethylaminopropyl)-3-ethylcarbodimide hydrochloride or 2-(1H-benzotriazole-1-y1)-1,1,3,3-tetramethyluronium tetrafluoro-borate, to synthesize Cbl-b-(ethyl-hexyl)-PAMA-OEt. To achieve optimal radiolabeling, $[^{99m}Tc(CO)_3(OH_2)_3]^+$ was prepared using the isolink kit by heating $[Na][^{99m}TcO_4]$. Cbl-b-(ethyl-hexyl)-PAMA-OEt was then incubated with $[^{99m}Tc(CO)_3(OH_2)_3]^+$ in 2-(*N*-morpholino)ethanesulfonic acid (MES) buffer at 75 °C under a nitrogen environment [194, 195].

3.2.3. Aptamers (Oligomers)

Aptamers are a rather novel class of compounds with potential as radiopharmaceutics because of their high target affinity and specificity; moreover, these probes can be custom designed towards

a specific target [196] such as cell surface pathogen-specific proteins or bacteria-specific receptors [197]. *S. aureus* specific aptamers SA20, SA23 and SA34 were successfully labeled with ^{99m}Tc, which showed high uptake in the infected site (*S. aureus*) compared to the muscle infected with *C. albicans* and zymosan developed inflammation [198]. The radiolabeling was carried out by adding tricine, EDDA into 0.9% saline and the aptamers followed by the addition of $SnCl_2.2H_2O$. After adjusting the pH to 7, the reaction vessel was sealed and a vacuum was created. $^{99m}TcO_4^-$ was added and the mixture refluxed to facilitate the radiolabeling (Scheme 27) [198].

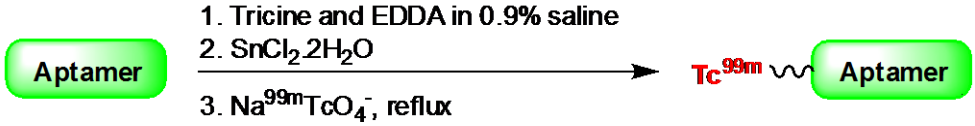

Scheme 27. Principle of direct ^{99m}Tc-radiolabeling of aptamers

Chen *et. al.* demonstrated the specificity of the radiolabeled oligomers towards the RNA of *S. aureus, K. pneumoniae* and *E. coli* [199]. The oligomers that were investigated included phosphorodiamidate morpholino (MORF), peptide nucleic acids (PNA), and phosphorothioate DNA (PS-DNA) that were conjugated with NHS-MAG_3 [200]. The MAG_3-conjugated oligomers were mixed with a solution of ammonium acetate, tartrate and freshly prepared $SnCl_2.2H_2O$ (in HCl/ ascorbate) and vortexed. Finally, $^{99m}TcO_4^-$ was added and the mixture was heated at 95 °C (Scheme 28) [199]. In another example, the same group demonstrated that the 12-mer phosphorodiamidate morpholino (MORF) oligomer, that was complementary to bacterial ribosomal RNA, was specific in its identification of *K. pneumoniae* in infected mouse muscles [201]. Radiolabeling was carried out in the similar manner as described above.

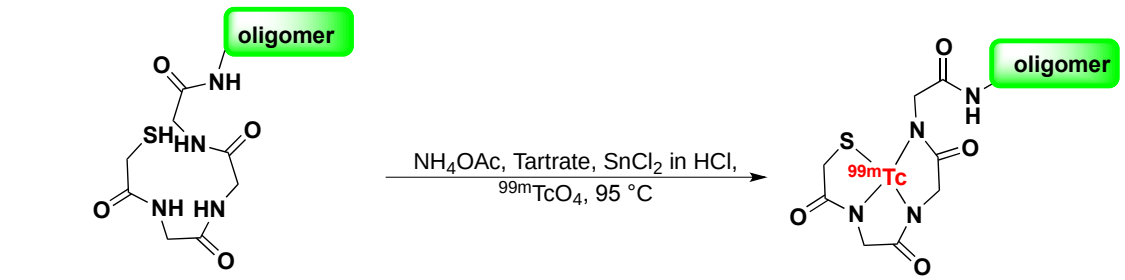

Oligomers = MORF or PNA or DNA

Scheme 28. Synthesis of ^{99m}Tc-NHS-MAG_3-(MORF/PNA/PS-DNA)

3.2.4. Puromycin

Puromycin is a protein synthesis inhibitor that affects the derivatization of immature polypeptide chains as polypeptidyl-puromycin [202]. Eigner *et. al.* emphasised the potential of ^{68}Ga-DOTA-Puromycin for imaging bacterial infections based on the fact that it can detect the protein

synthesis of the microbial colonies [203]. The study revealed that there is no accumulation of the radiotracer in sites of sterile inflammation; however, high contrast μPET/CT images were obtained in the subcutaneous colonies of *S. aureus* infected foci [203]. The investigators used commercially available DOTA-Pur for radiolabelling with ^{68}Ga. Briefly, DOTA-Puromycin was added to a solution of freshly eluted ^{68}Ga (in HCl) after pH adjustment and the reaction mixture was incubated at 95 °C until completion followed by purification through a Strata-X column [203].

3.2.5. Radiolabeled purines and pyrimidines

Herpes simplex virus 1 (HSV1) thymidine kinase (TK) is an important enzyme for the transfer of a phosphate group to the 5′ hydroxyl group of pyrimidines from ATP. HSV1-TK reporter gene system can be of importance as its substrate can be radiolabeled for tracing. These radiotracers are subsequently phosphorylated and cellularly trapped upon introduction of the charge of the phosphate group [204]. This mechanism was successfully implemented in transformed tumor cells imaging and based on this fact it was approached for imaging TKs of bacteria in mammals [205]. Bettegowda *et. al.* demonstrated the selectivity of iodine-125 (^{125}I)-radiolabeled 1-(2′-deoxy-2′-fluoro-5-iodo-1-β-D-arabinofuranosyl) -5-iodouracil (FIAU) towards TK of a wild-type *E. coli* strain [205]. Subsequent studies on ^{125}I-FIAU revealed its application for imaging musculoskeletal infections in patients [206]. For radiolabeling, 1-(2′-deoxy-2′-fluoro- β -D-arabinofuranoside)-uracil (FAU) was dissolved in HNO_3 and to this solution ^{125}I-NaI was added. The reaction was heated at 130 °C and finally quenched with a mixture of ACN/H_2O/triethylamine (Scheme 29).

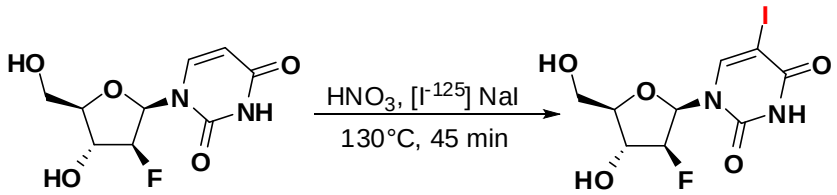

Scheme 29. Synthesis of ^{125}I-FIAU

3.2.6. Glycopyranose derivatives

Bacteria can utilize unique sugars such as maltose, sorbitol and trehalose as energy sources. However, mammalian cells are deficient in the transporters for these molecules which may bear great potential as probes for bacterial imaging [207]. The maltose derivatives 6-^{18}F-fluoromaltose and ^{18}F-maltohexanose (^{18}F-MH) have been synthesized and reported to be bacterial specific [208-210]. 6-^{18}F-fluoromaltose was reported to be taken up by both gram positive as well as gram negative bacteria; however, insignificant amounts were detected in tumor cells [209]. Likewise, ^{18}F-MH was also found to be selective and specific towards *E. coli*

showing minimal affinity towards mammalian cells [210]. For the synthesis of 6-^{18}F-fluoromaltose; ^{18}F-fluoride was eluted with a solution of K_2CO_3 and Kryptofix in water and acetonitrile. An anhydrous residue was obtained after evaporation of the solvent, which was then added to a 1,2,3-tri-O-acetyl-4-O-(2′,3′,-di-O-acetyl-4′,6′-benzylidene-α-D-glucopyranosyl)-6-deoxy-6-O-nosyl-D-glucopranosidic solution in ACN followed by heating at 80 °C. This intermediate compound was purified using a C-18 Sep-Pak cartridge. The purified product was then first hydrolyzed by HCl at 110 °C followed by addition of NaOH at room temperature to yield the 6-^{18}F-fluoromaltose (Scheme 30) [208].

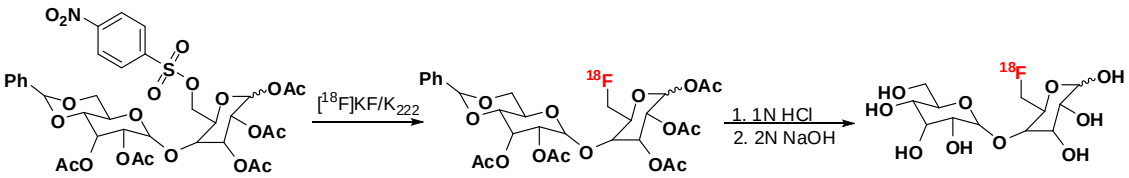

Scheme 30. Synthesis of 6-^{18}F-fluoromaltose

Radiochemical synthesis of ^{18}F-MH was obtained by cryptate-mediated nucleophilic substitution of maltohexose-brosylate precursor with K^{18}F (in ACN, at 110 °C). The compound synthesized was then hydrolyzed with NaOH (in water, at 110 °C) followed by acid neutralization at room temperature (Scheme 31) [210].

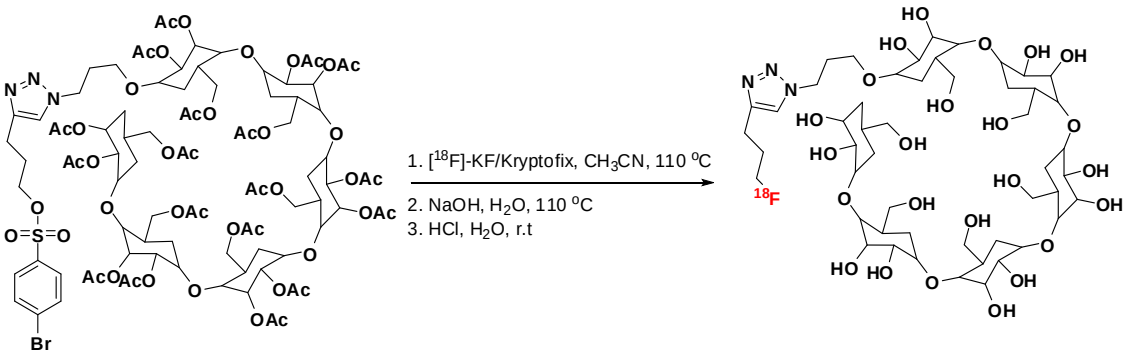

Scheme 31. Synthesis of ^{18}F-maltohexanose

Sorbitol is considered as a probe towards the identification of enterobacteriaceae because this class can selectively metabolize glycopyranose using the glycerol diffusion facilitator (glpF). The radiolabeled sorbitol derivative ^{18}F-fluorodesoxysorbitol (^{18}F-FDS) is reported to be target specific and also capable of identifying drug resistance [211-213]. ^{18}F-FDS can be synthesized by reduction of commercially available ^{18}F-FDG by $NaBH_4$ in water at 35 °C (Scheme 32) [211].

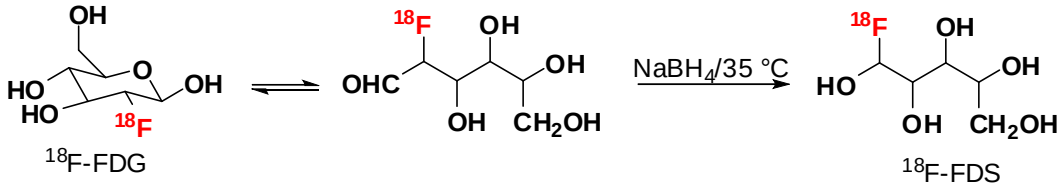

Scheme 32. Synthesis of ^{18}F-fluorodesoxysorbitol

The non-mammalian disaccharide trehalose is utilized by bacteria for stress protection, carbohydrate storage and even an energy source. It is also a constituent of the cell wall of some mycobacteria [214]. A trehalose derivative, 2-fluorotrehalose (2-FDT)-PET/CT, was successfully applied for the detection of tubercular lesions in a rabbit infection model bearing *Mycobacterium tuberculosis* HN878 [215]. The 2-fluorotrehalose (2-FDT) synthesis is a biomimetic process, inspired by the bacterial synthesis of trehalose from glucose. Chemo-enzymatic synthesis of 2-FDT occurs as a one-pot cascade reaction in which hexokinase transfers a phosphate from adenosine triphosphate (ATP) to ^{18}F-FDG (normally glucose in bacterial trehalose synthesis). OtsA then transfers the glucose from the donor UDP-glucose to the acceptor phosphorylated ^{18}F-FDG. Dephosphorylation gives the desired product that is affected by OtsB. The entire one-pot process is complete in 45 min.

Amino sugars are one of the essential components of the bacterial cell wall. In both gram negative and gram positive bacteria, they form the peptidoglycan backbone. Bacterial cell walls are composed of alternate sequences of *N*-acetylglucosamine and *N*-acetylmuramic acid, joined by oligopeptides. The use of *N*-acetylglucosamine as a radiotracer by incorporating a radioisotope bears potential hope for bacterial imaging. Martínez *et. al.* described the synthesis and application of 2-deoxy-2-(^{18}F)-fluoroacetamido-D-glucopyranose (^{18}F-FAG). They were capable of successfully identifying *E. coli* in infected rat models. The synthesis of ^{18}F-FAG was carried out by using 1,3,4,6-tetra-O-acetyl-2-deoxy-2-bromoacetamido-D-glucopyranose as a precursor with microwave heating. ^{18}F-fluorine eluted in a solution of K_2CO_3/ Kryptofix and was evaporated under microwave conditions (110 °C) in the presence of argon gas. Subsequently, the bromide precursor (in anhydrous ACN) was added to the dried $[K/K_{222}]^{+18}F^-$ complex followed by hydrolysis with sodium hydroxide and finally neutralized by the addition of HCl (Scheme 33) [216].

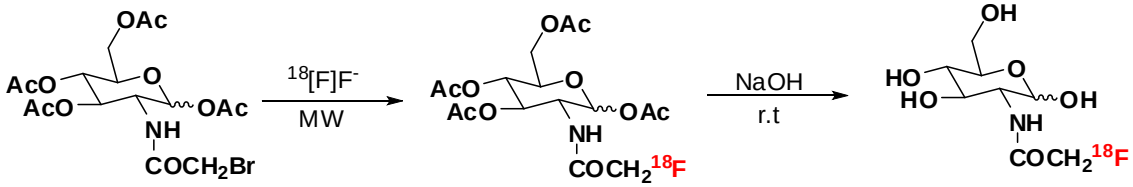

Scheme 33. Synthesis of ^{18}F-FAG

3.2.7. Siderophores

All microorganisms, including bacteria and fungi, require iron as a trace element for their growth [217]. However the presence of O_2 in the environment causes oxidation of ferrous (2^+) to ferric (3^+) iron which is insoluble. Bacteria produce siderophores; which are small peptide-like metabolites with the ability to chelate iron thereby making it available to the organism [218]. Moreover, a few siderophores also mediate the uptake of gallium [219, 220]. Recent investigations described the ^{68}Ga radiolabeling potential of siderophores namely triacetylfusarinine C (TAFC) and ferrioxamine E (FOXE). Radiolabeled ^{68}Ga-TAFC and ^{68}Ga-FOXE showed rapid accumulation as well as specificity towards *A. fumigatus* in infected lung tissues. However, it also showed moderate accumulation in sterile inflamed tissue and no affinity towards *S. aureus* infected muscle [66, 221, 222]. For radiolabeling TAFC (Scheme 34) and FOXE (Scheme 35), they are incubated with ^{68}Ga in acetate buffer at room temperature and at 80 °C respectively [221].

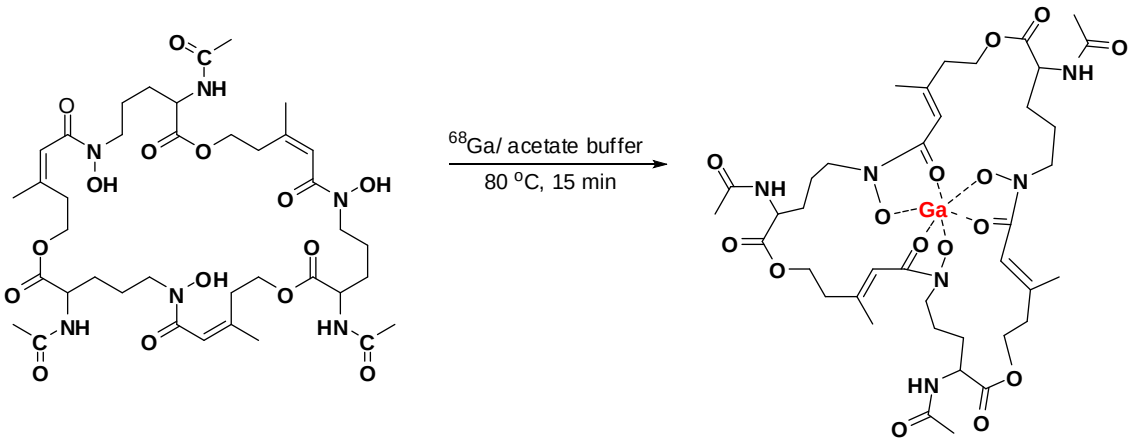

Scheme 34. Synthesis of ^{68}Ga-TAFC

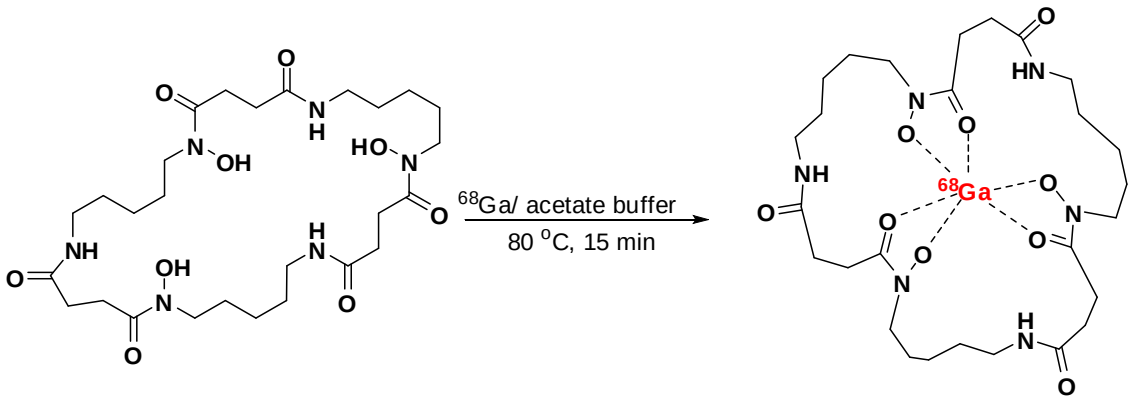

Scheme 35. Synthesis of ^{68}Ga-FOXE

Table 4 Novel biomimetic radiotracers for infection imaging

Compound class	Compound name	Radio-isotope	Targeted microorganism(s)	T/NT ratio	Labelling efficiency	Method	Reference
Vitamins	Biotin	^{111}In , ^{68}Ga	*S. aureus, M.tuberculosis, Aspergillus and Propionibacterium acnes*	--	>98%	SPECT/CT	[191]
	Cyano-cobalamin	^{99m}Tc	*S. aureus and E. coli*	--	95%	SPECT/CT scans	[194]
Aptamers	SA20, SA23 and SA34	^{99m}Tc	*S. aureus, C. albicans*	4.0 ± 0.5	91-93%	Gamma counter	[198]
	MORF, PNA, PS-DNA	^{99m}Tc	*S. aureus, K. pneumoniae* and *E. coli*	--	95%	SPECT/CT	[199]
Ribosomal inhibitors	Puromycin	^{68}Ga	*S. aureus*	--	65 ± 2.6 %	µPET/CT	[203]
Purins and Pyrimidins	FIAU	^{125}I	*S. aureus, E. faecalis, Proteus mirabilis, Pseudomonas aeruginosa etc*	14	50%	PET/CT	[205, 206]
Bacterial sugars	Maltose	^{18}F	*E. coli*		5-8%	PET	[208]
	Maltohexaose	^{18}F	*E.coli*	--	--	PET	[210]
	Sorbitol	^{18}F	*E. coli, S. aureus, Enterobacteriaceae*	12.4 ± 0.44	81±4%	PET/CT	[211]
	FAG	^{18}F	*E. coli*	--	9.7%±2.8%	PET	[216]
Siderophores	TAFC	^{68}Ga	*A. fumigatus*	5.81±6.05	--	PET/CT	[221]
	FOXE	^{68}Ga		6.64±2.91	--	PET/CT	[221]

4. Challenges and limitations in producing efficient infection imaging probes

The production of radiopharmaceuticals is often expensive and requires appropriate shielding or particular laboratory set-up to adhere to current guidelines and rules by incorporating good manufacturing procedures (GMP). A favorable imaging agent for infection imaging should be straightforward and rapid to manufacture, if possible at ambient temperatures. Easy-to-radiolabel kit solutions may allow for inexpensive probe manufacture and generates commercialization opportunities. The probe's clinical performance may be limited by its specific activity to assure a sensitive discovery of any unknown infection sites as only trace amounts of the biomolecule forms part of the radiopharmaceutical dose. In addition, most radiosynthesis suffer from the use of solvents during the radiolabeling approach, however it is desirable to eliminate all solvent agents as they may lead to unfavorable reactions or can manipulate the probe's pharmacokinetics and biodistribution. Regarding its chemical production, the desired imaging agent might be of neutral charge to avoid any unnecessary unspecific binding *in vivo* [223]. Moreover, the production of certain radioisotopes (^{11}C, ^{13}N, or ^{15}O) may be a logistical obstruction due to their exceptionally rapid radioactive decay. This may challenge their broad clinical application, except if being utilized on-site. There is also a significant radiation burden to personnel during production and whilst patient administration.

5. Conclusion

In this review article, we discussed the potential of established and novel probes available for non-invasive infection imaging. Even though substantial efforts were made to study the field of infection imaging tracers, only a handful of them are FDA approved and commercially available. Moreover, these bacterial imaging techniques are not regularly used for bacterial diagnosis in clinical setup. Thus far, and despite their challenging radiosyntheses, SPECT/CT using radiolabeled leukocytes is considered the gold standard procedure for the diagnosis of joint prosthesis, endocarditis, inflammatory bowel diseases and osteomyelitis. Since infectious diseases and bacterial resistance pair up to be an even greater threat to medical health and the world's economy; we foresee novel imaging technologies such as PET/MRI and SPECT/MRI using bacteria-unique probes to be the paradigm shift required to meet the urgent need for an early and better diagnosis of the pathogens!

References

[1] C. Bunchorntavakul, N. Chamroonkul, D. Chavalitdhamrong, Bacterial infections in cirrhosis: A critical review and practical guidance, World J Hepatol, 8 (2016) 307-321.

[2] D.M. Morens, G.K. Folkers, A.S. Fauci, The challenge of emerging and re-emerging infectious diseases, Nature, 430 (2004) 242-249.

[3] M. Cupić, I. Lazarević, A. Knezević, M. Stanojević, Conventional and molecular methods in diagnosis and monitoring of viral infection, Srp. Arh. Celok. Lek., 135 (2006) 589-593.

[4] S.J. Goldsmith, S. Vallabhajosula, Clinically proven radiopharmaceuticals for infection imaging: mechanisms and applications, in: Semin. Nucl. Med., Elsevier, 2009, pp. 2-10.

[5] C. Tsopelas, Radiotracers Used for the Scintigraphic Detection of Infection and Inflammation, Scientific World J., 2015 (2015) 1-33.

[6] A. Signore, S.J. Mather, G. Piaggio, G. Malviya, R.A. Dierckx, Molecular Imaging of Inflammation / Infection: Nuclear Medicine and Optical Imaging Agents and Methods, Chem. Rev., 110 (2010) 3112-3145.

[7] T. Ebenhan, O. Gheysens, H.G. Kruger, J.R. Zeevaart, M.M. Sathekge, Antimicrobial peptides: their role as infection-selective tracers for molecular imaging, Biomed Res Int, 2014 (2014) 867381.

[8] A. Bunschoten, M.M. Welling, M.F. Termaat, M. Sathekge, F.W.B. Van Leeuwen, Development and prospects of dedicated tracers for the molecular imaging of bacterial infections, Bioconjugate Chem., 24 (2013) 1971-1989.

[9] M. Sathekge, The potential role of 68Ga-labeled peptides in PET imaging of infection, Nucl. Med. Commun., 29 (2008) 663-665.

[10] A.A. Ordonez, E.A. Weinstein, L.E. Bambarger, V. Saini, Y.S. Chang, V.P. DeMarco, M.H. Klunk, M.E. Urbanowski, K.L. Moulton, A.M. Murawski, S. Pokkali, A.S. Kalinda, S.K. Jain, A Systematic Approach for Developing Bacteria-Specific Imaging Tracers, J. Nucl. Med., jnumed.116.181792. [Epub ahead of print] (2016).

[11] T.F. Massoud, S.S. Gambhir, Molecular imaging in living subjects: seeing fundamental biological processes in a new light, Genes Dev., 17 (2003) 545-580.

[12] J. Ady, Y. Fong, Imaging for Infection: From Visualization of Inflammation to Visualization of Microbes, Surg Infect (Larchmt), 15 (2014) 700-707.

[13] P.J. Mountford, M.J. Allsopp, A.C. Baird, C.I. North, F.M. Hall, C.P. Wwlls, A.J. Coakley, A study of leucocyte labelling efficiencies obtained with 111In-oxine, Nucl. Med. Commun., 6 (1985) 109-114.

[14] M. Roca, E.F. de Vries, F. Jamar, O. Israel, A. Signore, Guidelines for the labelling of leucocytes with 111In-oxine, Eur. J. Nucl. Med. Mol. Imaging, 37 (2010) 835-841.

[15] P.J. Mountford, A.G. Kettle, M.J. O'Doherty, A.J. Coakley, Comparison of technetium-99m-HM-PAO leukocytes with indium-111-oxine leukocytes for localizing intraabdominal sepsis, J. Nucl. Med., 31 (1990) 311-315.

[16] A. Signore, A.W. Glaudemans, The molecular imaging approach to image infections and inflammation by nuclear medicine techniques, Ann. Nucl. Med., 25 (2011) 681-700.

[17] V.K. Verma, S.S. Beevi, A. Tabassum, K. Kumaresan, R.S. Kamaraju, A.S. Arbab, L.K. Chelluri, In vitro assessment of cytotoxicity and labeling efficiency of 99mTc-HMPAO with stromal vascular fraction of adipose tissue, Nucl. Med. Biol., 41 (2014) 744-748.

[18] C.H. Green, Technetium-99m production issues in the United Kingdom, J Med Phys, 37 (2012) 66-71.

[19] R.D. Neirinckx, J.F. Burke, R.C. Harrison, A.M. Forster, A.R. Andersen, N.A. Lassen, The retention mechanism of technetium-99m-HM-PAO: intracellular reaction with glutathione, J. Cereb. Blood Flow Metab., 8 (1988) S4-S12.

[20] M. Chianelli, S. Mather, J. Martin-Comin, A. Signore, Radiopharmaceuticals for the study of 4 inflammatory processes: A review, Nucl. Med. Commun., 18 (1997) 437-458.

[21] R. Hanna, T. Braun, A. Levendel, F. Lomas, Radiochemistry and biostability of autologous leucocytes labelled with 99mTc-stannous colloid in whole blood, Eur. J. Nucl. Med., 9 (1984) 216-219.

[22] R.W. Hanna, F.E. Lomas, Identification of factors affecting technetium 99m leucocyte labelling by phagocytic engulfment and evelopment of an optimal technique, Eur. J. Nucl. Med., 12 (1986) 159-162.

[23] C. McClelland, E. Onuegbulem, N. Carter, M. Leahy, M.J. O'doherty, F. Pooley, T. O'doherty, R.J. Newsam, G. Ensing, P.J. Blower, 99mTc-SnF2 colloid 'LLK': particle size, morphology and leucocyte labelling behaviour, Nucl. Med. Commun., 24 (2003) 191-202.

[24] A.E. Southee, K.J. Lee, A.F. McLaughlin, P.W. Borham, G.J. Bautovich, J.G. Morris, Tc-99m white cell scintigraphy in suspected acute infection, Clin. Nucl. Med., 15 (1990) 71-75.

[25] K. Chik, M. Magee, W. Bruce, R. Higgs, M. Thomas, K. Allman, H. Van der Wall, Tc-99m stannous colloid-labeled leukocyte scintigraphy in the evaluation of the painful arthroplasty, Clin. Nucl. Med., 21 (1996) 838-843.

[26] S. Ramsay, J. Labrooy, R. Norton, B. Webb, Demonstration of different patterns of musculoskeletal, soft tissue and visceral involvement in melioidosis using 99mTc stannous colloid white cell scanning, Nucl. Med. Commun., 22 (2001) 1193-1199.

[27] S. Boyd, R. Nour, R. Quinn, E. McKay, S. Butler, Evaluation of white cell scintigraphy using indium-111 and technetium-99m labelled leucocytes, Eur. J. Nucl. Med., 20 (1993) 201-206.

[28] N. Carter, C. Eustance, S. Barrington, M. O'DOHERTY, A. Coakley, Imaging of abdominal infection using 99mTc stannous fluoride colloid labelled leukocytes, Nucl. Med. Commun., 23 (2002) 153-160.

[29] V. Kumar, Radiolabeled white blood cells and direct targeting of micro-organisms for infection imaging, Q. J. Nucl. Med. Mol. Imaging, 49 (2005) 325-338.

[30] C. Tsopelas, The radiopharmaceutical chemistry of 99mTc-tin fluoride colloid-labeled-leukocytes, Q. J. Nucl. Med. Mol. Imaging, 49 (2005) 319-324.

[31] K. Peacock, U. Porn, R. Howman-Giles, E. O'Loughlin, R. Uren, K. Gaskin, S. Dorney, R. Kamath, 99mTc-stannous colloid white cell scintigraphy in childhood inflammatory bowel disease, J. Nucl. Med., 45 (2004) 261-265.

[32] J. BOOTH, Assessment of inflammatory bowel disease activity by technetium 99m phagocyte scanning, Gastroenterology, 95 (1988) 989-996.

[33] P. Gibson, M. Lichtenstein, N. Salehi, G. Hebbard, J. Andrews, Value of positive technetium-99m leucocyte scans in predicting intestinal inflammation, Gut, 32 (1991) 1502-1507.

[34] M.R. Puncher, P.J. Blower, Labelling of leucocytes with colloidal tech netium-99m-SnF2: an investigation of the labelling process by autoradiography, Eur. J. Nucl. Med., 22 (1995) 101-107.

[35] B.H. Mock, D. English, Leukocyte labeling with technetium-99m tin colloids, J. Nucl. Med., 28 (1987) 1471-1477.

[36] H. Gallagher, S.C. Ramsay, J. Barnes, J. Maggs, N. Cassidy, N. Ketheesan, Neutrophil labeling with [99m Tc]-technetium stannous colloid is complement receptor 3-mediated and increases the neutrophil priming response to lipopolysaccharide, Nucl. Med. Biol., 33 (2006) 433-439.

[37] C.J. Palestro, Radionuclide Imaging of Musculoskeletal Infection: A Review, J. Nucl. Med., 57 (2016) 1406-1412.

[38] C.J. Palestro, A.W. Glaudemans, R.A. Dierckx, Multiagent imaging of inflammation and infection with radionuclides, Clin Transl Imaging, 1 (2013) 385-396.

[39] M. Horger, S.M. Eschmann, C. Pfannenberg, D. Storek, F. Dammann, R. Vonthein, C.D. Claussen, R. Bares, The value of SPET/CT in chronic osteomyelitis, Eur. J. Nucl. Med. Mol. Imaging, 30 (2003) 1665-1673.

[40] V. Graute, M. Feist, S. Lehner, A. Haug, P.E. Müller, P. Bartenstein, M. Hacker, Detection of low-grade prosthetic joint infections using 99mTc-antigranulocyte SPECT/CT: initial clinical results, Eur. J. Nucl. Med. Mol. Imaging, 37 (2010) 1751-1759.

[41] J. Meller, V. Ivancevic, M. Conrad, S. Gratz, Clinical value of immunoscintigraphy in patients with fever of unknown origin, J. Nucl. Med., 39 (1998) 1248.

[42] A. Hubalewska, D. Dudek, J. Dubiel, E. Płaczkiewicz-Jankowska, B. Huszno, A. Staszczak, W. Frasik, Screening for acute myocarditis—is scintigraphy with 99m Tc-anti-granulocyte BW 250/183 an answer, Nucl Med Rev Cent East Eur, 7 (2004) 165-169.

[43] T. Györke, L. Duffek, K. Bártfai, E. Makó, K. Karlinger, Á. Mester, Z. Tarján, The role of nuclear medicine in inflammatory bowel disease. A review with experiences of aspecific bowel activity using immunoscintigraphy with 99m Tc anti-granulocyte antibodies, Eur. J. Radiol., 35 (2000) 183-192.

[44] A. Blazeski, K. Kozloff, P. Scott, Besilesomab for imaging inflammation and infection in peripheral bone in adults with suspected osteomyelitis, Rep Med Imaging, 3 (2010) 1-11.

[45] A.W.J.M. Glaudemans, F. Galli, M. Pacilio, A. Signore, Leukocyte and bacteria imaging in prosthetic joint infection, Eur. Cell. Mater., 25 (2012) 61-77.

[46] S.J. Skehan, J.F. White, J.W. Evans, D.R. Parry-Jones, C.K. Solanki, J.R. Ballinger, E.R. Chilvers, A.M. Peters, Mechanism of accumulation of 99mTc-sulesomab in inflammation, J. Nucl. Med., 44 (2003) 11-18.

[47] S. Schroeter, L. Greiner-Bechert, LeukoScan protocol, Nucl. Med. Commun., 22 (2001) 841.

[48] S. Basu, T. Chryssikos, S. Moghadam-Kia, H. Zhuang, D.A. Torigian, A. Alavi, Positron emission tomography as a diagnostic tool in infection: present role and future possibilities, in: Semin. Nucl. Med., Elsevier, 2009, pp. 36-51.

[49] R. Kubota, S. Yamada, K. Kubota, K. Ishiwata, N. Tamahashi, T. Ido, IntratumoralDistribution of fluorine- 18-FluorodeoxyglucoseIn Vivo: High Accumulation in MacrophagesandGranulationTissuesStudied by Microautoradiograph, J. Nucl. Med., 33 (1992) 1972-1980.

[50] H.A. Jones, R.J. Clark, C.G. Rhodes, J.B. Schofield, T. Krausz, C. Haslett, In vivo measurement of neutrophil activity in experimental lung inflammation, Am. J. Respir. Crit. Care. Med., 149 (1994) 1635-1639.

[51] D.J. Weisdorf, P.R. Craddock, H.S. Jacob, Glycogenolysis versus glucose transport in human granulocytes: differential activation in phagocytosis and chemotaxis, Blood, 60 (1982) 888-893.

[52] J. Shearer, J. Amaral, M. Caldwell, Glucose metabolism of injured skeletal muscle: the contribution of inflammatory cells, Circ. Shock, 25 (1988) 131-138.

[53] M.J. Cline, R.I. Lehrer, Phagocytosis by human monocytes, Blood, 32 (1968) 423-435.

[54] N.D. McKay, B. Robinson, R. Brodie, N. Rooke-Allen, Glucose transport and metabolism in cultured human skin fibroblasts, Biochim. Biophys. Acta, Mol. Cell Res., 762 (1983) 198-204.

[55] K. Hamacher, H.H. Coenen, G. Stöcklin, Efficient Stereospecific Synthesis of No-Carrier-Added 2-[18F]-Fluoro-2-Deoxy-D-Glucose Using Aminopolyether Supported Nucleophilic Substitution, J. Nucl. Med., 27 (1986) 235-238.

[56] H.W. Kim, J.M. Jeong, Y.-S. Lee, D.Y. Chi, K.-H. Chung, D.S. Lee, J.-K. Chung, M.C. Lee, Rapid synthesis of [18F]FDG without an evaporation step using an ionic liquid, Appl. Radiat. Isot., 61 (2004) 1241-1246.

[57] C. LOWELL EDWARDS, R. Hayes, Tumor scanning with 67Ga citrate, J. Nucl. Med., 25 (1984) 724-726.

[58] V. Kumar, D.K. Boddeti, (68)Ga-radiopharmaceuticals for PET imaging of infection and inflammation, Recent Results Cancer Res., 194 (2013) 189-219.

[59] A. Rizzello, D. Di Pierro, F. Lodi, S. Trespidi, G. Cicoria, D. Pancaldi, C. Nanni, M. Marengo, M.C. Marzola, A. Al-Nahhas, Synthesis and quality control of 68Ga citrate for routine clinical PET, Nucl. Med. Commun., 30 (2009) 542-545.

[60] A. Aghanejad, A.R. Jalilian, K. Ardaneh, F. Bolourinovin, H. Yousefnia, A.B. Samani, Preparation and Quality Control of (68)Ga-Citrate for PET Applications, Asia Ocean J Nucl Med Biol, 3 (2015) 99-106.

[61] M. Vorster, B. Mokaleng, M.M. Sathekge, T. Ebenhan, A modified technique for efficient radiolabeling of 68Ga-citrate from a SnO2-based 68Ge/68Ga generator for better infection imaging, Hell. J. Nucl. Med., 16 (2013) 193-198.

[62] W. Becker, E. Schomann, W. Fischbach, W. Borner, K. Grüner, Comparison of 99Tcm-HMPAO and 111In-oxine labelled granulocytes in man: first clinical results, Nucl. Med. Commun., 9 (1988) 435-448.

[63] A. Delcourt, D. Huglo, T. Prangere, H. Benticha, F. Devemy, D. Tsirtsikoulou, M. Lepeut, P. Fontaine, M. Steinling, Comparison between Leukoscan®(Sulesomab) and Gallium-67 for the diagnosis of osteomyelitis in the diabetic foot, Diabetes Metab., 31 (2005) 125-133.

[64] M. Bester, P. Van Heerden, J. Klopper, H. Wasserman, S. Rubow, F. De Klerk, Imaging infection and inflammation in an African environment: Comparison of 99Tcm-HMPAO-labelled leukocytes and 67Ga-citrate, Nucl. Med. Commun., 16 (1995) 599-607.

[65] S. Takahama, Y. Kaku, E. Nakashima, R. Minami, M. Yamamoto, [The Usefulness of the Scan with 67Ga-citrate to Assess the Therapeutic Effect on Pneumocystis pneumonia with HIV-1 Infection], Kansenshogaku Zasshi, 89 (2015) 254-258.

[66] S. Auletta, F. Galli, C. Lauri, D. Martinelli, I. Santino, A. Signore, Imaging bacteria with radiolabelled quinolones, cephalosporins and siderophores for imaging infection: a systematic review, Clin Transl Imaging, 4 (2016) 229-252.

[67] K. Chen, X. Chen, Design and development of molecular imaging probes, Curr. Top. Med. Chem., 10 (2010) 1227-1236.

[68] T. Ebenhan, N. Chadwick, M.M. Sathekge, P. Govender, T. Govender, H.G. Kruger, B. Marjanovic-Painter, J.R. Zeevaart, Peptide synthesis, characterization and 68 Ga-radiolabeling of NOTA-conjugated ubiquicidin fragments for prospective infection imaging with PET/CT, Nucl. Med. Biol., 41 (2014) 390-400.

[69] K. Chen, P.S. Conti, Target-specific delivery of peptide-based probes for PET imaging, Adv. Drug Delivery Rev., 62 (2010) 1005-1022.

[70] L. Gentilucci, R. De Marco, L. Cerisoli, Chemical modifications designed to improve peptide stability: incorporation of non-natural amino acids, pseudo-peptide bonds, and cyclization, Curr. Pharm. Des., 16 (2010) 3185-3203.

[71] J. Thundimadathil, A. Gangakhedkar, Improving stability of peptide drugs through chemical modifications, Oligos and Peptides, 32 (2014) 35-38.

[72] T. Arnesen, Towards a functional understanding of protein N-terminal acetylation, PLoS Biol., 9 (2011) e1001074.

[73] H.C. Kolb, K. Chen, J.C. Walsh, Q. Liang, H.C. Padgett, F. Karimi, Click chemistry-derived cyclopeptide derivatives as imaging agents for integrins, in, Google Patents, 2010.

[74] A.J. Beer, R. Haubner, M. Goebel, S. Luderschmidt, M.E. Spilker, H.-J. Wester, W.A. Weber, M. Schwaiger, Biodistribution and pharmacokinetics of the αvβ3-selective tracer 18F-galacto-RGD in cancer patients, J. Nucl. Med., 46 (2005) 1333-1341.

[75] M.S. Morrison, S.-A. Ricketts, J. Barnett, A. Cuthbertson, J. Tessier, S.R. Wedge, Use of a novel Arg-Gly-Asp radioligand, 18F-AH111585, to determine changes in tumor vascularity after antitumor therapy, J. Nucl. Med., 50 (2009) 116-122.

[76] E. Mittra, M. Goris, A. Iagaru, A. Kardan, S. Liu, B. Shen, F. Chin, X. Chen, S. Gambhir, First in man studies of [18F] FPPRGD2: a novel PET radiopharmaceutical for imaging αvβ3 integrin levels, J. Nucl. Med., 51 (2010) 1433-1433.

[77] V. Rufini, M.L. Calcagni, R.P. Baum, Imaging of neuroendocrine tumors, in: Semin. Nucl. Med., Elsevier, 2006, pp. 228-247.

[78] C.J. Anderson, F. Dehdashti, P.D. Cutler, S.W. Schwarz, R. Laforest, L.A. Bass, J.S. Lewis, D.W. McCarthy, 64Cu-TETA-octreotide as a PET imaging agent for patients with neuroendocrine tumors, J. Nucl. Med., 42 (2001) 213-221.

[79] Z. Win, L. Rahman, J. Murrell, J. Todd, A. Al-Nahhas, The possible role of 68 Ga-DOTATATE PET in malignant abdominal paraganglioma, Eur. J. Nucl. Med. Mol. Imaging, 33 (2006) 506-506.

[80] G. Meisetschläger, T. Poethko, A. Stahl, I. Wolf, K. Scheidhauer, M. Schottelius, M. Herz, H.J. Wester, M. Schwaiger, Gluc-Lys ([18F] FP)-TOCA PET in patients with SSTR-positive tumors: biodistribution and diagnostic evaluation compared with [111In] DTPA-octreotide, J. Nucl. Med., 47 (2006) 566-573.

[81] A. Dimitrakopoulou-Strauss, P. Hohenberger, U. Haberkorn, H.R. Mäcke, M. Eisenhut, L.G. Strauss, 68Ga-labeled bombesin studies in patients with gastrointestinal stromal tumors: comparison with 18F-FDG, J. Nucl. Med., 48 (2007) 1245-1250.

[82] C.P. Brouwer, M. Wulferink, M.M. Welling, The pharmacology of radiolabeled cationic antimicrobial peptides, J. Pharm. Sci., 97 (2008) 1633-1651.

[83] M.R. Yeaman, N.Y. Yount, Mechanisms of antimicrobial peptide action and resistance, Pharmacol. Rev., 55 (2003) 27-55.

[84] S.M. Okarvi, Peptide-based radiopharmaceuticals: future tools for diagnostic imaging of cancers and other diseases, Med. Res. Rev., 24 (2004) 357-397.

[85] M.S. Akhtar, M.B. Imran, M.A. Nadeem, A. Shahid, Antimicrobial peptides as infection imaging agents: better than radiolabeled antibiotics, Int J Pept, 2012 (2012) 965238.

[86] P.S. Hiemstra, M.T. van den Barselaar, M. Roest, P.H. Nibbering, R. van Furth, Ubiquicidin, a novel murine microbicidal protein present in the cytosolic fraction of macrophages, J. Leukoc. Biol., 66 (1999) 423-428.

[87] C.P. Brouwer, S.J. Bogaards, M. Wulferink, M.P. Velders, M.M. Welling, Synthetic peptides derived from human antimicrobial peptide ubiquicidin accumulate at sites of infections and eradicate (multi-drug resistant) Staphylococcus aureus in mice, Peptides, 27 (2006) 2585-2591.

[88] G. Ferro-Flores, C. Arteaga de Murphy, M. Pedraza-Lopez, L. Melendez-Alafort, Y.M. Zhang, M. Rusckowski, D.J. Hnatowich, In vitro and in vivo assessment of 99mTc-UBI specificity for bacteria, Nucl. Med. Biol., 30 (2003) 597-603.

[89] M.S. Akhtar, J. Iqbal, M.A. Khan, J. Irfanullah, M. Jehangir, B. Khan, I. Ul-Haq, G. Muhammad, M.A. Nadeem, M.S. Afzal, M.B. Imran, 99mTc-labeled antimicrobial peptide ubiquicidin (29-41) accumulates less in Escherichia coli infection than in Staphlococcus aureus infection, J. Nucl. Med., 45 (2004) 849-856.

[90] C.P. Brouwer, F.F. Gemmel, M.M. Welling, Evaluation of 99mTc-UBI 29-41 scintigraphy for specific detection of experimental multidrug-resistant Staphylococcus aureus bacterial endocarditis, Q. J. Nucl. Med. Mol. Imaging, 54 (2010) 442-450.

[91] A. Lupetti, M.M. Welling, U. Mazzi, P.H. Nibbering, E.K. Pauwels, Technetium-99m labelled fluconazole and antimicrobial peptides for imaging of Candida albicans and Aspergillus fumigatus infections, Eur. J. Nucl. Med. Mol. Imaging, 29 (2002) 674-679.

[92] M.M. Welling, A. Paulusma-Annema, H.S. Balter, E.K. Pauwels, P.H. Nibbering, Technetium-99m labelled antimicrobial peptides discriminate between bacterial infections and sterile inflammations, Eur. J. Nucl. Med., 27 (2000) 292-301.

[93] L. Melendez-Alafort, A. Nadali, G. Pasut, E. Zangoni, R. De Caro, L. Cariolato, M.C. Giron, I. Castagliuolo, F.M. Veronese, U. Mazzi, Detection of sites of infection in mice using 99mTc-labeled PN(2)S-PEG conjugated to UBI and 99mTc-UBI: a comparative biodistribution study, Nucl. Med. Biol., 36 (2009) 57-64.

[94] L. Melendez-Alafort, M. Ramirez Fde, G. Ferro-Flores, C. Arteaga de Murphy, M. Pedraza-Lopez, D.J. Hnatowich, Lys and Arg in UBI: a specific site for a stable Tc-99m complex?, Nucl. Med. Biol., 30 (2003) 605-615.

[95] M.S. Akhtar, A. Qaisar, J. Irfanullah, J. Iqbal, B. Khan, M. Jehangir, M.A. Nadeem, M.A. Khan, M.S. Afzal, I. Ul-Haq, M.B. Imran, Antimicrobial peptide 99mTc-ubiquicidin 29-41 as human infection-imaging agent: clinical trial, J. Nucl. Med., 46 (2005) 567-573.

[96] D. Salber, J. Gunawan, K.J. Langen, E. Fricke, P. Klauth, W. Burchert, S. Zijlstra, Comparison of 99mTc- and 18F-ubiquicidin autoradiography to anti-Staphylococcus aureus immunofluorescence in rat muscle abscesses, J. Nucl. Med., 49 (2008) 995-999.

[97] S. Zijlstra, J. Gunawan, C. Freytag, W. Burchert, Synthesis and evaluation of fluorine-18 labelled compounds for imaging of bacterial infections with pet, Appl. Radiat. Isot., 64 (2006) 802-807.

[98] T. Ebenhan, J.R. Zeevaart, J.D. Venter, T. Govender, G.H. Kruger, N.V. Jarvis, M.M. Sathekge, Preclinical evaluation of 68Ga-labeled 1,4,7-triazacyclononane-1,4,7-triacetic acid-ubiquicidin as a radioligand for PET infection imaging, J. Nucl. Med., 55 (2014) 308-314.

[99] Y. Date, M. Nakazato, K. Shiomi, H. Toshimori, K. Kangawa, H. Matsuo, S. Matsukura, Localization of human neutrophil peptide (HNP) and its messenger RNA in neutrophil series, Ann. Hematol., 69 (1994) 73-77.

[100] T. Ganz, M.E. Selsted, D. Szklarek, S. Harwig, K. Daher, D.F. Bainton, R.I. Lehrer, Defensins. Natural peptide antibiotics of human neutrophils, J. Clin. Invest., 76 (1985) 1427.

[101] C. Wilde, J. Griffith, M. Marra, J. Snable, R. Scott, Purification and characterization of human neutrophil peptide 4, a novel member of the defensin family, J. Biol. Chem., 264 (1989) 11200-11203.

[102] A. Singh, A. Bateman, Q. Zhu, S. Shimasaki, F. Esch, S. Solomon, Structure of a novel human granulocyte peptide with anti-ACTH activity, Biochem. Biophys. Res. Commun., 155 (1988) 524-529.

[103] J.F. Gera, A. Lichtenstein, Human neutrophil peptide defensins induce single strand DNA breaks in target cells, Cell. Immunol., 138 (1991) 108-120.

[104] S. Sharma, I. Verma, G. Khuller, Antibacterial activity of human neutrophil peptide-1 against Mycobacterium tuberculosis H37Rv: in vitro and ex vivo study, Eur. Respir. J., 16 (2000) 112-117.

[105] M.M. Welling, P.S. Hiemstra, M.T. van den Barselaar, A. Paulusma-Annema, P.H. Nibbering, E. Pauwels, W. Calame, Antibacterial activity of human neutrophil defensins in experimental infections in mice is accompanied by increased leukocyte accumulation, J. Clin. Invest., 102 (1998) 1583-1590.

[106] E. Pauwels, M. Welling, R. Feitsma, D. Atsma, W. Nieuwenhuizen, The labeling of proteins and LDL with 99m Tc: a new direct method employing KBH 4 and stannous chloride, Nucl. Med. Biol., 20 (1993) 825-833.

[107] J. Stolk, J. Camps, H. Feitsma, J. Hermans, J. Dijkman, E. Pauwels, Pulmonary deposition and disappearance of aerosolised secretory leucocyte protease inhibitor, Thorax, 50 (1995) 645-650.

[108] P.A. Raj, K.J. Antonyraj, T. Karunakaran, Large-scale synthesis and functional elements for the antimicrobial activity of defensins, Biochem. J., 347 (2000) 633-641.

[109] A. Belaaouaj, Neutrophil elastase-mediated killing of bacteria: lessons from targeted mutagenesis, Microbes Infect., 4 (2002) 1259-1264.

[110] L. Robert, W. Hornbeck, Elastin and elastases, vol I, CRC Press, FL, 1989.

[111] B.L. Roberts, W. Markland, A.C. Ley, R.B. Kent, D.W. White, S.K. Guterman, R.C. Ladner, Directed evolution of a protein: selection of potent neutrophil elastase inhibitors displayed on M13 fusion phage, Proc Natl Acad Sci U S A., 89 (1992) 2429-2433.

[112] A.C. Ley, R.C. Ladner, S.K. Guterman, B.L. Roberts, W. Markland, R.B. Kent, Engineered human-derived kunitz domains that inhibit human neutrophil elastase, in, Google Patents, 1997.

[113] M. Rusckowski, T. Qu, J. Pullman, R. Marcel, A.C. Ley, R.C. Ladner, D.J. Hnatowich, Inflammation and Infection Imaging with a 99mTc-Neutrophil Elastase Inhibitor in Monkeys, J. Nucl. Med., 41 (2000) 363-374.

[114] D.J. Hnatowich, T. Qu, F. Chang, A.C. Ley, Labeling peptides with technetium-99m using a bifunctional chelator of a N-hydroxysuccinimide ester of mercaptoacetyltriglycine, J. Nucl. Med., 39 (1998) 56-64.

[115] M. Liberatore, A. Pala, S. Scaccianoce, C. Anagnostou, U. Di Tondo, E. Calandri, P. D'Elia, M.D. Gross, D. Rubello, Microbial Targeting of 99mTc-Labeled Recombinant Human β-Defensin-3 in an Animal Model of Infection: A Feasibility Pilot Study, J. Nucl. Med., 50 (2009) 823-826.

[116] A. Weinberg, S. Krisanaprakornkit, B. Dale, Epithelial antimicrobial peptides: review and significance for oral applications, Crit. Rev. Oral Biol. Med., 9 (1998) 399-414.

[117] J. Harder, J. Bartels, E. Christophers, J.-M. Schröder, Isolation and characterization of human β-defensin-3, a novel human inducible peptide antibiotic, J. Biol. Chem., 276 (2001) 5707-5713.

[118] J.-R. García, F. Jaumann, S. Schulz, A. Krause, J. Rodríguez-Jiménez, U. Forssmann, K. Adermann, E. Klüver, C. Vogelmeier, D. Becker, Identification of a novel, multifunctional β-defensin (human β-defensin 3) with specific antimicrobial activity, Cell Tissue Res., 306 (2001) 257-264.

[119] H.P. Jia, B.C. Schutte, A. Schudy, R. Linzmeier, J.M. Guthmiller, G.K. Johnson, B.F. Tack, J.P. Mitros, A. Rosenthal, T. Ganz, Discovery of new human β-defensins using a genomics-based approach, Gene, 263 (2001) 211-218.

[120] R. Alberto, R. Schibli, A. Egli, A.P. Schubiger, U. Abram, T.A. Kaden, A Novel Organometallic Aqua Complex of Technetium for the Labeling of Biomolecules: Synthesis of

[99mTc(OH2)3(CO)3]+ from [99mTcO4]- in Aqueous Solution and Its Reaction with a Bifunctional Ligand, J. Am. Chem. Soc., 120 (1998) 7987-7988.

[121] F. Schanbacher, R.E. Goodman, R. Talhouk, Bovine mammary lactoferrin: implications from messenger ribonucleic acid (mRNA) sequence and regulation contrary to other milk proteins, J. Dairy Sci., 76 (1993) 3812-3831.

[122] I.A. García-Montoya, T.S. Cendón, S. Arévalo-Gallegos, Q. Rascón-Cruz, Lactoferrin a multiple bioactive protein: An overview, Biochim. Biophys. Acta, Gen. Subj., 1820 (2012) 226-236.

[123] B. Van der Strate, L. Beljaars, G. Molema, M. Harmsen, D. Meijer, Antiviral activities of lactoferrin, Antiviral Res., 52 (2001) 225-239.

[124] Y.E. Öztafl, N. Özgünefl, Lactoferrin: a multifunctional protein, Adv Mol Med, 1 (2005) 149-154.

[125] D.A. Rodríguez-Franco, L. Vázquez-Moreno, M.G. Ramos-Clamont, Actividad antimicrobiana de la lactoferrina: Mecanismos y aplicaciones clínicas potenciales, Rev Latino-am Microbiol, 47 (2005) 101-111.

[126] P. Nibbering, E. Ravensbergen, M. Welling, L. Van Berkel, P. Van Berkel, E. Pauwels, J. Nuijens, Human lactoferrin and peptides derived from its N terminus are highly effective against infections with antibiotic-resistant bacteria, Infect. Immun., 69 (2001) 1469-1476.

[127] A.M. van der Does, P.J. Hensbergen, S.J. Bogaards, M. Cansoy, A.M. Deelder, H.C. van Leeuwen, J.W. Drijfhout, J.T. van Dissel, P.H. Nibbering, The human lactoferrin-derived peptide hLF1-11 exerts immunomodulatory effects by specific inhibition of myeloperoxidase activity, J. Immunol., 188 (2012) 5012-5019.

[128] H.S. de Koster, R. Amons, W.E. Benckhuijsen, M. Feijlbrief, G.A. Schellekens, J.W. Drijfhout, The use of dedicated peptide libraries permits the discovery of high affinity binding peptides, J. Immunol. Methods, 187 (1995) 179-188.

[129] A. Signore, M. Chianelli, C. D'Alessandria, A. Annovazzi, Receptor targeting agents for imaging inflammation/infection: where are we now?, Q. J. Nucl. Med. Mol. Imaging, 50 (2006) 236-242.

[130] M.M. Welling, A. Lupetti, H.S. Balter, S. Lanzzeri, B. Souto, A.M. Rey, E.O. Savio, A. Paulusma-Annema, E.K. Pauwels, P.H. Nibbering, 99mTc-labeled antimicrobial peptides for detection of bacterial and Candida albicans infections, J. Nucl. Med., 42 (2001) 788-794.

[131] O. Langer, M. Brunner, M. Zeitlinger, S. Ziegler, U. Müller, G. Dobrozemsky, E. Lackner, C. Joukhadar, M. Mitterhauser, W. Wadsak, In vitro and in vivo evaluation of [18F] ciprofloxacin for the imaging of bacterial infections with PET, Eur. J. Nucl. Med. Mol. Imaging, 32 (2005) 143-150.

[132] M. Brunner, O. Langer, G. Dobrozemsky, U. Müller, M. Zeitlinger, M. Mitterhauser, W. Wadsak, R. Dudczak, K. Kletter, M. Müller, [18F] Ciprofloxacin, a new positron emission tomography tracer for noninvasive assessment of the tissue distribution and pharmacokinetics of ciprofloxacin in humans, Antimicrob. Agents Chemother., 48 (2004) 3850-3857.

[133] B.D. Davis, Mechanism of bactericidal action of aminoglycosides, Microbiol. Rev., 51 (1987) 341-350.

[134] L.P. Kotra, J. Haddad, S. Mobashery, Aminoglycosides: Perspectives on Mechanisms of Action and Resistance and Strategies to Counter Resistance, Antimicrob. Agents Chemother., 44 (2000) 3249-3256.

[135] A. Badbarin, A.R. Jalilian, H. Yousefnia, M. Mazidi, F. Bolourinovin, Optimized preparation and evaluation of 99mTc-Streptomycin, Iran J Nucl Med, 24 (2016) 46-50.

[136] E. Widyasari, M. Sriyani, T. Wibawa, W. Nuraeni, Preparation of 99m Tc-Kanamycin Using a Direct Labeling Method, Atom Indones., 41 (2015) 131-137.

[137] K. Özker, İ. Urgancioĝlu, 99mTc-gentamicin: Chemical and biological evaluation, Eur. J. Nucl. Med., 6 (1981) 173-176.

[138] A. Van't Veen, D. Gommers, S.J. Verbrugge, P. Wollmer, J.W. Mouton, P.P. Kooij, B. Lachmann, Lung clearance of intratracheally instilled 99mTc-tobramycin using pulmonary surfactant as vehicle, Br. J. Pharmacol., 126 (1999) 1091-1096.

[139] D.J. Weber, N.E. Tolkoff-Rubin, R.H. Rubin, Amoxicillin and potassium clavulanate: an antibiotic combination. Mechanism of action, pharmacokinetics, antimicrobial spectrum, clinical efficacy and adverse effects, Pharmacotherapy, 4 (1984) 122-136.

[140] D. Ilem-Ozdemir, O. Caglayan-Orumlu, M. Asikoglu, H. Ozkilic, F. Yilmaz, M. Hosgor-Limoncu, Evaluation of 99mTc-amoxicillin sodium as an infection imaging agent in bacterially infected and sterile inflamed rats, J. Radioanal. Nucl. Chem., 308 (2016) 995-1004.

[141] F. Yurt Lambrecht, O. Yilmaz, P. Unak, B. Seyitoglu, K. Durkan, H. Baskan, Evaluation of 99mTc-Cefuroxime axetil for imaging of inflammation, J. Radioanal. Nucl. Chem., 277 (2008) 491-494.

[142] M. Sohaib, Z. Khurshid, S. Roohi, Labelling of ceftriaxone with 99mTc and its bio-evaluation as an infection imaging agent, J. Label. Compd. Radiopharm., 57 (2014) 652-657.

[143] M. Motaleb, M. El-Kolaly, A. Ibrahim, A.A. El-Bary, Study on the preparation and biological evaluation of 99mTc–gatifloxacin and 99mTc–cefepime complexes, J. Radioanal. Nucl. Chem., 289 (2011) 57-65.

[144] V.G. Barreto, G. Rabiller, F. Iglesias, V. Soroa, F. Tubau, M. Roca, J. Martin-Comin, Gammagrafía con 99m Tc-ceftizoxima en ratas normales y en ratas con absceso inducido, Rev. Esp. Med. Nucl., 24 (2005) 312-318.

[145] S. Mirshojaei, M. Gandomkar, R. Najafi, S.S. Ebrahimi, M. Babaei, A. Shafiei, M. Talebi, Radio labeling, quality control and biodistribution of 99mTc-cefotaxime as an infection imaging agent, J. Radioanal. Nucl. Chem., 287 (2011) 21-25.

[146] M.A. Motaleb, Preparation of 99mTc-cefoperazone complex, a novel agent for detecting sites of infection, J. Radioanal. Nucl. Chem., 272 (2007) 167-171.

[147] P.E. Reynolds, Structure, biochemistry and mechanism of action of glycopeptide antibiotics, Eur. J. Clin. Microbiol. Infect. Dis., 8 (1989) 943-950.

[148] M. Motaleb, M. El-Tawoosy, S. Mohamed, I. Borei, H. Ghanem, A. Massoud, 99m Tc-labeled teicoplanin and its biological evaluation in experimental animals for detection of bacterial infection, Radiochemistry, 56 (2014) 544-549.

[149] S. Roohi, A. Mushtaq, S.A. Malik, Synthesis and biodistribution of 99mTc-Vancomycin in a model of bacterial infection, Radiochim. Acta, 93 (2005) 415-418.

[150] T. Tenson, M. Lovmar, M. Ehrenberg, The Mechanism of Action of Macrolides, Lincosamides and Streptogramin B Reveals the Nascent Peptide Exit Path in the Ribosome, J. Mol. Biol., 330 (2003) 1005-1014.

[151] T.H. Bokhari, F.A. Rizvi, S. Roohi, S. Hina, M. Ahmad, M. Khalid, M. Iqbal, Preparation, biodistribution and scintigraphic evaluation of (99m) Tc-lincomycin, Pak J Pharm Sci, 1 (2015) 1965-1970.

[152] S. Hina, M.I. Rajoka, S. Roohi, A. Haque, M. Qasim, Preparation, biodistribution, and scintigraphic evaluation of 99mTc-clindamycin: an infection imaging agent, Appl. Biochem. Biotechnol., 174 (2014) 1420-1433.

[153] M. Sanad, Labeling and biological evaluation of 99m Tc-azithromycin for infective inflammation diagnosis, Radiochemistry, 55 (2013) 539-544.

[154] E. Borai, M. Sanad, A. Fouzy, Optimized chromatographic separation and biological evaluation of 99m Tc-clarithromycin for infective inflammation diagnosis, Radiochemistry, 58 (2016) 84-91.

[155] M.T. Ercan, T. Aras, I.S. Ünsal, Evaluation of 99mTc-erythromycin and 99mTc-streptomycin sulphate for the visualization of inflammatory lesions, Int. J. Rad. Appl. Instrum. B, 19 (1992) 803-806.

[156] S.S. Sastry, R. Jayaraman, Inhibitors of nitrofuran reduction in Escherichia coli: evidence for their existence, partial purification, binding of nitrofurantoin in vitro, and implications for nitrofuran resistance, Arch. Biochem. Biophys., 236 (1985) 252-259.

[157] S.Q. Shah, A.U. Khan, M.R. Khan, Radiosynthesis of 99mTc-nitrofurantoin a novel radiotracer for in vivo imaging of Escherichia coli infection, J. Radioanal. Nucl. Chem., 287 (2011) 417-422.

[158] K.T. Bain, E.T. Wittbrodt, Linezolid for the treatment of resistant gram-positive cocci, Ann. Pharmacother., 35 (2001) 566-575.

[159] F.Y. Lambrecht, O. Yilmaz, K. Durkan, P. Unak, E. Bayrak, Preparation and biodistribution of [131I] linezolid in animal model infection and inflammation, J. Radioanal. Nucl. Chem., 281 (2009) 415-419.

[160] K. Britton, D. Wareham, S. Das, K. Solanki, H. Amaral, A. Bhatnagar, A. Katamihardja, J. Malamitsi, H. Moustafa, V. Soroa, Imaging bacterial infection with 99mTc-ciprofloxacin (Infecton), J. Clin. Pathol., 55 (2002) 817-823.

[161] R.H. Siaens, H.J. Rennen, O.C. Boerman, R. Dierckx, G. Slegers, Synthesis and comparison of 99mTc-enrofloxacin and 99mTc-ciprofloxacin, J. Nucl. Med., 45 (2004) 2088-2094.

[162] M. Motaleb, Radiochemical and biological characteristics of 99mTc-difloxacin and 99mTc-pefloxacin for detecting sites of infection, J. Label. Compd. Radiopharm., 53 (2010) 104-109.

[163] M. Motaleb, Preparation and biodistribution of 99mTc-lomefloxacin and 99mTc-ofloxacin complexes, J. Radioanal. Nucl. Chem., 272 (2007) 95-99.

[164] S.Q. Shah, M.R. Khan, Radiocharacterization of the 99mTc–rufloxacin complex and biological evaluation in Staphylococcus aureus infected rat model, J. Radioanal. Nucl. Chem., 288 (2011) 373-378.

[165] I. Ibrahim, M. Motaleb, K. Attalah, Synthesis and biological distribution of 99mTc–norfloxacin complex, a novel agent for detecting sites of infection, J. Radioanal. Nucl. Chem., 285 (2010) 431-436.

[166] M.E. Moustapha, H.A. Shweeta, M.A. Motaleb, Technetium-labeled danofloxacin complex as a model for infection imaging, Arabian J. Chem, 9 (2016) S1928–S1934.

[167] A. Singh, J. Verma, A. Bhatnagar, A. Ali, Tc-99m labeled sparfloxacin: A specific infection imaging agent, World J Nucl Med, 2 (2003) 103-109.

[168] S. Shahzad, M.A. Qadir, R. Rasheed, S. Anwar, M. Ahmed, In Vivo Studies 99mTc-Levofloxacin Freeze Dried Kits in Salmonella typhi, Pseudomonas aeruginosa, and Escherichia coli, Lat. Am. J. Pharm, 34 (2015) 760-765.

[169] S.Q. Shah, M.R. Khan, Radiosynthesis and biological evaluation of the 99m Tc-tricarbonyl moxifloxacin dithiocarbamate complex as a potential Staphylococcus aureus infection radiotracer, Appl. Radiat. Isot., 69 (2011) 686-690.

[170] S.Q. Shah, M.R. Khan, S.M. Ali, Radiosynthesis of 99mTc (CO) 3-clinafloxacin dithiocarbamate and its biological evaluation as a potential Staphylococcus aureus infection radiotracer, Nucl Med Mol Imaging, 45 (2011) 248-254.

[171] S.Q. Shah, A.U. Khan, M.R. Khan, 99mTc (CO) 3–Garenoxacin dithiocarbamate synthesis and biological evolution in rats infected with multiresistant Staphylococcus aureus and penicillin-resistant Streptococci, J. Radioanal. Nucl. Chem., 288 (2011) 171-176.

[172] A.J. Fischman, J.W. Babich, N.M. Alpert, J. Vincent, R.A. Wilkinson, R.J. Callahan, J.A. Correia, R.H. Rubin, Pharmacokinetics of 18F-labeled trovafloxacin in normal and Escherichia coli-infected rats and rabbits studied with positron emission tomography, Clin. Microbiol. Infect., 3 (1997) 63-72.

[173] A.J. Fischman, E. Livni, J. Babich, N. Alpert, Y. Liu, E. Thom, R. Cleeland, B. Prosser, R. Callahan, J. Correia, Pharmacokinetics of 18F-labeled fleroxacin in rabbits with Escherichia coli infections, studied with positron emission tomography, Antimicrob. Agents Chemother., 36 (1992) 2286-2292.

[174] D. Satpati, C. Arjun, R. Krishnamohan, G. Samuel, S. Banerjee, 68Ga-labeled Ciprofloxacin Conjugates as Radiotracers for Targeting Bacterial Infection, Chem. Biol. Drug Des., 87 (2016) 680-686.

[175] N. Singh, A. Bhatnagar, Clinical Evaluation of Efficacy of 99mTC-Ethambutol in Tubercular Lesion Imaging, Tuberc Res Treat, 2010 (2010) 1-9.

[176] S.Q. Shah, A.U. Khan, M.R. Khan, Radiosynthesis and biodistribution of 99m Tc-rifampicin: a novel radiotracer for in-vivo infection imaging, Appl. Radiat. Isot., 68 (2010) 2255-2260.

[177] G. Samuel, K. Kothari, S. Banerjee, T. Das, S. Subramanian, M. Kameshwaran, M. Pillai, M. Venkatesh, On the 99mTc-labeling of isoniazid with different 99mTc cores, J. Label. Compd. Radiopharm., 48 (2005) 363-377.

[178] L. Liu, Y. Xu, C. Shea, J.S. Fowler, J.M. Hooker, P.J. Tonge, Radiosynthesis and bioimaging of the tuberculosis chemotherapeutics isoniazid, rifampicin and pyrazinamide in baboons, J. Med. Chem., 53 (2010) 2882-2891.

[179] I. Chopra, M. Roberts, Tetracycline Antibiotics: Mode of Action, Applications, Molecular Biology, and Epidemiology of Bacterial Resistance, Microbiol. Mol. Biol. Rev., 65 (2001) 232-260.

[180] D. İlem-Özdemir, M. Asikoglu, H. Ozkilic, F. Yilmaz, M. Hosgor-Limoncu, S. Ayhan, 99mTc-Doxycycline hyclate: a new radiolabeled antibiotic for bacterial infection imaging, J. Label. Compd. Radiopharm., 57 (2014) 36-41.

[181] E. Weinstein, L. Liu, A. Ordonez, H. Wang, J.M. Hooker, P. Tonge, S. Jain, Noninvasive determination of 2-[18F]-fluoroisonicotinic acid hydrazide pharmacokinetics by positron emission tomography in Mycobacterium tuberculosis-infected mice, Antimicrob. Agents Chemother., 56 (2012) 6284-6290.

[182] J. Martin-Comin, V. Soroa, G. Rabiller, R. Galli, L. Cuesta, M. Roca, Diagnosis of bone infection with 99mTc-ceftizoxime, Rev. Esp. Med. Nucl., 23 (2004) 357.

[183] A. Kaul, P.P. Hazari, H. Rawat, B. Singh, T.C. Kalawat, S. Sharma, A.K. Babbar, A.K. Mishra, Preliminary evaluation of technetium-99m-labeled ceftriaxone: infection imaging agent for the clinical diagnosis of orthopedic infection, Int. J. Infect. Dis., 17 (2013) e263-e270.

[184] J. Stanek, S. Mairinger, T. Wanek, C. Kuntner, M. Müller, O. Langer, Automated radiosynthesis of [18 F] ciprofloxacin, Appl. Radiat. Isot., 99 (2015) 133-137.

[185] L. Sarda, A. Saleh-Mghir, C. Peker, A. Meulemans, A.-C. Crémieux, D. Le Guludec, Evaluation of 99mTc-ciprofloxacin scintigraphy in a rabbit model of Staphylococcus aureus prosthetic joint infection, J. Nucl. Med., 43 (2002) 239-245.

[186] S.I. Sazonova, Y.B. Lishmanov, N.V. Varlamova, V.S. Skuridin, Y.N. Ilushenkova, M.R. Karpova, Y.A. Nesterov, Synthesis and experimental study of norfloxacin labeled with technecium-99m as a potential agent for infection imaging, Iran J Nucl Med, 23 (2015) 73-81.

[187] S.Q. Shah, M.R. Khan, Radiolabeling of gemifloxacin with technetium-99m and biological evaluation in artificially Streptococcus pneumoniae infected rats, J. Radioanal. Nucl. Chem., 288 (2011) 307-312.

[188] S.Q. Shah, A.U. Khan, M.R. Khan, Radiosynthesis, biodistribution and scintigraphy of the 99mTc-Teicoplanin complex in artificially infected animal models, J. Label. Compd. Radiopharm., 54 (2011) 145-149.

[189] F. Virzi, B. Fritz, M. Rusckowski, M. Gionet, H. Misra, D. Hnatowich, New indium-111 labeled biotin derivatives for improved immunotargeting, Int. J. Rad. Appl. Instrum. B, 18 (1991) 719725-723726.

[190] P.A. Erba, A.G. Cataldi, C. Tascini, A. Leonildi, C. Manfredi, G. Mariani, E. Lazzeri, 111In-DTPA-Biotin uptake by Staphylococcus aureus, Nucl. Med. Commun., 31 (2010) 994-997.

[191] E. Lazzeri, P. Erba, M. Perri, R. Doria, C. Tascini, G. Mariani, Clinical impact of SPECT/CT with In-111 biotin on the management of patients with suspected spine infection, Clin. Nucl. Med., 35 (2010) 12-17.

[192] E. Blom, B. Långström, I. Velikyan, 68Ga-labeling of biotin analogues and their characterization, Bioconjugate Chem., 20 (2009) 1146-1151.

[193] B. Seetharam, N. Li, Transcobalamin II and its cell surface receptor, Vitam. Horm., 59 (2000) 337-366.

[194] D. Baldoni, R. Waibel, P. Bläuenstein, F. Galli, V. Iodice, A. Signore, R. Schibli, A. Trampuz, Evaluation of a Novel Tc-99m Labelled Vitamin B12 Derivative for Targeting Escherichia coli and Staphylococcus aureus In Vitro and in an Experimental Foreign-Body Infection Model, Mol. Imaging Biol., 17 (2015) 829-837.

[195] R. Waibel, H. Treichler, N.G. Schaefer, D.R. van Staveren, S. Mundwiler, S. Kunze, M. Küenzi, R. Alberto, J. Nüesch, A. Knuth, New derivatives of vitamin B12 show preferential targeting of tumors, Cancer Res., 68 (2008) 2904-2911.

[196] M. Gijs, A. Aerts, N. Impens, S. Baatout, A. Luxen, Aptamers as radiopharmaceuticals for nuclear imaging and therapy, Nucl. Med. Biol., 43 (2016) 253-271.

[197] Y.S. Kim, J. Chung, M.Y. Song, J. Jurng, B.C. Kim, Aptamer cocktails: enhancement of sensing signals compared to single use of aptamers for detection of bacteria, Biosens. Bioelectron., 54 (2014) 195-198.

[198] S.R. dos Santos, C.R. Corrêa, A.L.B. de Barros, R. Serakides, S.O. Fernandes, V.N. Cardoso, A.S.R. de Andrade, Identification of Staphylococcus aureus infection by aptamers directly radiolabeled with technetium-99m, Nucl. Med. Biol., 42 (2015) 292-298.

[199] L. Chen, Y. Wang, D. Cheng, X. Liu, S. Dou, G. Liu, D.J. Hnatowich, M. Rusckowski, 99m Tc-MORF oligomers specific for bacterial ribosomal RNA as potential specific infection imaging agents, Bioorg. Med. Chem., 21 (2013) 6523-6530.

[200] Y. Wang, G. Liu, D.J. Hnatowich, Methods for MAG3 conjugation and 99mTc radiolabeling of biomolecules, Nat. Protoc., 1 (2006) 1477-1480.

[201] L. Chen, D. Cheng, G. Liu, S. Dou, Y. Wang, X. Liu, Y. Liu, M. Rusckowski, Detection of Klebsiella. Pneumoniae Infection with an Antisense Oligomer Against its Ribosomal RNA, Mol. Imaging Biol., 18 (2016) 527-534.

[202] M. Azzam, I. Algranati, Mechanism of puromycin action: fate of ribosomes after release of nascent protein chains from polysomes, Proc Natl Acad Sci U S A., 70 (1973) 3866-3869.

[203] S. Eigner, D. Beckford Vera, O. Lebeda, K. Eigner Henke, 68Ga-DOTA-Puromycin: In vivo imaging of bacterial infection, J. Nucl. Med., 54 (2013) 1218.

[204] R.G. Blasberg, J.G. Tjuvajev, Molecular-genetic imaging: current and future perspectives, J. Clin. Invest., 111 (2003) 1620-1629.

[205] C. Bettegowda, C.A. Foss, I. Cheong, Y. Wang, L. Diaz, N. Agrawal, J. Fox, J. Dick, L.H. Dang, S. Zhou, Imaging bacterial infections with radiolabeled 1-(2′-deoxy-2′-fluoro-β-D-arabinofuranosyl)-5-iodouracil, Proc. Natl. Acad. Sci. U. S. A., 102 (2005) 1145-1150.

[206] L.A. Diaz Jr, C.A. Foss, K. Thornton, S. Nimmagadda, C.J. Endres, O. Uzuner, T.M. Seyler, S.D. Ulrich, J. Conway, C. Bettegowda, Imaging of musculoskeletal bacterial infections by [124 I] FIAU-PET/CT, PLoS One, 2 (2007) e1007.

[207] W. Boos, H. Shuman, Maltose/maltodextrin system of Escherichia coli: transport, metabolism, and regulation, Microbiol. Mol. Biol. Rev., 62 (1998) 204-229.

[208] M. Namavari, G. Gowrishankar, A. Hoehne, E. Jouannot, S.S. Gambhir, Synthesis of [18F]-labelled Maltose Derivatives as PET Tracers for Imaging Bacterial Infection, Mol. Imaging Biol., 17 (2015) 168-176.

[209] G. Gowrishankar, M. Namavari, E.B. Jouannot, A. Hoehne, R. Reeves, J. Hardy, S.S. Gambhir, Investigation of 6-[18 F]-fluoromaltose as a novel PET tracer for imaging bacterial infection, PLoS One, 9 (2014) e107951.

[210] X. Ning, W. Seo, S. Lee, K. Takemiya, M. Rafi, X. Feng, D. Weiss, X. Wang, L. Williams, V.M. Camp, Fluorine-18 labeled maltohexaose images bacterial infections by PET, Angewandte Chemie (International ed. in English), 53 (2014) 14096–14101.

[211] Z.-B. Li, Z. Wu, Q. Cao, D.W. Dick, J.R. Tseng, S.S. Gambhir, X. Chen, The synthesis of 18F-FDS and its potential application in molecular imaging, Mol. Imaging Biol., 10 (2008) 92-98.

[212] E.A. Weinstein, A.A. Ordonez, V.P. DeMarco, A.M. Murawski, S. Pokkali, E.M. MacDonald, M. Klunk, R.C. Mease, M.G. Pomper, S.K. Jain, Imaging Enterobacteriaceae infection in vivo with 18F-fluorodeoxysorbitol positron emission tomography, Sci. Transl. Med., 6 (2014) 259ra146-259ra146.

[213] S. Yao, H. Xing, W. Zhu, Z. Wu, Y. Zhang, Y. Ma, Y. Liu, L. Huo, Z. Zhu, Z. Li, Infection imaging with 18 F-FDS and first-in-human evaluation, Nucl. Med. Biol., 43 (2016) 206-214.

[214] K.M. Backus, H.l. Boshoff, C.S. Barry, O. Boutureira, M.K. Patel, F. D'Hooge, S.S. Lee, L.E. Via, K. Tahlan, C.E. Barry, B.G. Davis, Uptake of unnatural trehalose analogs as a reporter for Mycobacterium tuberculosis, Nat. Chem. Biol., 7 (2011) 228-235.

[215] S.R. Rundell, Z.L. Wagar, L.M. Meints, C.D. Olson, M.K. O'Neill, B.F. Piligian, A.W. Poston, R.J. Hood, P.J. Woodruff, B.M. Swarts, Deoxyfluoro-d-trehalose (FDTre) analogues as potential PET probes for imaging mycobacterial infection, Org. Biomol. Chem., 14 (2016) 8598-8609.

[216] M.E. Martínez, Y. Kiyono, S. Noriki, K. Inai, K.S. Mandap, M. Kobayashi, T. Mori, Y. Tokunaga, V.N. Tiwari, H. Okazawa, New radiosynthesis of 2-deoxy-2-[18 F] fluoroacetamido-D-glucopyranose and its evaluation as a bacterial infections imaging agent, Nucl. Med. Biol., 38 (2011) 807-817.

[217] M. Wittenwiler, Mechanisms of Iron Mobilization by Siderophores, Master Studies in Environmental Sciences Master, ETH Zürich, (2007).

[218] E.-I. Koh, J.P. Henderson, Microbial copper-binding siderophores at the host-pathogen interface, J. Biol. Chem., 290 (2015) 18967-18974.

[219] R.A. Atkinson, A.L.M. Salah El Din, B. Kieffer, J.-F. Lefèvre, M.A. Abdallah, Bacterial iron transport: 1H NMR determination of the three-dimensional structure of the gallium complex

of pyoverdin G4R, the peptidic siderophore of Pseudomonas putida G4R, Biochemistry, 37 (1998) 15965-15973.

[220] T. Emery, P.B. Hoffer, Siderophore-mediated mechanism of gallium uptake demonstrated in the microorganism Ustilago sphaerogena, J. Nucl. Med., 21 (1980) 935-939.

[221] M. Petrik, G.M. Franssen, H. Haas, P. Laverman, C. Hörtnagl, M. Schrettl, A. Helbok, C. Lass-Flörl, C. Decristoforo, Preclinical evaluation of two (68)Ga-siderophores as potential radiopharmaceuticals for Aspergillus fumigatus infection imaging, Eur. J. Nucl. Med. Mol. Imaging, 39 (2012) 1175-1183.

[222] M. Petrik, H. Haas, P. Laverman, M. Schrettl, G.M. Franssen, M. Blatzer, C. Decristoforo, (68)Ga-Triacetylfusarinine C and (68)Ga-Ferrioxamine E for Aspergillus Infection Imaging: Uptake Specificity in Various Microorganisms, Mol. Imaging Biol., 16 (2014) 102-108.

[223] C.A. Boswell, D.B. Tesar, K. Mukhyala, F.-P. Theil, P.J. Fielder, L.A. Khawli, Effects of Charge on Antibody Tissue Distribution and Pharmacokinetics, Bioconjugate Chem., 21 (2010) 2153-2163.

Chapter 3

A Facile Synthesis of NODASA-Functionalized Peptide

Jyotibon Dutta[a], Praveen K. Chinthakindi[a], Per I. Arvidsson[a,c], Beatriz G. de la Torre[a], Hendrik G. Kruger[a], Thavendran Govender[a], Tricia Naicker[*a], Fernando Albericio[*a,b,d,e,f]

[a] *Catalysis and Peptide Research Unit, School of Health Sciences, University of KwaZulu-Natal, Durban 4001, South Africa*
[b] *School of Chemistry and Physics, University of KwaZulu-Natal, Durban 4001, South Africa*
[c] *Science for Life Laboratory, Drug Discovery & Development Platform & Division of Translational Medicine and Chemical Biology, Department of Medical Biochemistry and Biophysics, Karolinska Institutet, Stockholm, Sweden*
[d] *CIBER-BBN, Networking Centre on Bioengineering, Biomaterials and Nanomedicine, Barcelona Science Park, 08028 Barcelona, Spain*
[e] *Department of Chemistry, College of Science, King Saud University, P.O. Box 2455,Riyadh 11451, Saudi Arabia*
[f] *Department of Organic Chemistry, University of Barcelona, 08028-Barcelona, Spain*

*Correspondence to: *naickert1@ukzn.ac.za, albericio@ukzn.ac.za*

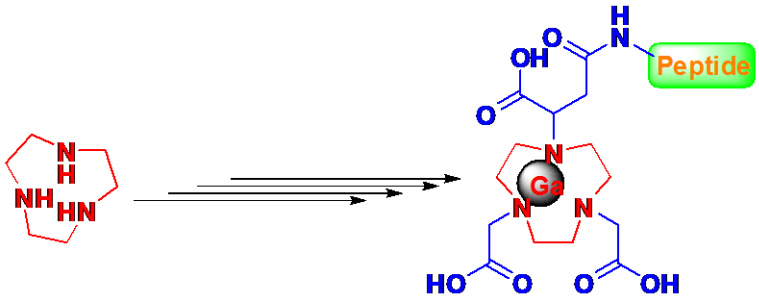

6

- On and off-resin synthetic approach
- Potential PET imaging agent
- Peptide-functionalized NODASA
- Overall 84% yield

Abstract

Herein, we report a mild and efficient synthesis of a NODASA-functionalized peptide, which was initiated with a Michael addition reaction between monomethyl fumarate and 1,4,7-triazacyclononane.

In radiopharmaceutics, chelators are small organic molecules that can form stable coordination complexes with radiometals (radioactive isotopes of various metals) and can be delivered to the target of interest in vivo [1]. Based on the type of radiometal-ion selectivity it can either be used in disease diagnosis or therapeutics [2]. In disease diagnosis; metal ions comprising of positron- or γ-emitting radionuclides and are used in positron emission tomography (PET) [3-5] and single-photon emission computed tomography (SPECT),[6, 7] respectively. The α- and β-ion generating radioisotopes are widely employed as therapeutics in cancer treatment [8-13]. Due to its noninvasive, quantitative, and highly specific nature, PET imaging has become a powerful tool for diagnostic or therapeutic purposes. Some of the common radiometals which can be used in PET imaging are ^{68}Ga, ^{64}Cu, ^{86}Y, ^{89}Zr, and ^{44}Sc metal ions [1]. Among various radiometals used

for PET, ^{68}Ga is of choice due to its availability from enduring ^{68}Ge/^{68}Ga generator systems which offers a cost-effective alternative to the radionuclides produced by a cyclotron [5, 14]. Bifunctional chelators (BFC) are typically used for the development of radiolabeling; focusing on the in vivo target specificity and specific metal-binding capabilities. BFC contain two parts; one is a functional group which can readily react with the targeting molecule (e.g., peptides, antibodies, and nanoparticles) as well as provide a stable covalent bond to it and the other is to form a strong complex with the metal ion ensuring its undesired release within the recipient [15-18].

Significant development has been achieved in the field of oncology in the context of radiolabeled peptides for tissue localization and therapy [19]. In comparison to small molecules, antibodies, and proteins as a carrier, peptides show distinctive advantages. They are reasonably lower molecular weight, easier to synthesize with the development of solid-phase synthesis, compatible to couple with various chelators, bind many significant biological targets, display excellent tumor penetration, and shows rapid clearance from the recipient. Moreover, as a therapeutic, it shows minimal side effects compared to conventional drugs and it is non immunogenic [20, 21].

A well-known BFC, 1,4,7-triazacyclononane-*N*′,*N*′,*N*′′-tri acetic acid (NOTA); is a cyclic polyamino carboxylic ligand which is one of the first and most efficient chelators of ^{64}Cu and $^{67/68}$Ga [2, 22], therefore much research and development into its derivatives has been done [2]. Contrary to its popularity, a large excess of NOTA is required for the complexation with a peptide (Figure 1) as well as the high cost associated with its commercial form [23].

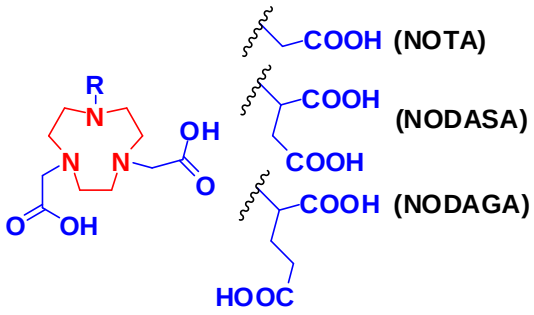

Figure 1 NOTA, NODASA and NODAGA

NOTA derivatives namely NODASA and NODAGA (Figure 1) contain an additional carboxylic acid moiety within the macrocycle allowing the core to better saturate the hexadentate coordination of the metal ion as well as provide a site for attachment of a peptide [19].

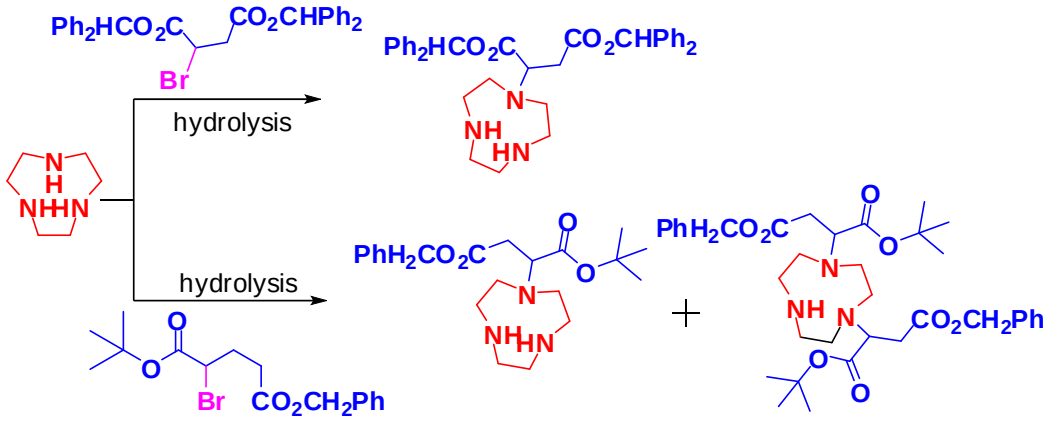

Scheme 1 NODASA [24] and NODAGA [25] synthesis.

In literature noncommercially available bis(diphenyl methyl) *d*,*l*-bromosuccinate [24] and α-bromoglutaric acid 1-*tert*-butyl ester 5-benzyl [25] are typically described for the synthesis of NODASA and NODAGA, respectively (Scheme 1). Hence, there is a need to provide a more convenient synthetic approach for these functionalized chelator derivatives and their coupling to peptides. Herein, we report a new and facile synthetic route for the preparation of peptide-functionalized NODASA on solid phase from readily available and cheaper starting material.

The model peptide, YGGF from the parent peptide YGGFL, is a part of the enkephalin sequence. Coupling of each amino acid was carried out with HBTU/DIPEA in DMF and each step was monitored by the ninhydrin test. Single coupling for one hour with excess of Fmoc-protected amino acids were sufficient for completion of the reaction. The pure peptide product was observed in analytical HPLC when a small portion of the peptide was cleaved from the resin.

Initially, the NODASA synthesis was carried out with the coupling of 4-(benzyloxy)-3-bromo-4-oxobutanoic acid to a peptide on resin followed by addition of 1,4,7-triazacyclononane; this was unsuccessful due to the HBr elimination reaction (Scheme 2). Subsequently, monomethyl fumarate was attached to the peptide on resin, and the addition with 1,4,7-triazacyclononane was attempted, however, this reaction did not yield the product.

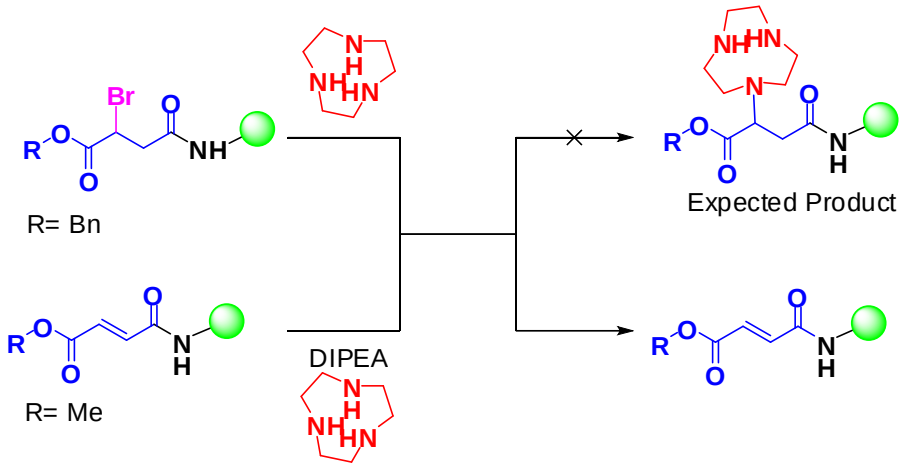

Scheme 2

Next, a Michael addition reaction between monomethyl fumarate and 1,4,7-triazacyclononane (Scheme 3) was carried out in solution. To our delight, the reaction proceeded to the desired product and proved to be regioselective for the C3 position of the alkane and was confirmed using 2D NMR spectroscopy. It was recrystallized in DMF with a yield of 94%. This product (**1**) was also confirmed by LC–MS (positive mode, at *m/z* = 260). In order to prevent self-polymerization of **1** during the amide coupling reaction, protection of the free secondary amines with Fmoc-OSu was carried out.

Compound **2** was then easily coupled to the model peptide YGGF with standard coupling reagents, DIC/Oxyma-Pure. The reaction was monitored by cleaving a small portion of the resin and further analysis via HPLC. Complete conversion into the desired diastereomeric product was observed at *m/z* = 1127. It was then subject to a standard Fmoc deprotection to yield compound **3** which was monitored by HPLC and confirmed by LC–MS.

The resulting free secondary amines were then successfully alkylated on resin with *tert*-butyl bromoacetate in the presence of DIPEA. Complete conversion into the product was observed using analytical HPLC and LC–MS (positive mode) and showed its corresponding *m/z* = 799 for compound **4**. Thereafter, base hydrolysis of the ester was achieved on resin with LiOH in THF–MeOH to furnish derivative **5** which was confirmed from analytical HPLC with 100% conversion of the ester. The *tert*-butyl groups were removed simultaneously with cleavage of the peptide from the resin using TFA/H_2O/TIS. The final product **6** was analyzed by analytical HPLC followed by LC–MS characterization. Analytical HPLC showed 100% conversion into the product with its corresponding *m/z* = 785 and an isolated yield of 84% [26].

An application of the conjugated functionalized peptide product was metal chelation with cold gallium. A period of 30 minutes at room temperature was adequate for $GaCl_3$ in the presence of NaOAc for the complete complexation of NODASA–YGGF (**6**). The stability of gallium complexation was further analyzed by 500-fold excess of EDTA. However, EDTA was challenged for 0, 30, 60, 120, 180, and 240 min showing no significant release of gallium from the complex confirming the resistance towards *trans* chelation.

In this study we described a facile seven-step synthesis and purification of NODASA with a model peptide. The combination of on- and off-resin synthetic approach was employed. We also successfully demonstrated the efficient conjugation of cold gallium to this NODASA–YGGF chelator as a potential PET imaging agent. The synthetic route provides a cheap and simple alternative to commercially available functionalized NODASA in the current market and could be applied to various peptides of choice.

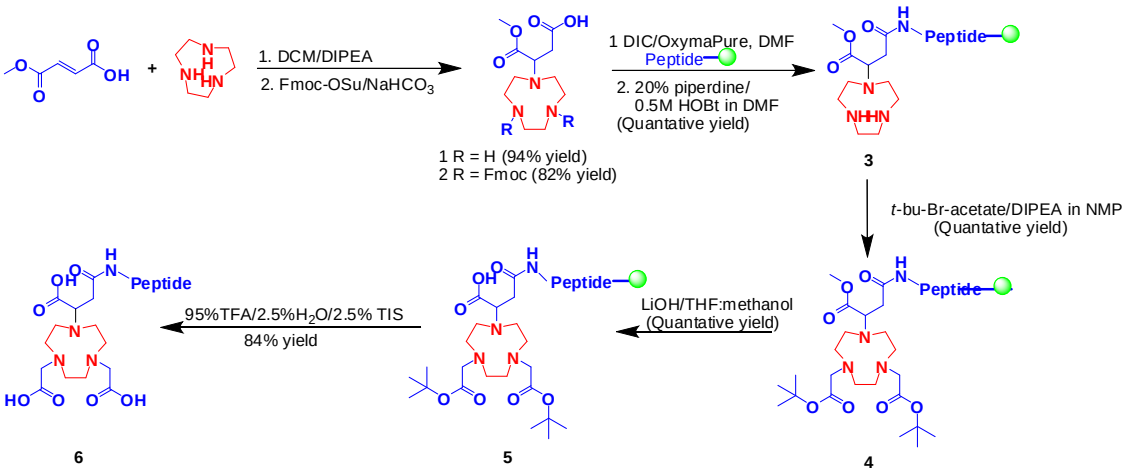

Scheme 3

Acknowledgment

This work was funded in part by the following: National Research

Foundation (NRF) and the University of KwaZulu-Natal. Luxembourg

Biotech Ltd. is acknowledged for the generous gift of coupling reagents.

Supporting Information

Supporting information for this article is available online at

http://dx.doi.org/10.1055/s-0035-1561970.

References and Notes

[1] E.W. Price, C. Orvig, Matching chelators to radiometals for radiopharmaceuticals, Chem. Soc. Rev., 43 (2014) 260-290.

[2] L. Lattuada, A. Barge, G. Cravotto, G.B. Giovenzana, L. Tei, The synthesis and application of polyamino polycarboxylic bifunctional chelating agents, Chem. Soc. Rev., 40 (2011) 3019-3049.

[3] M. Shokeen, C.J. Anderson, Molecular Imaging of Cancer with Copper-64 Radiopharmaceuticals and Positron Emission Tomography (PET), Acc Chem Res., 42 (2009) 832-841.

[4] K. Tanaka, K. Fukase, PET (positron emission tomography) imaging of biomolecules using metal-DOTA complexes: a new collaborative challenge by chemists, biologists, and physicians for future diagnostics and exploration of in vivo dynamics, Org. Biomol. Chem., 6 (2008) 815-828.

[5] M. Fani, J.P. André, H.R. Maecke, 68Ga-PET: a powerful generator-based alternative to cyclotron-based PET radiopharmaceuticals, Contrast Media Mol. Imaging, 3 (2008) 53-63.

[6] J. R. Dilworth, S. J. Parrott, The biomedical chemistry of technetium and rhenium, Chem. Soc. Rev., 27 (1998) 43-55.

[7] C.J. Anderson, M.J. Welch, Radiometal-Labeled Agents (Non-Technetium) for Diagnostic Imaging, Chem. Rev., 99 (1999) 2219-2234.

[8] W.A. Volkert, T.J. Hoffman, Therapeutic Radiopharmaceuticals, Chem. Rev., 99 (1999) 2269-2292.

[9] C.S. Cutler, C.J. Smith, G.J. Ehrhardt, T.T. Tyler, S.S. Jurisson, E. Deutsch, Current and Potential Therapeutic Uses of Lanthanide Radioisotopes, Cancer Biother. Radiopharm., 15 (2000) 531-545.

[10] M.R. McDevitt, G. Sgouros, R.D. Finn, J.L. Humm, J.G. Jurcic, S.M. Larson, D.A. Scheinberg, Radioimmunotherapy with alpha-emitting nuclides, Eur J Nucl Med, 25 (1998) 1341-1351.

[11] S. Hassfjell, M.W. Brechbiel, The Development of the α-Particle Emitting Radionuclides 212Bi and 213Bi, and Their Decay Chain Related Radionuclides, for Therapeutic Applications, Chem. Rev., 101 (2001) 2019-2036.

[12] M. Miederer, D.A. Scheinberg, M.R. McDevitt, Realizing the potential of the Actinium-225 radionuclide generator in targeted alpha particle therapy applications, Adv. Drug Deliv. Rev., 60 (2008) 1371-1382.

[13] P.A. Schubiger, R. Alberto, A. Smith, Vehicles, Chelators, and Radionuclides: Choosing the "Building Blocks" of an Effective Therapeutic Radioimmunoconjugate, Bioconjugate Chem., 7 (1996) 165-179.

[14] P.J. Riss, C. Kroll, V. Nagel, F. Rösch, NODAPA-OH and NODAPA-(NCS)n: Synthesis, 68Ga-radiolabelling and in vitro characterisation of novel versatile bifunctional chelators for molecular imaging, Bioorg. Med. Chem. Lett., 18 (2008) 5364-5367.

[15] L.M. De León-Rodríguez, Z. Kovacs, The Synthesis and Chelation Chemistry of DOTA−Peptide Conjugates, Bioconjugate Chem., 19 (2008) 391-402.

[16] J. Fichna, A. Janecka, Synthesis of Target-Specific Radiolabeled Peptides for Diagnostic Imaging, Bioconjugate Chem., 14 (2003) 3-17.

[17] S. Liu, D.S. Edwards, Bifunctional Chelators for Therapeutic Lanthanide Radiopharmaceuticals, Bioconjugate Chem., 12 (2001) 7-34.

[18] G. Anderegg, F. Arnaud-Neu, R. Delgado, J. Felcman, K. Popov, Critical evaluation of stability constants of metal complexes of complexones for biomedical and environmental applications* (IUPAC Technical Report), in: Pure and Applied Chemistry, 2005, pp. 1445.

[19] M. Jamous, U. Haberkorn, W. Mier, Synthesis of Peptide Radiopharmaceuticals for the Therapy and Diagnosis of Tumor Diseases, Molecules, 18 (2013) 3379.

[20] S. Liu, The role of coordination chemistry in the development of target-specific radiopharmaceuticals, Chem. Soc. Rev., 33 (2004) 445-461.

[21] M. Fani, H.R. Maecke, S.M. Okarvi, Radiolabeled Peptides: Valuable Tools for the Detection and Treatment of Cancer, Theranostics, 2 (2012) 481-501.

[22] M. Takahashi, S. Takamoto, The preparation of trivalent metal chelates with some N3O3-type ligands, Bull. Chem. Soc. Jpn., 50 (1977) 3413-3414.

[23] B. Guérin, S. Ait-Mohand, M.-C. Tremblay, V. Dumulon-Perreault, P. Fournier, F. Bénard, Total Solid-Phase Synthesis of NOTA-Functionalized Peptides for PET Imaging, Org. Lett., 12 (2010) 280-283.

[24] J. P. Andre, H. R. Maecke, J. P. Andre, M. Zehnder, L. Macko, K. G. Akyel, 1,4,7-Triazacyclononane-1-succinic acid-4,7-diacetic acid (NODASA): a new bifunctional chelator for radio gallium-labelling of biomolecules, Chem. Commun., (1998) 1301-1302.

[25] K.-P. Eisenwiener, M.I.M. Prata, I. Buschmann, H.-W. Zhang, A.C. Santos, S. Wenger, J.C. Reubi, H.R. Mäcke, NODAGATOC, a New Chelator-Coupled Somatostatin Analogue Labeled with [67/68Ga] and [111In] for SPECT, PET, and Targeted Therapeutic Applications of Somatostatin Receptor (hsst2) Expressing Tumors, Bioconjugate Chem., 13 (2002) 530-541.

[26] **General Procedure for the Synthesis of 1-Amino-2-benzyl-15-[4, 4,7-triazonan-1-yl]-11-(4-hydroxybenzyl)-1,4,7,10,13-pentaoxo-3,6,9,12-tetraazahexadecan-16-oic Acid (5)**, The functionalized peptide on resin **4**; 0.0125 mmol was swelled in 1.0 ml CH_2Cl_2 for 5 min followed by filtration, and 1.0 mL of 1 M LiOH (dissolved in MeOH and THF in 1:1 ratio) was added. The reaction was carried out for a period of 30 min at room temperature. The completion of the reaction was monitored by cleaving an aliquot of the compound from the resin and checked by LC–MS as well as analytical HPLC. The resin was washed with about 5.0 mL of THF (2×), DMF (2×), and CH_2Cl_2 (2×) consecutively. Compound 5 (0.0125 mmol) was deprotected and cleaved from the resin using a cocktail of 1.0 mL TFA/H_2O/thioanisole (95:2.5:2.5) over 2 h. The resin was removed by filtration and washed with 1 mL TFA. Further, TFA was evaporated with the aid of N_2 gas bubbling through the mixture. The peptide was then precipitated in 5.0 mL of ice-cold Et_2O. The precipitated peptide was centrifuged and the Et_2O solution was decanted. It was then dissolved in 1.0 mL of water and freeze dried without further purification which gave a yield of 84%. The purity of the synthesis was checked by analytical RP-HPLC which showed

100% purity and characterized by LC–MS. HRMS (ESI+): m/z calcd. for $C_{36}H_{49}N_8O_{12}$ [M + H]: 785.3464; found: 785.3434.

Supporting information

General information:

All the chemicals were purchased from commercial sources and used without further purification. Mono-methyl fumarate, tert-butyl bromoacetate, *N*,*N*-diisopropylethylamine (DIPEA), lithium hydroxide (LiOH), tetrahydrofuran (THF), dichloromethane (DCM), dimethylformamide (DMF) were purchased form Sigma-Aldrich. 1,4,7 triazacyclononane was purchased from Leap LabChem. Fmoc-Phe-OH, Fmoc-Gly-OH, Fmoc-Tyr (tBu)-OH, Fmoc-OSu and rinkamide MBHA were purchased from GL Biochem (Shanghai). Coupling reagents used were **1**-[bis(dimethylamino)methylene]-1*H*-1,2,3-triazolo[4,5-*b*] pyridinium 3-oxid hexafluorophosphate (HATU) from Luxembourg Biotech, *N*,*N*-diisopropylethylamine (DIPEA) from Sigma-Aldrich , *N,N′*-diisopropylcarbodiimide **(**DIC) (Fluka, lot number BCBK8348 V) and oxyma (Luxembourg Biotech).

All compounds were analyzed by RP-HPLC (Agilent 1100, USA). Runs were performed using a linear gradient of solvent A (0.1% TFA in H_2O) and solvent B (0.1% TFA in ACN); where the gradient was 5% B to 95% B in 15 min at a flow rate of 1 ml/min. All the synthetic steps were further characterized using LCMS (Shimadzu 2020 UFLC-MS, Japan) with an YMC-Triart C18 (5 μm, 4.6 × 150 mm) column for their respective masses. NMR spectra (^{1}H NMR, ^{13}C NMR, HMBC and HSQC) were recorded on a Bruker AVANCE III 400 MHz spectrometer using deuterated methanol as the solvent. HRMS was carried out on a Bruker microTOF-QII.

Peptide synthesis:

The model peptide YGGF was synthesized using Fmoc chemistry in solid phase at 0.1 mmol scale. Amino acids were dissolved in 1.0 ml of DMF along with HATU and DIPEA followed by addition to the resin. The ratio of Fmoc protected amino acid to free amine was 2:1 and each coupling was carried out for 1hr. A ratio of 1:1:2 of amino acid: HATU: DIPEA was employed in the synthesis. Fmoc deprotection was performed in 4.0 ml of 20% piperdine in DMF for 5 minutes twice. In all the steps the resin was washed with approx. 5.0 ml of DMF (2 x), DCM (2 x) and DMF (2 x) consecutively. An aliquot of the synthesized peptide was cleaved from the resin and monitored by HPLC as well as LCMS.

4-Methoxy-4-oxo-3-(1,4,7-triazonan-1-yl)butanoic acid (1):

1,4,7-triazacyclononane (991.5 mg, 2.0 equiv.) and DIPEA (1.33 ml, 2.0 equiv.) were dissolved in 10 ml DCM. To this solution, 500 mg (1.0 equiv.) of Mono-methyl fumarate pre dissolved in

1.0 ml DCM was added drop-wise over a period of 10-15 min. After 2 hr of agitation, the DCM was removed *in vacuo*. The product was further dissolved in 4.0 ml DMF and kept overnight at -20 ºC for the precipitation of the (1). The DMF was decanted and the residual DMF was co-evaporated with toluene *in vacuo* which gave a yield of 94%. **^{1}HNMR (400 MHz, MeOD):** δ 3.36 (1H, t), 2.93 (2H, m), 2.74 (2H, m), 2.61-2.70 (2H, m), 2.58 (2H, m), 2.56 (3H, s), 2.36-2.51 (5H, m), 2.24 (1H, m) ; **^{13}C NMR (100 MHz, MeOD):** δ 179.4, 175.3, 64.4, 52.2 (2), 50.3, 46.8 (2), 45.8 (2), 35.1. HRMS (ESI^{+}): calcd. for $C_{11}H_{22}N_3O_4$ [M+H] 260.1605; found 260.1612.

***3-(4,7-Bis(((9H-fluoren-9-yl)methoxy)carbonyl)-1,4,7-triazonan-1-yl)-4-methoxy-4-oxobutanoic acid* (2):**

Compound 1 (100 mg, 1.0 equiv.) and $NaHCO_3$ (162 mg, 5 equiv.) was dissolved in 60 ml of water and acetone (1:1). The mixture was cooled down to 0 ºC and 286 mg (2.2 equiv.) of Fmoc-OSu pre-dissolved in 2.0 ml acetone was added dropwise over a period of 10-15 min followed by overnight stirring. The reaction was then concentrated *in vacuo* and extracted with diethyl ether to remove the unreacted Fmoc-OSu. Thereafter, the resulting reaction mixture was acidified with 10 ml 1M HCl followed by extraction of the compound with 50 ml diethyl ether. The organic layer was evaporated *in vacuo* to give a white solid yielding 82%. LCMS (positive mode) showed desired m/z 704. The product was then used for the next step without further purification.

Methyl 1-amino-2-benzyl-11-(4-hydroxybenzyl)-1,4,7,10,13-pentaoxo-15-(1,4,7-triazonan-1-yl)-3,6,9,12-tetraazahexadecan-16-oate on resin (3):

Compound 2 was coupled to the synthesized peptide on resin at 0.0125 mmol scale. Compound (2) was dissolved in 0.5 ml of DMF along with DIC and OxymaPure followed by 2 min activation. The entire mixture was then added to the resin containing the model peptide and the reaction was carried out for 16 hr. A ratio of 1:1:1: (2):DIC:OxymaPure was used in the synthesis. Compound (2) to free amine ratio was 2:1. In all the steps resin was washed with about 5.0 ml each of DMF (2 x), DCM (2 x) and DMF (2 x). The Fmoc group was removed using 4.0 ml of 20% piperdine in DMF along with 0.5M HOBt to produce compound 3. The resin was washed using approx. 5.0 ml of DMF (2 x) and DCM (2 x) consecutively. An aliquot of the synthesized peptide was cleaved from the resin and monitored by analytical HPLC as well as LCMS. LCMS (positive mode) showed desired m/z 683.

Tert-butyl 2,2'-(7-(18-amino-17-benzyl-8-(4-hydroxybenzyl)-3,6,9,12,15,18-hexaoxo-2-oxa-7,10,13,16-tetraazaoctadecan-4-yl)-1,4,7-triazonane-1,4-diyl)diacetate on resin (4):

Compound (3); 0.0125 mmol was swelled with 1 ml DCM for 5 min followed by filtration, to which tert-butyl bromoacetate (5.5 µl, 3.0 equiv.) and DIPEA (6.5 µl, 3.0 equiv.) in 0.4 ml of

NMP was added and the reaction mixture left to stir for 2.5 hr [1]. The resin was washed with approx. 5.0 ml of DMF (2x) and DCM (2x) consecutively. An aliquot of the synthesized compound was cleaved from the resin and monitored by analytical HPLC. LCMS (positive mode) showed its desired m/z 799.

1-amino-2-benzyl-15-(4,7-bis(2-tert-butoxy-2-oxoethyl)-1,4,7-triazonan-1-yl)-11-(4-hydroxybenzyl)-1,4,7,10,13-pentaoxo-3,6,9,12-tetraazahexadecan-16-oic acid (5):

The functionalized peptide on resin (4); 0.0125 mmol was swelled in 1.0 ml DCM for 5 min followed by filtration, and 1.0 ml of 1M LiOH (dissolved in methanol and THF in 1:1 ratio) was added. The reaction was carried out for a period of 30 min at room temperature. The completion of the reaction was monitored by cleaving an aliquot of the compound from the resin and checked by LCMS as well as analytical HPLC. The resin was washed with about 5.0 ml of THF (2x), DMF (2x), and DCM (2x) consecutively. Compound 5 (0.0125 mmol) was deprotected and cleaved from the resin using a cocktail of 1.0 ml TFA:H_2O:thioanisole (95:2.5:2.5) over 2 hr. The resin was removed by filtration and washed with 1 ml TFA. Further, TFA was evaporated with the aid of N_2 gas bubbling through the mixture. The peptide was then precipitated in 5.0 ml of ice-cold diethyl ether. The precipitated peptide was centrifuged and the diethyl ether solution was decanted. It was then dissolved in 1.0 ml of water and freeze dried without further purification which gave a yield of 84%. The purity of the synthesis was checked by analytical RP-HPLC which showed 100% purity and characterized by LCMS. HRMS (ESI^+): calcd. for $C_{36}H_{49}N_8O_{12}$ [M+H] 785.3464; found 785.3434.

Conjugation of cold Ga to NODASA-Peptide:

Cold Ga was labelled to NODASA peptide as described before by Peter A. Knetsch *et. al* [2]. 1.0 mg of NODASA-peptide (**6**) was dissolved in 828 µl of water; 167 µl 1.9M sodium acetate and 5 µl of 0.7M $^{69}GaCl_3$. The solution was allowed to react for 15 min at room temperature. Excess $^{69}GaCl_3$ was filtered through a SPE C18 cartridge and conjugated NODASA-Peptide was eluted in 50% methanol. The ^{69}Ga conjugation was further confirmed by ESI-LCMS. HRMS (ESI^+): calcd. for $C_{36}H_{46}GaN_8O_{12}$ [M+H] 851.2486; found 851.2534.

Transchelation assay:

The stability of ^{69}Ga NODAGA complexation was carried out by the EDTA challenge as described by previous researchers [3]. ^{69}Ga [NODASA]-peptide was incubated with 500 fold excess of EDTA at room temperature. Samples were tested for transchelation at six different time points i.e. 0 min, 30 min, 60 min, 120 min, 180 min and 240 min respectively and monitored using Q-TOF LCMS.

Reference:

[1] B. Guérin, S. Ait-Mohand, M.-C. Tremblay, V. Dumulon-Perreault, P. Fournier, F. Bénard, Total Solid-Phase Synthesis of NOTA-Functionalized Peptides for PET Imaging, Organic Letters, 12 (2010) 280-283.

[2] P. Knetsch, M. Petrik, C. Griessinger, C. Rangger, M. Fani, C. Kesenheimer, E. von Guggenberg, B. Pichler, I. Virgolini, C. Decristoforo, R. Haubner, [68Ga]NODAGA-RGD for imaging αvβ3 integrin expression, Eur J Nucl Med Mol Imaging, 38 (2011) 1303-1312.

[3] J. Strand, H. Honarvar, A. Perols, A. Orlova, R.K. Selvaraju, A.E. Karlström, V. Tolmachev, Influence of Macrocyclic Chelators on the Targeting Properties of ⁶⁸Ga-Labeled Synthetic Affibody Molecules: Comparison with ¹¹¹In-Labeled Counterparts, PLoS ONE, 8 (2013) e70028.

Spectral Data

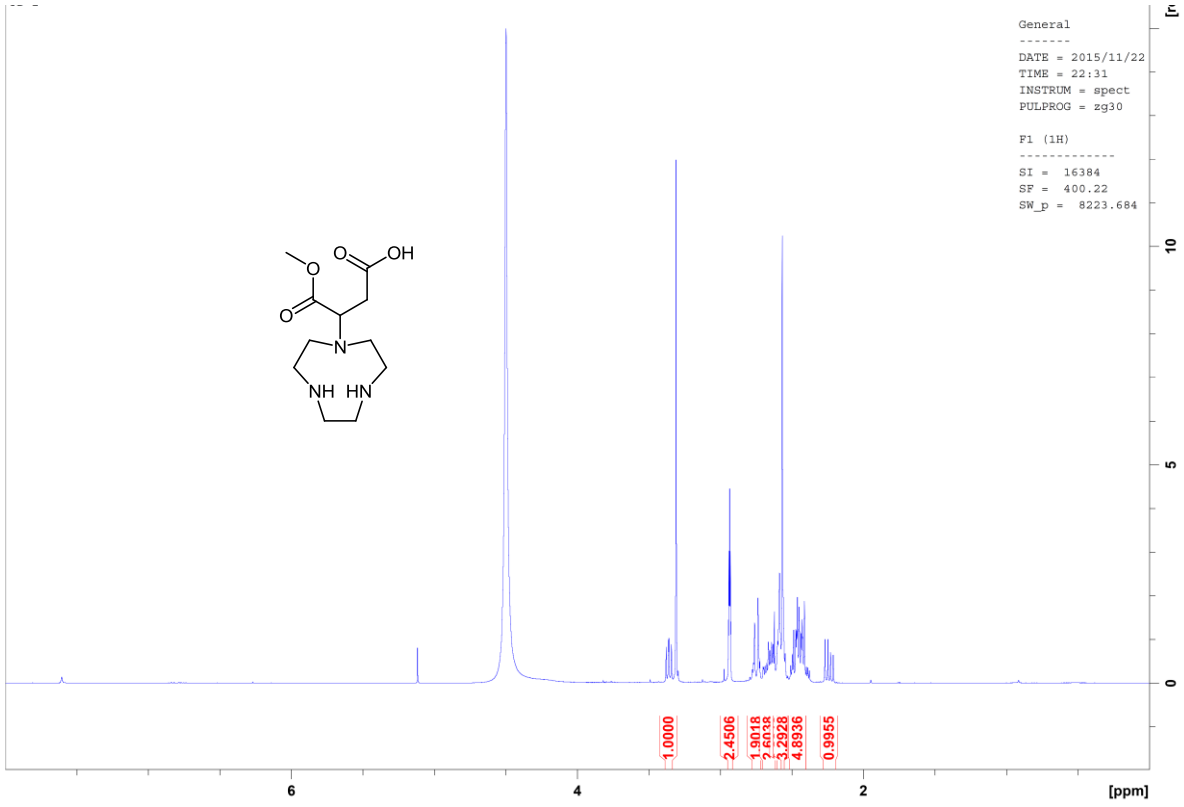

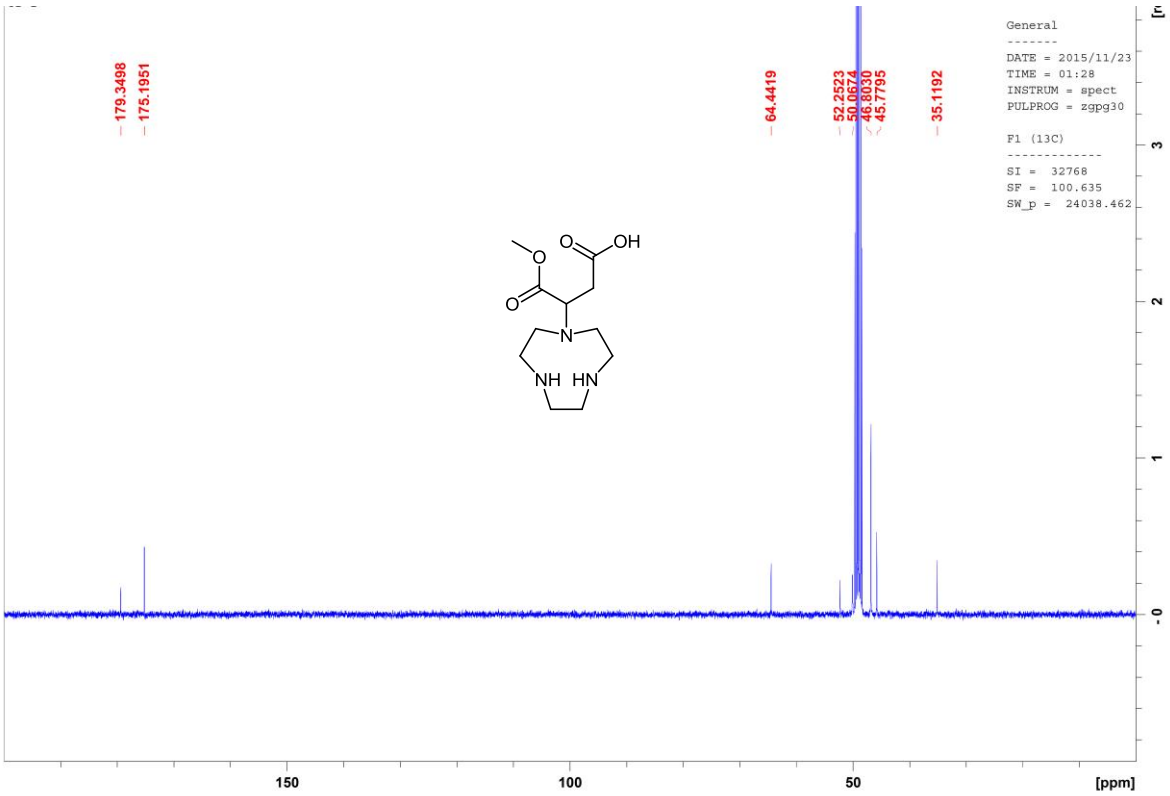
179.3498
175.1951
64.4419
52.2523
50.0674
46.8030
45.7795
35.1192
General
DATE = 2015/11/23
TIME = 01:28
INSTRUM = spect
PULPROG = zgpg30
F1 (13C)
SI = 32768
SF = 100.635
SW_p = 24038.462
O
OH
O
N
NH HN
150
100
50
[ppm]

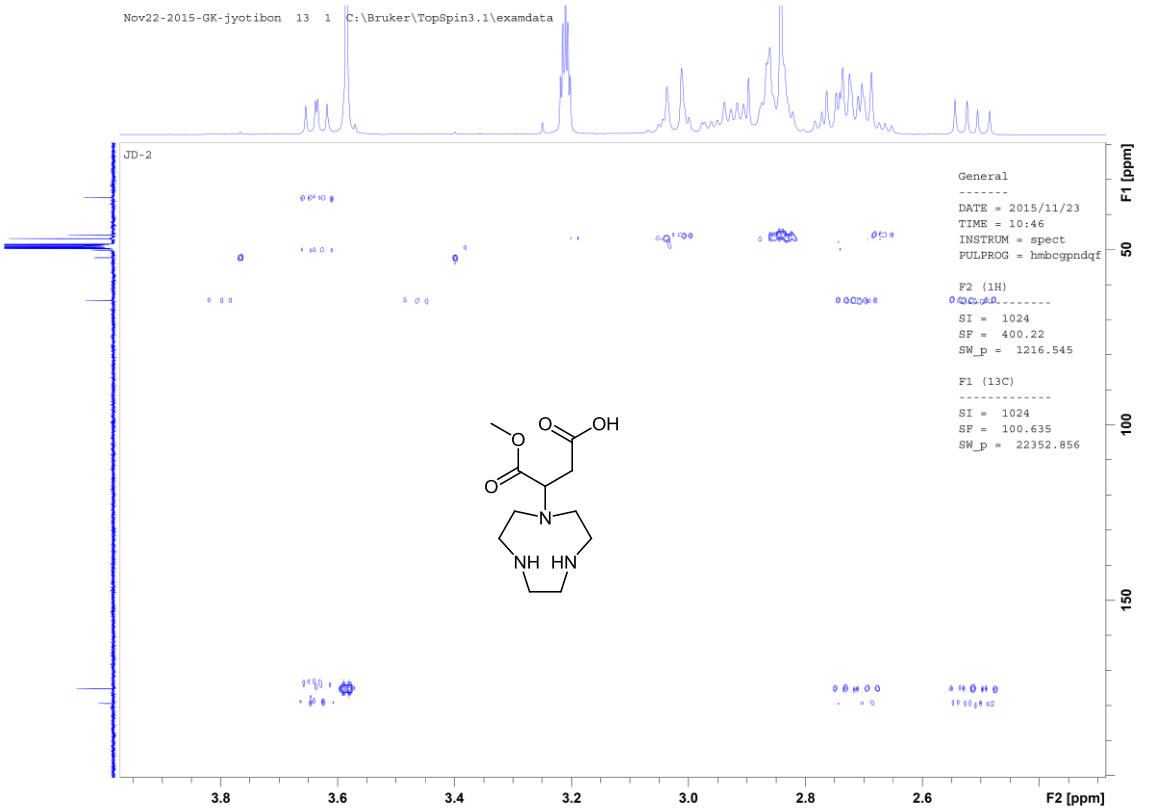
Nov22-2015-GK-jyotibon 13 1 C:\Bruker\TopSpin3.1\examdata
JD-2
General
DATE = 2015/11/23
TIME = 10:46
INSTRUM = spect
PULPROG = hmbcgpndqf
F2 (1H)
SI = 1024
SF = 400.22
SW_p = 1216.545
F1 (13C)
SI = 1024
SF = 100.635
SW_p = 22352.856
O
OH
O
N
NH HN
F1 [ppm]
F2 [ppm]
3.8
3.6
3.4
3.2
3.0
2.8
2.6

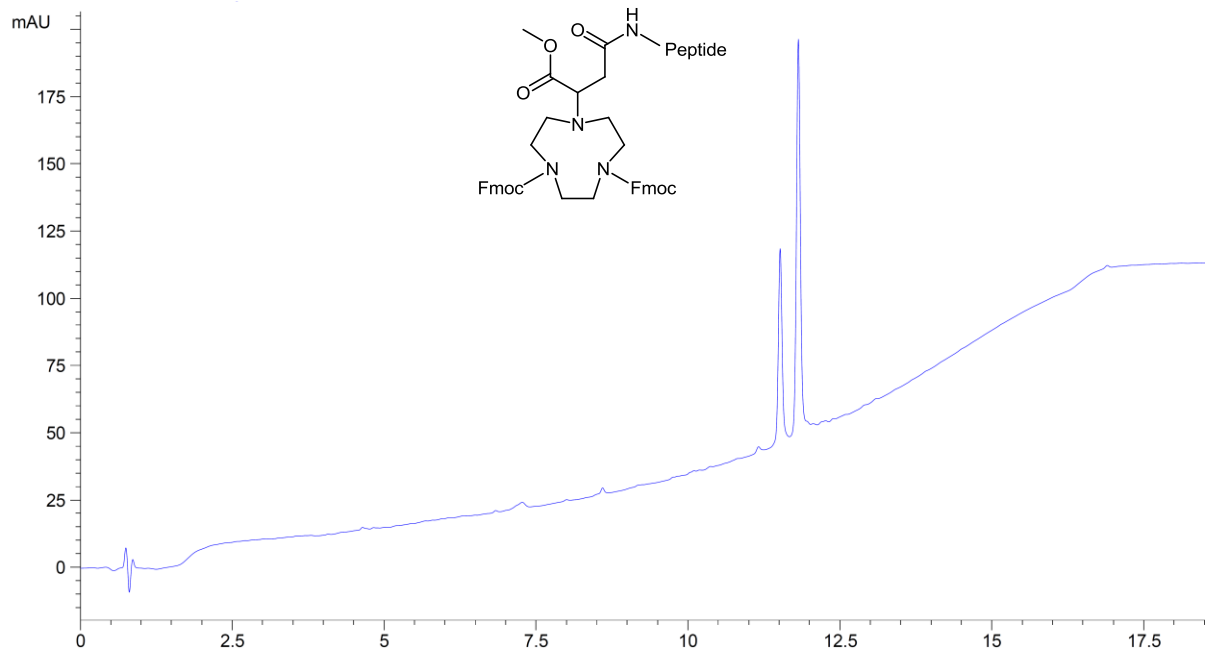
mAU
175
150
125
100
75
50
25
0
0
2.5
5
7.5
10
12.5
15
17.5
O
O
H
N
Peptide
N
N
N
Fmoc
Fmoc

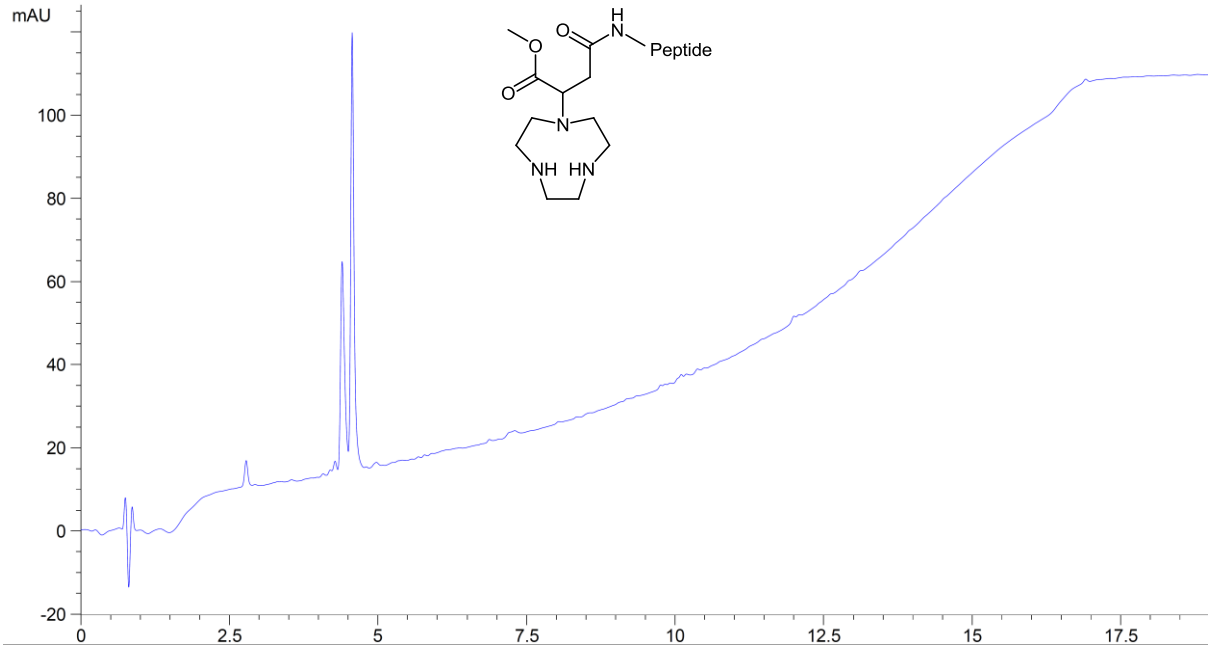
mAU
100
80
60
40
20
0
-20
0
2.5
5
7.5
10
12.5
15
17.5
O
O
H
N
Peptide
N
NH
HN

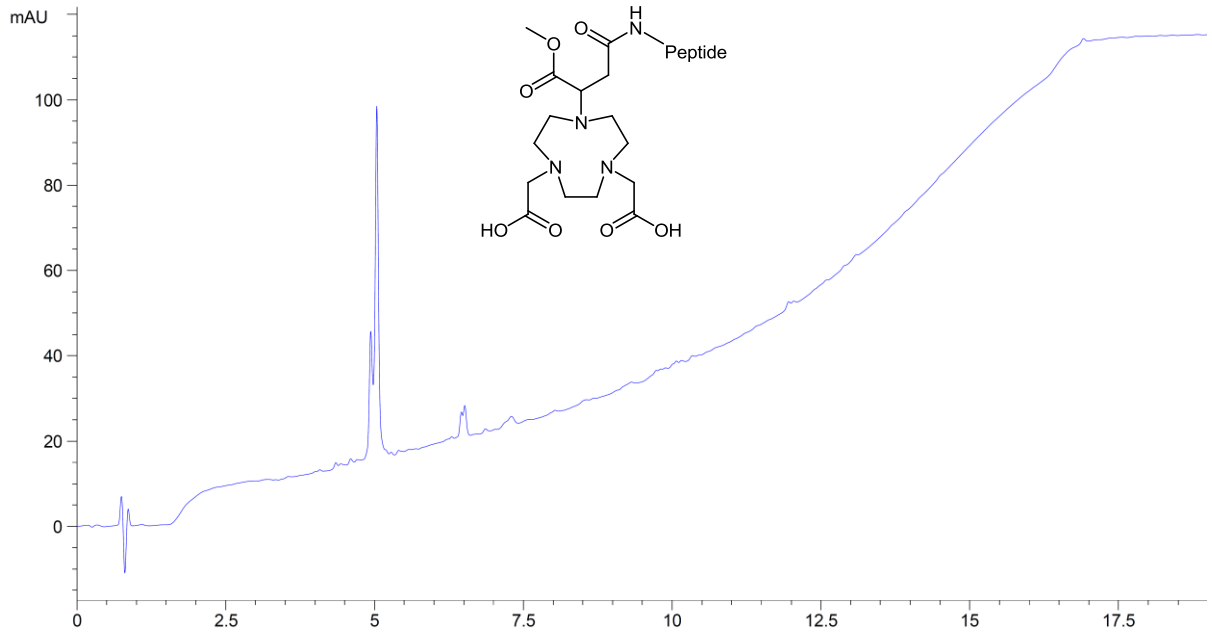
mAU
100
80
60
40
20
0
0
2.5
5
7.5
10
12.5
15
17.5
H
N
O
Peptide
O
O
N
N
N
HO
O
O
OH

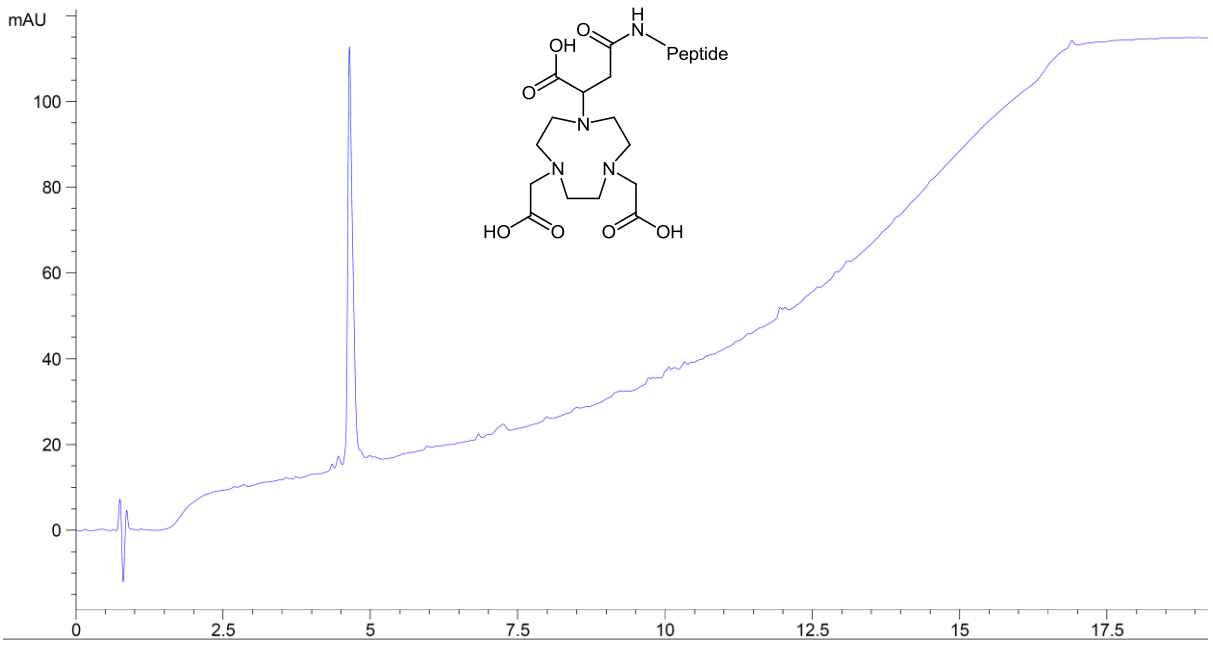
mAU
100
80
60
40
20
0
0
2.5
5
7.5
10
12.5
15
17.5
H
N
O
Peptide
OH
O
N
N
N
HO
O
O
OH

Chapter 4

Optimized Microwave Assisted Synthesis of LL37, a Cathelicidin Human Antimicrobial Peptide

Jyotibon Dutta,[a] Suhas Ramesh,[a] Siduduzo M. Radebe,[a] Anou M. Somboro,[a,b] Beatriz G. de la Torre,[a,d] Hendrik G. Kruger,[a] Sabiha Y. Essack,[b] Fernando Albericio,[a,c,d,e,f] and Thavendran Govender[a*]

[a] Catalysis and Peptide Research Unit, Department of Pharmacy, School of Health Sciences, University of KwaZulu-Natal, Durban, South Africa
[b]Antimicrobial Research Unit, School of Health Sciences, University of KwaZulu-Natal, Durban, 4001, South Africa
[c]Institute for Research in Biomedicine and CIBER-BBN, Barcelona 08028, Spain
[d]School of Chemistry, Yachay Tech, Yachay City of Knowledge, 100119-Urcuqui, Ecuador
[e]School of Chemistry and Physics, University of Kwazulu-Natal, Durban 4001, South Africa
[f]Department of Organic Chemistry, University of Barcelona, Barcelona 08028, Spain

** Correspondence to: Thavendran Govender, E-mail: govenderthav@ukzn.ac.za*

Abstract

LL37, a human cathelecidin antimicrobial peptide comprising 37 amino acids has emerged as one of the vital therapeutic peptides associated with a number of biological applications. In this context, we herein report a highly efficient and optimized methodology for the synthesis of LL37 through SPPS assisted by microwave power. Standard conditions employing uronium coupling reagents was unsatisfactory from the 20th amino acid residue onwards. A segmentation approach revealed that the amide bond formation between the Val and Ile was identified as the problematic coupling. It was found that DIC/OxymaPure in conjunction with THF as the solvent gave best results during manual coupling of 20th position Ile and required double coupling as revealed by HPLC and MALDI-TOF MS. In order to verify the synthesis, antibacterial testing was carried out and the results revealed comparable values with that of literature reported.

Keywords: LL37, SPPS, Microwave, DIC, OxymaPure, THF

Abbreviations

DCC: *N,N′*-Dicyclohexylcarbodiimide; DIC: *N,N′*-Diisopropylcarbodiimide; DIPEA: *N,N*-Diisopropylethylamine; DMF: *N,N*-Dimethylformamide; HATU: 1-[Bis(dimethylamino)methylene]-1H-1,2,3-triazolo[4,5-b]pyridinium-3-oxidhexafluorophosphate; HBTU: *N*-[(1H-benzotriazol-1-yl)(dimethylamino)methylene]-*N*-methylmethanaminium hexafluorophosphate *N*-oxide; HOBt: 1-Hydroxybenzotriazole; PyBOP:

(Benzotriazol-1-yloxy) tripyrrolidinophosphonium hexafluorophosphate; TFA: Trifluoroacetic acid; THF: Tetrahydrofuran

1. Introduction

Since the discovery of human cathelicidin protein in 1995 [1], extensive research has been conducted on LL37. This is a 37 amino acid residue of human cationic antimicrobial peptide (hCAP18) from the *C*-terminus and has a linear structure (Fig. 1) [1]. LL37 is widely associated with the innate immune system and is found in various body fluids and cells such as neutrophil granulocytes and human squamous epithelia [1, 2]. Besides its use as a first line of defence for antimicrobial activities, this peptide also plays a role in angiogenesis, cytokine production, histamine release, cell migration, and chemotaxis [3-8]. These biological roles enable LL37 to regulate immune responses, wound healing and neovascularization in injured tissues [7, 8] and hence can be considered as a peptide of high therapeutic value. Studies reveal contradictory involvement of the antimicrobial peptide in cancer [9-14]. Recently, the role of LL37 has been described in anti-tumor activity and tumor surveillance [9, 13, 14]. However, in contrast, different researchers have also reported oncogenic effects [10, 12]. As this peptide shows diversified biological activities, relatively large quantities are required to study its mechanism both in culture conditions as well as in animal models.

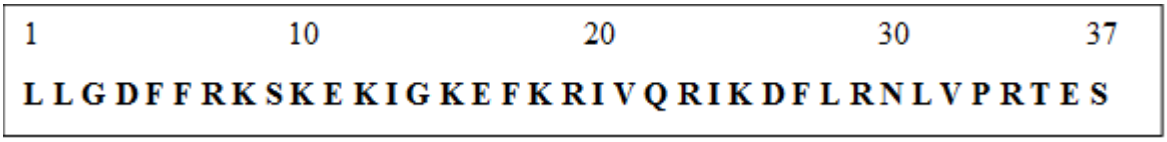

Fig. 1 Primary structure of full length human LL37; Amino acids have been numbered sequentially from the *N*-terminus and the same has been used throughout the text

LL37 being a "good old" peptide, synthesis of which is routinely carried out in several laboratories. Johansson *et al.* first described the use of *t*-butoxycarbonyl amino acid derivatives for the solid-phase synthesis of LL37 using double coupling of arginine, glutamine, and asparagine residues [15]. Since then Fmoc chemistry have been the choice approach reported by many research groups [5, 6, 16-22]. All of the syntheses described were vague with regards to reaction conditions, yields and purities. Till now LL37 has been synthesised using various coupling reagents including HATU/DIEA [22], PyBOP [22], DIC/HOBt [18], and DCC/HOBt [20]. But none of these articles describe the synthetic conditions/protocols employed. Moreover, to the best of our knowledge there are no reports comparing the efficiency of coupling reagents for the synthesis of this peptide.

The established method of microwave assisted solid phase peptide synthesis has revolutionised this field. It has been reported to not only increase coupling efficiency but to also overcome near impossible coupling steps and in shorter time [23-26]. Microwave energy activates molecules based on its dipole rotation or ionic conduction, subsequently rapid heating of the molecule [27]. The heating efficiency is subjective to reactants, solvents, reaction volumes and the mode of mixing [28]. In microwave assisted peptide synthesis optimization of the temperature remains the critical factor to evade side reactions and racemization [29].

ChemMatrix® resin performs extremely well compared to polystyrene resins in the solid-phase synthesis of hydrophobic, highly structured peptides such as poly-Arg peptide and *β*-amyloid (1-42) [30-34]. Thus, ChemMatrix resins have been reported as the resin of choice for synthesis of hydrophobic and long peptides [31-33].

In view of the aforementioned shortcomings, in this communication we would like to describe for the first time the complete synthetic approach of LL37 aided by microwave assisted solid phase peptide synthesis using ChemMatrix resin. We also compared the coupling efficacies of HATU/DIPEA, HBTU/DIPEA and DIC/OxymaPure coupling systems.

2. Materials and Methods

2.1. Reagents

All 9-fluorenylmethoxycarbonyl (Fmoc) protected amino acids and coupling reagents were purchased from GLS Biochem Systems, Inc., China and OxymaPure from (Luxembourg Biotechnologies Ltd., Israel). The side chain functionalities were protected with *tert*butyl (Asp, Glu, Ser, Thr), *tert*-butyloxycarbonyl (Lys), NG-2,2,4,6,7-pentamethyldihydrobenzofuran-5-sulfonyl (Arg), and trityl (Asn, Gln) groups. Rink amide-ChemMatrix resin (Loading: 0.48 mmol/g) was purchased from PCAS BioMatrix Inc (USA). All solvents for synthesis and purification were of HPLC grade and purchased from Sigma-Aldrich (Germany).

2.2. Peptide Synthesis

Peptides were synthesized on a 0.1 mmol scale using a CEM microwave peptide synthesizer (USA).

2.2.1. Deprotection:

Fmoc deprotection was carried out with 20% piperidine/DMF (v/v) along with 0.1M HOBt under microwave condition at 70 °C for 2 min. Based on the previous experience/ literature, we thought Asp would lead to aspartimide formation in the sequence. Several acids have been used in order to protonate piperidine thereby reducing the aspartimide formation. In this sense, we have used

readily available, less expensive additive, HOBt (*p*Ka = 4.60) in piperidine to reduce aspartimide formation [35].

2.2.2. Coupling

Coupling was performed using various combinations of reagents and solvents. Amino acid/HBTU/DIPEA in DMF 1:1:2; Amino acid/HATU/DIPEA in DMF 1:1:2 and using Amino acid/DIC/OxymaPure in DMF 1:1:2; Amino acid/DIC/OxymaPure in THF 1:1:1. The ratio of amino acid to free amine on the resin was 5:1 for all amino acids used in the peptide synthesizer. DMF top and bottom washes were performed between deprotection and coupling steps. The standard microwave settings from the manufacturer were modified according to Table 1. All manual coupling were performed with 1:1:1 Amino acid/DIC/OxymaPure in THF using three equivalents of the respective amino acids [36].

Table 1 Coupling conditions under different activating reagents used in this study

Coupling reagents	Coupling condition	Temperature (°C)	Time (S)
HBTU/ DIPEA (Complete sequence)	mw	25	1,500
		75	300
HATU/ DIPEA (Complete sequence)	mw	25	1,500
		75	300
DIC/ OxymaPure in DMF (segment synthesis: 17+Ile+19)	mw	25	1,500
		75	300
	mw	75	300
DIC/ OxymaPure in THF	No mw	25	3,600

2.2.3. Cleavage

Peptides were cleaved from the resin employing a mixture of 95:2.5:2.5 TFA/thioanisole/water for two hours.

2.2.4. Purification of LL37

LL37 was purified directly via an ACE C_{18} preparative column (150 x 21.2 mm). A two-buffer system was employed utilizing TFA as the ion-pairing agent. Buffer A consisted of 0.1 % TFA/H_2O (v/v) and buffer B consisted of 0.1 % TFA/acetonitrile (v/v). A gradient of 20–70 %

buffer B over 30 min with a flow rate of 10 mL/min was used with UV detection at 220 nm and the fractions with purity >95 % were pooled, evaporated to 10 mL, frozen in liquid nitrogen and lyophilized.

2.3. Peptide analysis

Peptides were analyzed with an Agilent 1100 HPLC on a Waters XBridge C_{18} column (50 x 3.6 mm) over 15 min using a gradient of 5-95 % buffer B at a flow rate of 1 mL/min and UV detected at 220 nm. MALDI was performed with an Autoflex III instrument (Bruker), recorded in linear mode using α-cyano-4-hydroxycinnamic acid (HCCA) as matrix.

2.4. Antibacterial test

The antimicrobial activity of LL37 was tested against two gram positive bacteria *S. aureus* ATCC 25923 and *E. faecalis* ATCC 29212; along with two gram negative bacteria *E. coli* ATCC 25922 and *S. enterica* ATCC 10708 using broth dilution method as described previously [37].

3. Results and Discussion

3.1. LL37 synthetic approaches

Our initial attempts to synthesize the complete sequence of LL37 was with the uronium coupling reagents; HBTU and HATU, which gave poor results as analysed by HPLC. For these uronium coupling reagents double coupling was performed for all Ser, Arg, Val, Leu and Ile amino acids residues. A MALDI-TOF mass spectrum (Fig. 2) illustrates the non-specific products which are mainly found in the region from m/z 2100 to m/z 3100 along with a weak signal for the desired product at m/z 4493. Analysis of this region, lead us to conclude that m/z 2179 represented the peptide fragment with 21–37 amino acid residues incorporating two *t*Bu protecting groups due to incomplete deprotection. This can be confirmed by the presence of a peak at m/z 4604 that is representative our desired peptide also with two *t*Bu protecting groups. Subsequently, signals at m/z 2292, 2449, 2578, 2726, 2853 and 2982 represented fragments up to the 20^{th}, 19^{th}, 18^{th}, 17^{th}, 16^{th} and 15^{th} amino acid residues respectively. These results implied that the coupling efficiency decreased from the 20^{th} amino acid residue, i.e. the coupling of ^{20}Ile to ^{21}Val which persisted up to the 15^{th} position.

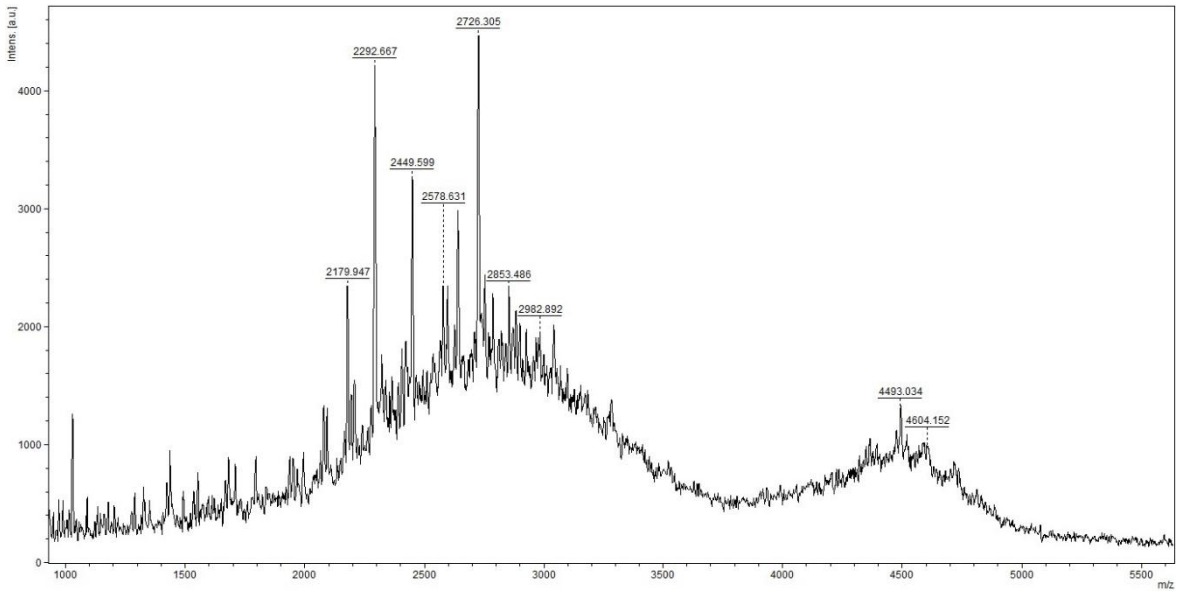

Fig. 2 MALDI analysis of full sequence synthesis of LL37 using HATU/DIPEA as coupling reagent

To investigate further, we performed the segment extension approach using HATU/DIPEA and the fragments identified were 33–37, 21–32, 16–20 and 11–15 (Fig. 3). In this approach, the amino acid sequence corresponding to the region 33-37, gave the desired peptide mass (LCMS ESI: m/z 587) and was successfully extended to residue 21 (Fig. S1). This efficient synthesis was realised with single coupling of the amino acids for 5 min at 75 °C under microwave conditions besides for Arg residues that needed double couplings of 25 min at 25 °C followed by 5 min at 75 °C. Further extension of the segment (i.e. residues 16–20) gave less resolved HPLC traces and MALDI TOF MS revealed non-specific masses along with the desired peptide at m/z 2742 (Fig. S2). Even though the above mentioned coupling conditions were maintained, nonspecific masses at m/z 2170, 2207, 2291, 2447, 2575, 2613 as well as at 2638 were observed. These results correspond to inefficient coupling in this region which was increased upon further extension up to the 11th residue which gave rise to corresponding non-specific masses at m/z 2200–3300 (Fig. 4). These findings proved that LL37 has difficult fragments with respect to coupling especially from the 16-20 amino acid residues.

Fig. 3 Fragment-based synthetic approach of LL37 (I) fragment 33-37 (II) fragment 21-37, (III) fragment 16-37, (IV) fragment 11-37 and (V) fragment 1-37. Difficult coupling region/ amino acids as found out experimentally are shown in red.

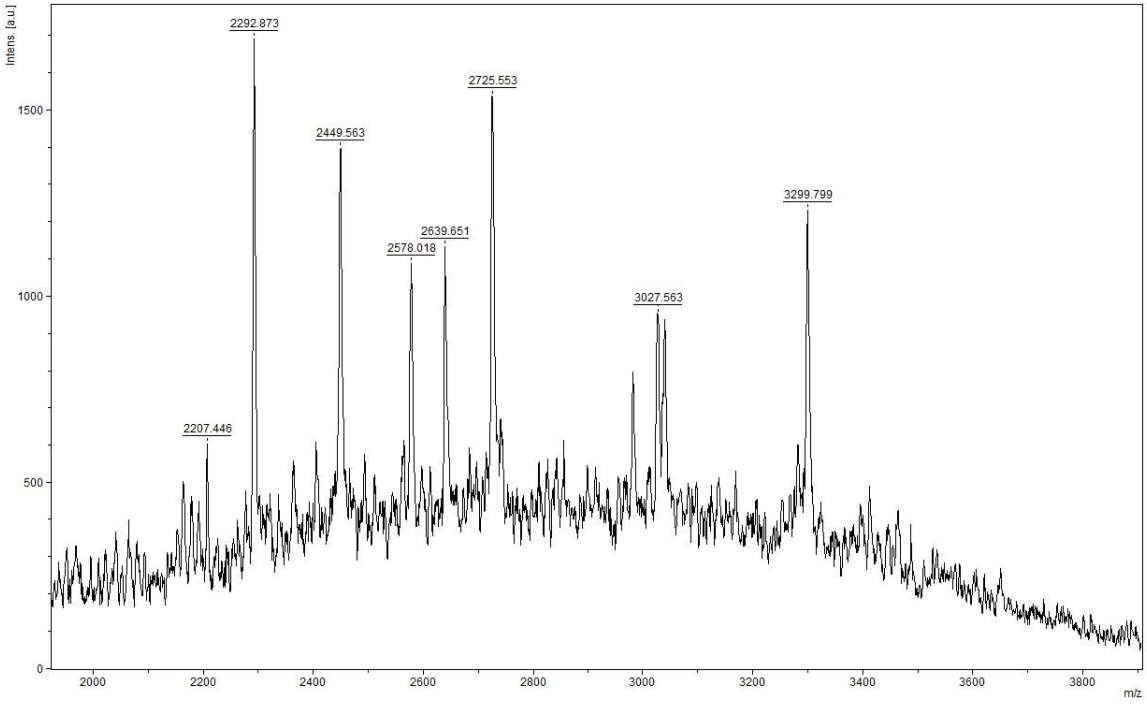

Fig. 4 MALDI analysis of the extended peptide fragment (11-37)

In the next approach we synthesized the peptide with the amino acids sequence ‘‘21–37’’ in the synthesizer with HATU/DIPEA. We decided to use extended coupling times over the region 16–20 and therefore needed to change the coupling reagents and conditions. A DIC-mediated coupling condition was chosen because it is more stable at extended durations under reaction conditions than standalone reagents such as HATU or HBTU [38]. Carbodiimide methods are usually used in combination with additives, mainly *N*-hydroxyamine such as HOBt, HOAt and OxymaPure [39, 40], from these OxymaPure was elected as benzotriazole derivatives (HOBt and

HOAt) showed explosive properties [41]. Furthermore, OxymaPure showed superior performance over HOBt and in some cases similar results to HOAt [39, 40, 42]. Recently, we observed that using THF instead of DMF in combination with DIC/OxymaPure and ChemMatrix resin at room temperature showed an approximately double coupling efficiency than DMF during synthesis of difficult sequences containing Aib (α-α-disubstituted amino acid) such as Aib-enkephalin and Aib-ACP analogues [36]. The subsequent amino acid residues; Ile, Arg, Lys and Phe were sequentially coupled to the 21-37 amino acid sequence manually using DIC/OxymaPure in THF and monitored by ninhydrin test for free amines. The Ile residue showed necessity for double couplings for 1 hour each; but the other amino acid residues *viz.* Arg, Lys and Phe required only single coupling reactions. This confirmed that the Ile in the 20^{th} position is a problematic coupling residue as well as DIC/OxymaPure in THF is a better combination of coupling system for the segment Phe-Lys-Arg-Ile-Val in LL37. We synthesized the 21–37 fragment in the automated synthesizer using DIC/OxymaPure in DMF under microwave conditions. The following ^{20}Ile amino acid residue was double coupled manually using DIC/OxymaPure as coupling reagent in THF for one hour each at ambient temperatures. Subsequent extension of the sequence after this residue was completed in the synthesizer under microwave conditions and resulted in the desired peptide with a strong signal for m/z 4493 in MALDI-TOF MS of the crude product. The HPLC analysis of the crude product showed a much improved profile with a 52 % purity (Fig. 5a) (pure HPLC trace has been shown in Fig. 6 and MALDI-TOF MS in Fig. S3). We then compared if the synthesis of the entire sequence would benefit from these promising conditions as we found in our recent report [36] but was disasspointed with a lower crude yield of 40 % (Fig. 5b) that we attribute to the possible solubility properties associated with extended peptides. Recently, we came across an article described by Collins *et al.* [30] in which they have established a new protocol for solid-phase synthesis of some standard peptides. The method involves shorter coupling times with higher temperatures, as less as 2 min at 90 °C under microwave power. They were also successful in reducing the percentage of waste that would be generated by earlier methodologies. Inspired by this, we were interested to incorporate these conditions given in this report with minor modifications. In this direction, we used DIC/OxymaPure-enabled microwave assisted SPPS of LL37 using 5 min coupling time at 75 °C and obtained the product in a crude yield of 32 % (Fig. 5c).

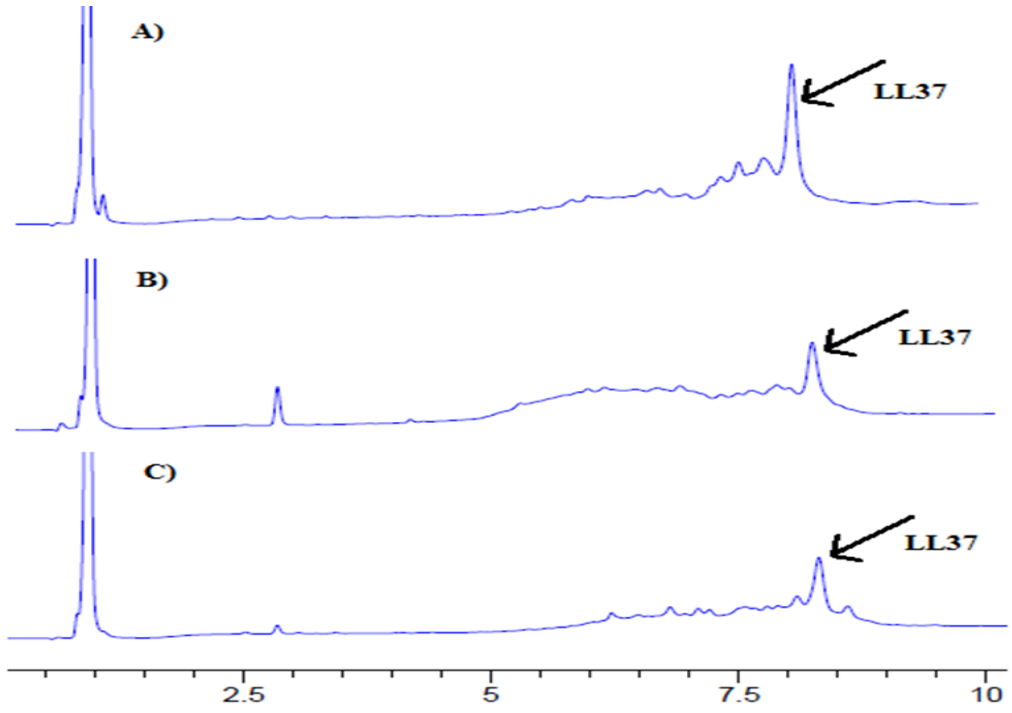

Fig. 5 HPLC chromatograms of synthesis of LL37 (a) modified protocol wherein only 20Ile was coupled manually using DIC/OxymaPure/THF (b) using DIC/OxymaPure/THF under NO microwave power (c) complete sequence using DIC/Oxyma/DMF under microwave

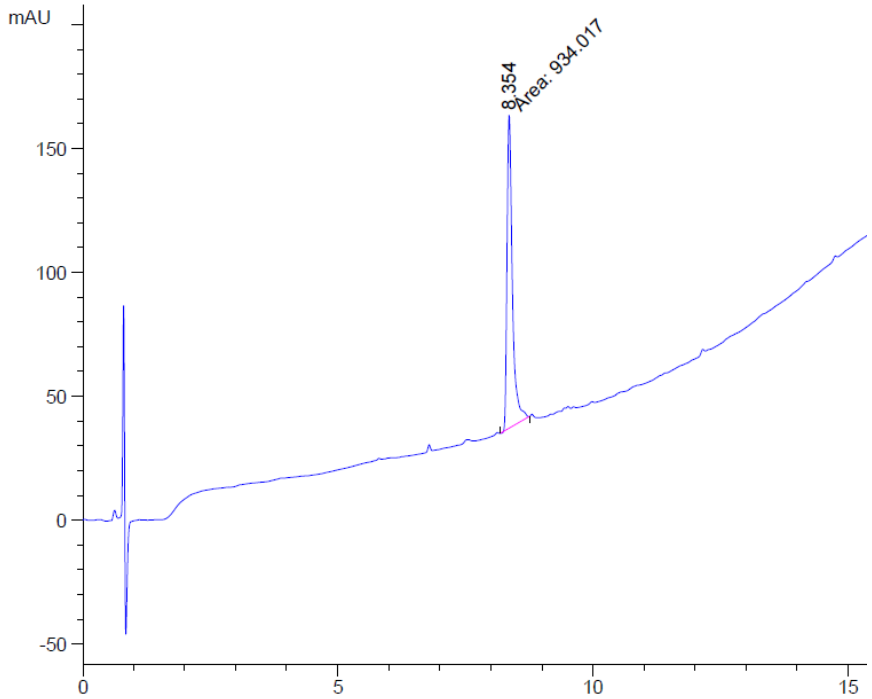

Fig. 6 HPLC chromatogram of purified LL37 obtained by using modified protocol

3.2. Antimicrobial activities

The HPLC purified LL37 was tested for its antimicrobial activity against *S. aureus* ATCC 25923, *E. faecalis* ATCC 29212, *E. coli* ATCC 25922 and *S. enterica* ATCC 10708. The corresponding MICs were listed in Table 2 which resembled with the previous report [37].

Table 2 Antimicrobial activity of pure synthetic LL37

Peptide	**Gram positive bacteria MIC (µg/mL)**		**Gram negative bacteria MIC (µg/mL)**	
	S. aureus *ATCC* 25923	*E. faecalis* *ATCC 29212*	*E. coli* *ATCC 25922*	*S. enterica* *ATCC 10708*
LL37	64	64	32	32

4. Conclusion

In short, we were successful in identifying the difficult region of LL37 peptide and described an efficient synthesis by microwave assisted SPPS with the necessity of manually coupling 20th Ile residue. The use of THF in combination with DIC/OxymaPure in the key coupling step could open a new vista for other difficult peptides also. We further conclude that DIC/OxymaPure system is better than the HBTU/DIPEA and HATU/DIPEA for this synthesis. We also verified the antimicrobial activity of the peptide against a panel of Gram positive and Gram negative bacteria which exhibited MICs comparable to previously reported values. Therefore this work happens to be of sufficient scientific interest from the view of researchers as well as pharmaceutical companies to prepare in bulk quantities.

Acknowledgements:

The authors would like to thank the National Research Foundation, SA; Aspenpharmacare, SA; and the University of KwaZulu-Natal, Durban, SA for having funded this project.

Conflict of Interest: Authors declare no conflict of interest

Human and Animal Rights and Informed Consent: This article does not contain any studies with human or animal subjects performed by any of the authors.

Reference

[1] J.W. Larrick, M. Hirata, R.F. Balint, J. Lee, J. Zhong, S.C. Wright, Human CAP18: a novel antimicrobial lipopolysaccharide-binding protein, Infect. Immun., 63 (1995) 1291-1297.

[2] M.F. Nilsson, B. Sandstedt, O. Sorensen, G. Weber, N. Borregaard, M. Stahle-Backdahl, The human cationic antimicrobial protein (hCAP18), a peptide antibiotic, is widely expressed in human squamous epithelia and colocalizes with interleukin-6, Infect. Immun., 67 (1999) 2561-2566.

[3] K. Gill, B.K. Mohanti, A.K. Singh, B. Mishra, S. Dey, The over expression of cathelicidin peptide LL37 in head and neck squamous cell carcinoma: The peptide marker for the prognosis of cancer, Cancer Biomark., 10 (2011) 125-134.

[4] M. Kajiya, H. Shiba, H. Komatsuzawa, K. Ouhara, T. Fujita, K. Takeda, Y. Uchida, N. Mizuno, H. Kawaguchi, H. Kurihara, The Antimicrobial Peptide LL37 Induces the Migration of Human Pulp Cells: A Possible Adjunct for Regenerative Endodontics, J. Endod., 36 (2010) 1009-1013.

[5] M. Kittaka, H. Shiba, M. Kajiya, T. Fujita, T. Iwata, K. Rathvisal, K. Ouhara, K. Takeda, T. Fujita, H. Komatsuzawa, H. Kurihara, The antimicrobial peptide LL37 promotes bone regeneration in a rat calvarial bone defect, Peptides, 46 (2013) 136-142.

[6] M. Kittaka, H. Shiba, M. Kajiya, K. Ouhara, K. Takeda, K. Kanbara, T. Fujita, H. Kawaguchi, H. Komatsuzawa, H. Kurihara, Antimicrobial peptide LL37 promotes vascular endothelial growth factor-A expression in human periodontal ligament cells, J. Periodontal Res., 48 (2013) 228-234.

[7] R. Koczulla, G. von Degenfeld, C. Kupatt, Kr, xF, F. tz, S. Zahler, T. Gloe, Issbr, xFc, K. cker, P. Unterberger, M. Zaiou, C. Lebherz, A. Karl, P. Raake, A. Pfosser, P. Boekstegers, U. Welsch, P.S. Hiemstra, C. Vogelmeier, R.L. Gallo, M. Clauss, R. Bals, An angiogenic role for the human peptide antibiotic LL-37/hCAP-18, J. Clin. Invest., 111 (2003) 1665-1672.

[8] D. Yang, Q. Chen, A.P. Schmidt, G.M. Anderson, J.M. Wang, J. Wooters, J.J. Oppenheim, O. Chertov, LL-37, the neutrophil granule- and epithelial cell-derived cathelicidin, utilizes formyl peptide receptor-like 1 (FPRL1) as a receptor to chemoattract human peripheral blood neutrophils, monocytes, and T cells, J. Exp. Med., 192 (2000) 1069-1074.

[9] C.-M. Chuang, A. Monie, A. Wu, C.-P. Mao, C.-F. Hung, Treatment with LL-37 Peptide Enhances Antitumor Effects Induced by CpG Oligodeoxynucleotides Against Ovarian Cancer, Hum. Gene Ther., 20 (2009) 303-313.

[10] S.B. Coffelt, S.L. Tomchuck, K.J. Zwezdaryk, E.S. Danka, A.B. Scandurro, Leucine Leucine-37 Uses Formyl Peptide Receptor–Like 1 to Activate Signal Transduction Pathways, Stimulate Oncogenic Gene Expression, and Enhance the Invasiveness of Ovarian Cancer Cells, Mol. Cancer Res., 7 (2009) 907-915.

[11] D. Vandamme, B. Landuyt, W. Luyten, L. Schoofs, A comprehensive summary of LL-37, the factotum human cathelicidin peptide, Cell. Immunol., 280 (2012) 22-35.

[12] G. Weber, C. Chamorro, F. Granath, A. Liljegren, S. Zreika, Z. Saidak, B. Sandstedt, S. Rotstein, R. Mentaverri, F. Sanchez, A. Pivarcsi, M. Stahle, Human antimicrobial protein hCAP18/LL-37 promotes a metastatic phenotype in breast cancer, Breast Cancer Res., 11 (2009) R6.

[13] W.K.K. Wu, J.J.Y. Sung, K.F. To, L. Yu, H.T. Li, Z.J. Li, K.M. Chu, J. Yu, C.H. Cho, The host defense peptide LL-37 activates the tumor-suppressing bone morphogenetic protein

signaling via inhibition of proteasome in gastric cancer cells, J. Cell. Physiol., 223 (2010) 178-186.

[14] W.K.K. Wu, G. Wang, S.B. Coffelt, A.M. Betancourt, C.W. Lee, D. Fan, K. Wu, J. Yu, J.J.Y. Sung, C.H. Cho, Emerging roles of the host defense peptide LL-37 in human cancer and its potential therapeutic applications, Int. J. Cancer, 127 (2010) 1741-1747.

[15] J. Johansson, G.H. Gudmundsson, M.n.E. Rottenberg, K.D. Berndt, B. Agerberth, Conformation-dependent Antibacterial Activity of the Naturally Occurring Human Peptide LL-37, J. Biol. Chem., 273 (1998) 3718-3724.

[16] R. Bucki, J.J. Pastore, P. Randhawa, R. Vegners, D.J. Weiner, P.A. Janmey, Antibacterial Activities of Rhodamine B-Conjugated Gelsolin-Derived Peptides Compared to Those of the Antimicrobial Peptides Cathelicidin LL37, Magainin II, and Melittin, Antimicrob. Agents Chemother., 48 (2004) 1526-1533.

[17] M. Gabriel, K. Nazmi, E.C. Veerman, A.V. Nieuw Amerongen, A. Zentner, Preparation of LL-37-Grafted Titanium Surfaces with Bactericidal Activity, Bioconjug. Chem., 17 (2006) 548-550.

[18] E. Kamysz, E. Sikorska, A. Karafova, M. Dawgul, Synthesis, biological activity and conformational analysis of head-to-tail cyclic analogues of LL37 and histatin 5, J. Pept. Sci., 18 (2012) 560-566.

[19] K. Midorikawa, K. Ouhara, H. Komatsuzawa, T. Kawai, S. Yamada, T. Fujiwara, K. Yamazaki, K. Sayama, M.A. Taubman, H. Kurihara, K. Hashimoto, M. Sugai, Staphylococcus aureus Susceptibility to Innate Antimicrobial Peptides, β-Defensins and CAP18, Expressed by Human Keratinocytes, Infect. Immun., 71 (2003) 3730-3739.

[20] Y.H. Nan, J.-K. Bang, B. Jacob, I.-S. Park, S.Y. Shin, Prokaryotic selectivity and LPS-neutralizing activity of short antimicrobial peptides designed from the human antimicrobial peptide LL-37, Peptides, 35 (2012) 239-247.

[21] S.M. Travis, N.N. Anderson, W.R. Forsyth, C. Espiritu, B.D. Conway, E.P. Greenberg, P.B. McCray, R.I. Lehrer, M.J. Welsh, B.F. Tack, Bactericidal Activity of Mammalian Cathelicidin-Derived Peptides, Infect. Immun., 68 (2000) 2748-2755.

[22] I. Zelezetsky, A. Pontillo, L. Puzzi, N. Antcheva, L. Segat, S. Pacor, S. Crovella, A. Tossi, Evolution of the primate cathelicidin - correlation between structural variations and antimicrobial activity, J. Biol. Chem., 281 (2006) 19861-19871.

[23] B. Bacsa, B. Desai, G. Dibó, C.O. Kappe, Rapid solid-phase peptide synthesis using thermal and controlled microwave irradiation, J. Pept. Sci., 12 (2006) 633- 638.

[24] J.M. Collins, N.E. Leadbeater, Microwave energy: a versatile tool for the biosciences, Org. Biomol. Chem., 5 (2007) 1141-1150.

[25] M. Erdelyi, A. Gogoll, Rapid microwave-assisted solid phase peptide synthesis, Synthesis, 11 (2002) 1592-1596.

[26] H.M. Yu, S.T. Chen, K.T. Wang, Enhanced coupling efficiency in solid-phase peptide synthesis by microwave irradiation, J. Org. Chem., 57 (1992) 4781-4784.

[27] G. Vanier, Microwave-Assisted Solid-Phase Peptide Synthesis Based on the Fmoc Protecting Group Strategy (CEM), in: K.J. Jensen, P. Tofteng Shelton, S.L. Pedersen (Eds.) Peptide Synthesis and Applications, Humana Press, 2013, pp. 235-249.

[28] V. Made, S. Els-Heindl, A.G. Beck-Sickinger, Automated solid-phase peptide synthesis to obtain therapeutic peptides, Beilstein J. Org. Chem., 10 (2014) 1197-1212.

[29] S.A. Palasek, Z.J. Cox, J.M. Collins, - Limiting racemization and aspartimide formation in microwave-enhanced Fmoc solid phase peptide synthesis, J. Pept. Sci., 13 (2007) 143- 148.

[30] J.M. Collins, K.A. Porter, S.K. Singh, G.S. Vanier, High-Efficiency Solid Phase Peptide Synthesis (HE-SPPS), Org. Lett., 16 (2014) 940-943.

[31] B. de la Torre, A. Jakab, D. Andreu, Polyethyleneglycol-Based Resins as Solid Supports for the Synthesis of Difficult or Long Peptides, Int. J. Pept. Res. Ther., 13 (2007) 265-270.

[32] F. García-Martín, M. Quintanar-Audelo, Y. García-Ramos, L.J. Cruz, C. Gravel, R. Furic, S. Côté, J. Tulla-Puche, F. Albericio, ChemMatrix, a poly (ethylene glycol)-based support for the solid-phase synthesis of complex peptides, J. Comb. Chem., 8 (2006) 213-220.

[33] F. García-Martín, P. White, R. Steinauer, S. Côté, J. Tulla-Puche, F. Albericio, The synergy of ChemMatrix resin® and pseudoproline building blocks renders Rantes, a complex aggregated chemokine, Biopolymers, 84 (2006) 566-575.

[34] K. Muthusamy, F. Albericio, P.I. Arvidsson, P. Govender, H.G. Kruger, G.E.M. Maguire, T. Govender, Microwave assisted SPPS of amylin and its toxicity of the pure product to RIN-5F cells, Biopolymers, 94 (2010) 323-330.

[35] G.B. Fields, R.H. Angeletti, L.F. Bonewald, W.T. Moore, A.J. Smith, J.T. Stults, L.C. Williams, Correlation of cleavage techniques with side-reactions following solid-phase peptide synthesis, in, Academic, 1995, pp. 539-546.

[36] G.A.A. Yahya E. Jad, Sherine N. Khattab, Beatriz G. de la Torre, Thavendran Govender, Hendrik G. Kruger, Ayman El-Faham and Fernando Albericio. , Peptide Synthesis Beyond DMF: THF and ACN as Excellent and Greener Alternatives. , Org. Biomol. Chem., 13 (2014) 2393-2398.

[37] R.N. Murugan, B. Jacob, E.-H. Kim, M. Ahn, H. Sohn, J.-H. Seo, C. Cheong, J.-K. Hyun, K.S. Lee, S.Y. Shin, J.K. Bang, Non hemolytic short peptidomimetics as a new class of potent and broad-spectrum antimicrobial agents, Bioorg. Med. Chem. Lett., 23 (2013) 4633-4636.

[38] J. Hachmann, M. Lebl, Search for optimal coupling reagent in multiple peptide synthesizer, Biopolymers, 84 (2006) 340-347.

[39] R. Subirós-Funosas, F. Albericio, A. El-Faham, N-Hydroxylamines for Peptide Synthesis, in: PATAI'S Chemistry of Functional Groups, John Wiley & Sons, Ltd, 2009, pp. 1-108.

[40] R. Subirós-Funosas, R. Prohens, R. Barbas, A. El-Faham, F. Albericio, Oxyma: An Efficient Additive for Peptide Synthesis to Replace the Benzotriazole-Based HOBt and HOAt with a Lower Risk of Explosion, Chem.--Eur. J., 15 (2009) 9394-9403.

[41] K.D. Wehrstedt, P.A. Wandrey, D. Heitkamp, Explosive properties of 1-hydroxybenzotriazoles, J. Hazard. Mater., 126 (2005) 1-7.

[42] R. Subiros-Funosas, S.N. Khattab, L. Nieto-Rodriguez, A. El-Faham, F. Albericio, Advances in Acylation Methodologies Enabled by Oxyma-Based Reagents, Aldrichim. Acta, 46 (2013) 21-40.

Supporting information

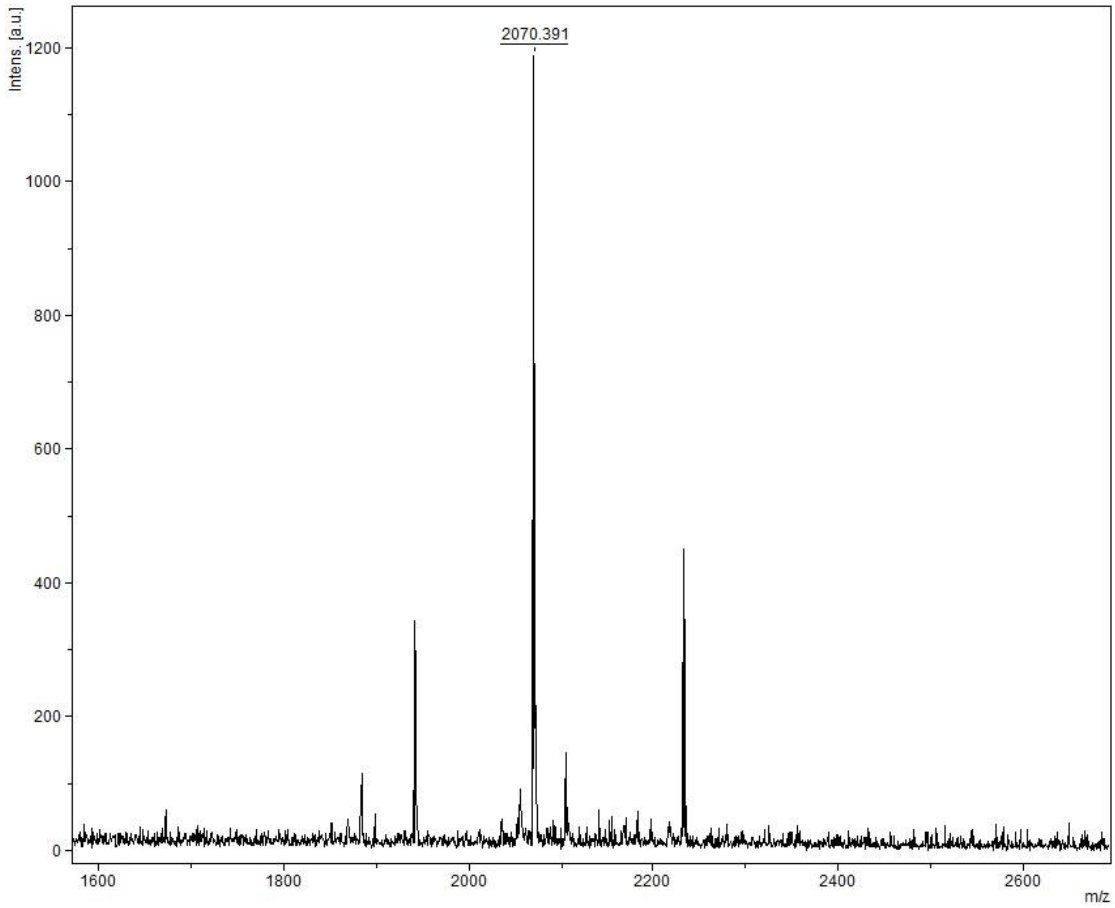

Fig. S1 MALDI-TOF MS spectrum of last seventeen amino acid residues of LL37 (20-37)

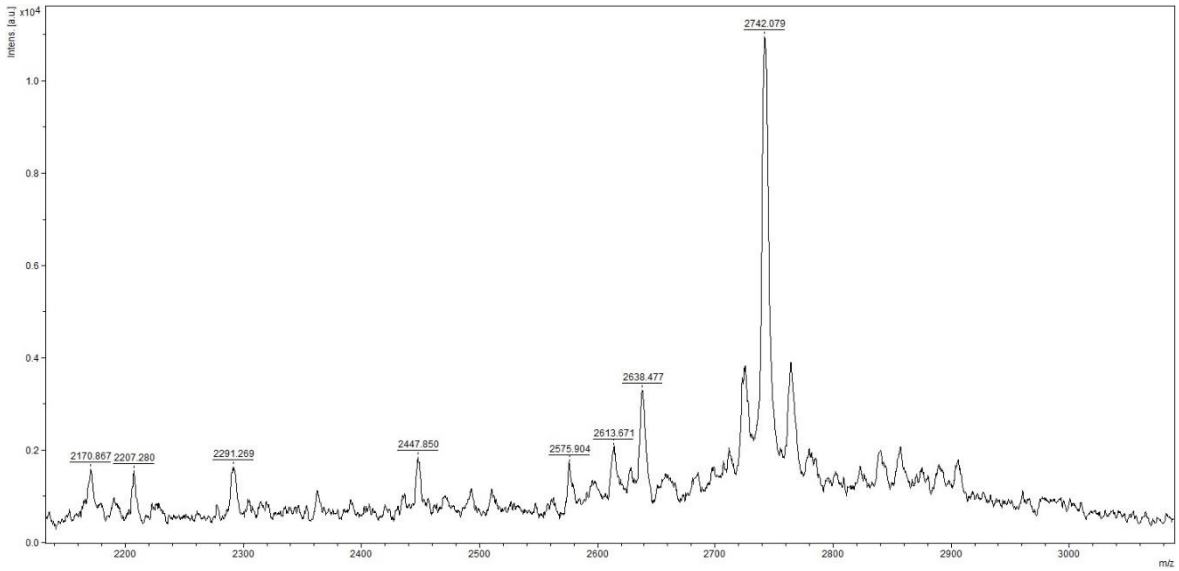

Fig. S2 MALDI analysis of the extended peptide fragment (16-37)

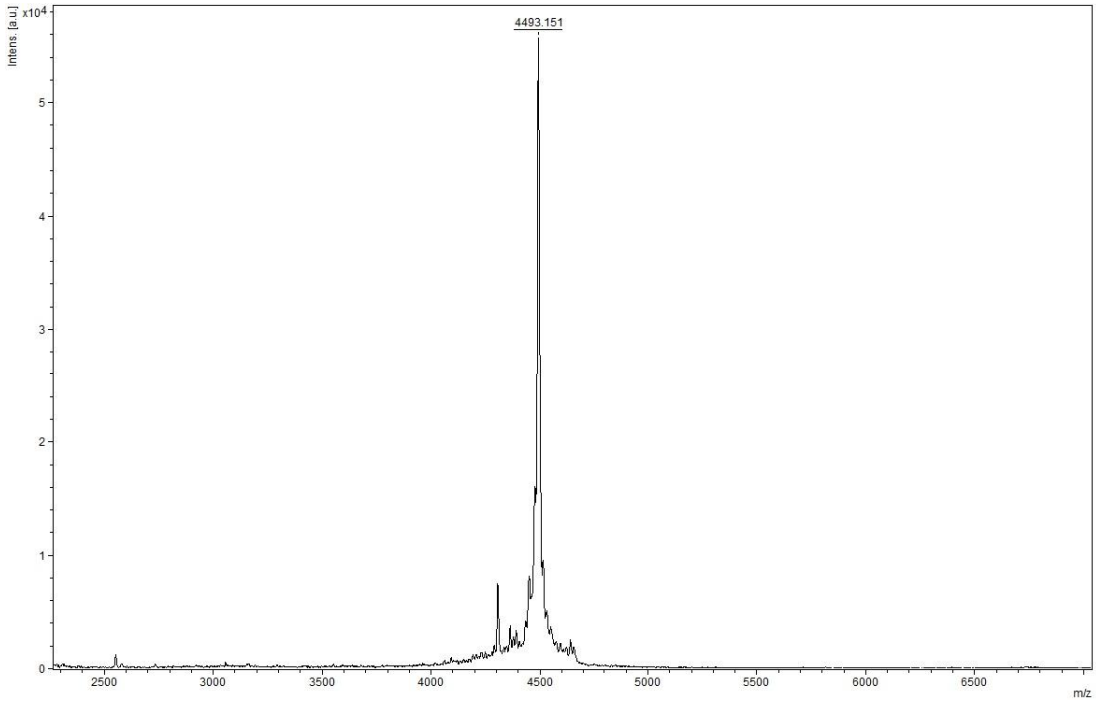

Fig. S3 MALDI-TOF MS spectrum of HPLC purified LL37 obtained by using modified protocol

Chapter 5

Synthesis, *in vitro* evaluation and ^{68}Ga-radiolabeling of CDP1 towards PET/CT imaging of bacterial infection

Jyotibon Dutta[1], Sooraj Baijnath[1], Anou M. Somboro[1], Savania Nagiah[2], Fernando Albericio[1, 3], Beatriz G. de la Torre[1], Biljana Marjanovic-Painter[5], Jan Rijn Zeevaart[6], Mike Sathekge[7], Hendrik G. Kruger[1], Anil Chuturgoon[2], Tricia Naicker[1], Thomas Ebenhan[7] and Thavendran Govender[1]*

[1]*Catalysis and Peptide Research Unit, School of Health Sciences and School of Chemistry and Physics, University of KwaZulu-Natal, Durban 4001, South Africa*
[2]*Discipline of Medical Biochemistry, School of Laboratory Medicine and Medical Sciences, College of Health Sciences, University of KwaZulu Natal, Durban, South Africa*
[3]*School of Chemistry and Physics, University of KwaZulu-Natal, University Road, Westville, Durban 4001, South Africa*
[4]*The South African Nuclear Energy Corporation (Necsa), Building P1600, Radiochemistry, Pelindaba, Brits, 0240, South Africa.*
[5]*Department of Science and Technology, Preclinical Drug Development Platform, North West University, 11 Hoffman St, Potchefstroom, 2520, South Africa.*
[6]*Department of Nuclear Medicine, University of Pretoria, Pretoria, South-Africa*
[7]*University of Pretoria & Steve Biko Academic Hospital, Crn Malherbe and Steve Biko Rd, Pretoria, 0001, South Africa.*

* Corresponding author. E-mail address: *govenderthav@ukzn.ac.za* (*Thavendran Govender)*

KEYWORDS: LL37, NODAGA, PET, Infection, Bacteria, Solid-phase peptide synthesis, CDP1

Running title ^{68}Ga-CDP1 for PET/CT imaging of bacterial infections

Abstract

Bacterial infections are a major concern in the human health sector due to poor diagnosis and development of multi drug resistant strains. PET/CT provides a means for the noninvasive detection and localization of the infectious foci; however, the radiotracers available are either cumbersome to prepare or its exact contribution towards the imaging is not yet established. Human antimicrobial peptides are of interest for development as PET radiotracers as they are an integral component of the immune system, non-immunogenic towards the recipient and show selectivity towards pathogens such as bacteria. Herein we report on the potential of LL37, a human cathelecidin antimicrobial peptide, as a radiotracer for bacterial imaging. Bi-functional chelator 1,4,7-triazacyclononane,1-glutaric acid-4,7-acetic acid (NODAGA) was utilized to functionalize the antimicrobial peptide, which in turn was capable of chelating gallium. The synthesized ^{nat}Ga-CDP1 showed bacterial selectivity and low affinity towards hepatic cells, which are favorable characteristics for further preclinical application.

1. Introduction

Bacterial infections are one of the fastest growing disease risk factors in health care despite significant global developments in antimicrobial chemotherapy. Infection still remains a major cause of morbidity and mortality due to poor diagnosis and increasing drug resistance [1]. Due to the numerous mechanisms of pathogenesis, early stage diagnosis is crucial in the effective prevention and treatment of bacterial infections [2]. The general, bacterial identification procedure involves culturing and examining the microorganism from the suspected site of contagion, which are time consuming, laborious and require skilled personnel [3-5]. Alternatively, Magnetic Resonance Imaging (MRI) [6], Computerized Tomography (CT) [7] and ultrasound can be used for the detection and localization of these pathogens by identifying the inflammatory changes in the local anatomy, water content in tissue or capillary permeability as a result of the infectious lesions [6, 7]. However, it is difficult for these methods to differentiate between sterile inflammation and bacterial infection in the absence of anatomical landmarks [2, 8, 9]. With the disadvantages associated with anatomy-based scanning systems, Positron Emission Tomography Computerized Tomography (PET/CT) imaging plays a key role in the diagnosis of diseases [10]. One of the methods to differentiate infection from sterile inflammation is to use radiolabeled agents that have an affinity to the bacterial cell. To date, various biomimetics, antimicrobials, leukocytes, antibodies, bacteriophages, antibiotics, sorbitol, maltose, maltohexaose, and siderophores have been made available for bacterial radiopharmaceutical imaging, but each approach has its own limitations [3-5, 10-16]. Despite of exponential growth in radiopharmaceutics, very few of them are commercially available and approved by Food and Drug Administration (FDA) for bacterial imaging; these includes radiolabeled leukocytes (^{111}In-oxine-leukocyte, ^{99m}Tc-HMPAO-leukocute and ^{99m}Tc-Stannous Colloid), radiolabeled anti-granulocyte antibodies (^{99m}Tc-Sulesomab and ^{99m}Tc-Besilesomab), 2-deoxy-2-(^{18}F)fluoro-D-glucose (^{18}F-FDG) and $^{67/68}$Ga-citrate. From these imaging techniques, ^{18}F-FDG-PET/CT has been considered for infection diagnosis for a long period of time, but its exact contribution has not yet been determined [17]. Radiolabeled leukocytes is considered to be the gold standard of infection imaging; however it is time consuming, labor intensive and requires blood handling [8]. Moreover, commercially available Gallium-67-(^{67}Ga-) citrate shows low specificity along with high energy γ radiation and longer half-life (78 hr) exposing patients to increased radioabsorption [18]. Due aforesaid disadvantages, antimicrobial peptides can be consider as potential candidate for PET tracer as it tend to accumulate at the infection sites rather than sterile inflammation due to their preferential binding to bacteria over mammalian cells [4, 19]. Since many of the antimicrobial peptides target bacterial cell wall proteins and lipids which are absent in mammalian cells, this feature makes them excellent candidates for infection imaging

[20]. Recently, ^{68}Ga-DOTA-TBIA101, a small radiolabeled depsidomycin-derived bioconjugate has been used to detect infection sites using PET/CT scanning and is an excellent example of how radiolabeled peptides can be employed to distinguish infection from inflammation [12]. Moreover, ^{68}Ga-NOTA-UBI fragments were also reported to show bacterial selectivity and specificity *in vitro* [21]. Furthermore, human neutrophil peptide, neutrophil elastase inhibitor peptide human β-defensin and human lactoferrin-derived peptide have also been successfully evaluated for imaging bacterial infection [22-25].

LL37, a linear human cationic antimicrobial peptide (hCAP18) comprising of 37 amino acid residues from the C-terminus [26] is widely associated with the innate immune response. LL37 is found in squamous epithelium and neutrophil granulocytes and is constitutively released into the extracellular space [26, 27]. This peptide is attributed towards the neutralization of the bioactive molecules of the bacterial cell wall as well as growth inhibition [28, 29]. In addition to its antimicrobial activities as a first line defense mechanism, this peptide is also linked with chemotaxis, histamine release, angiogenesis, cell migration, and cytokine production [30-32]. These biotic roles facilitate the LL37 modulation of the immune response, neovascularization of injured tissues and wound healing [31, 32]. Because of its close association with the innate human immune response, we envisaged the suitability of LL37 as a potential radiotracer for the diagnosis of infection. Furthermore and although the synthesis of this kind of large peptides can be considered a challenge, our group recently reported an optimized solid phase synthesis of LL37 [33].

Presently, LL37 radiolabeled compounds have not been reported for differentiating infection from inflammation. The bifunctional chelator, 1,4,7-triazacyclononane,1-glutaric acid-4,7-acetic acid (NODAGA), has gained popularity for radiolabeling of peptides because of its in vivo stability [34]. In this proof of concept study, we developed NODAGA-functionalized LL37 and conjugated it with ^{nat}Ga. We also present ^{nat}Ga-CDP1 uptake in different bacteria and a hepatocellular carcinoma (HepG2) cell line. Additionally, the radiosynthesis of CDP1 with the PET radioisotope gallium-68, including its identification by radio-HPLC/UV analysis is reported.

2. Methods and Materials

2.1. Materials

NODAGA(tBu)$_3$ was purchased from CheMatech (Dijon, France). All Fmoc protected amino acids, coupling reagents and the resin Rink Amide-MBHA were purchased from GLS Biochem Systems, Inc., (Shanghai, China). $GaCl_3$ was purchased from sigma-aldrich® (Germany).

2.2. Peptide synthesis

LL37 was synthesized as described in our previous publication using SPPS and Fmoc chemistry on 0.1 mmol scale [33]. The synthesis was confirmed by cleaving an aliquoted amount of resin followed by matrix-assisted laser-desorption ionization (MALDI) (Autoflex III smartbeam; Bruker Daltonics, Bremen, Germany) analysis. MALDI (positive mode) showed the product with m/z 4493.

2.1.1. Coupling of NODAGA(tBu)3 to the peptide and cleavage

NODAGA(tBu)$_3$ was coupled to LL37 on resin at 0.1 mmol scale using *N,N′*-diisopropylcarbodiimide (DIC)/OxymaPure to synthesize CDP1. The mixture of NODAGA(tBu)$_3$, DIC and OxymaPure was dissolved in tetrahydrofuran (THF) (0.1 ml) and allowed to react for 16 hr at room temperature. The ratio of NODAGA (tBu)$_3$/DIC/OxymaPure was 1:1:1 whereas NODAGA (tBu)$_3$ to free amine ratio was 1.2:1. Excess reagents were removed by washing the resin with 5 ml of THF (2 x) and DCM (2 x), consecutively. The tBu protected NODAGA attached to side chain protected LL37 peptide was finally cleaved from the resin using a cocktail of 1.0 ml TFA:H_2O:thioanisole (95:2.5:2.5) over a 2 hr period. During cleavage of the peptide from the resin, all protective groups were also removed. The resin was removed by filtration and washed with TFA (1.0 ml), which was then evaporated upon bubbling of N_2 gas through the mixture. The peptide was precipitated in 5.0 ml of ice-cold diethyl ether and centrifuged. The precipitate was then dissolved in 1.0 ml of water and further purified using prep-HPLC. The final product was characterized by MALDI-MS, revealing an m/z 4849 for CDP1 in positive mode.

2.1.2. CDP1 purification

CDP1 was purified on an ACE C18 preparative column (150 x 21.2 mm) by preparative HPLC (Shimadzu, Kyoto, Japan). A two-buffer system consisting of 0.1 % formic acid (FA)/H_2O (v/v) and 0.1 % FA/acetonitrile (v/v) were employed. A gradient of 15–80 % of 0.1 % FA/acetonitrile (v/v) over 30 min with a flow rate of 10 ml/min was used and the fractions were characterized by LC-MS (Shimadzu, Kyoto, Japan). Fractions which showed the desired mass were pooled and lyophilized and store for use in further experiments. The retention time of the compound on prep-HPLC was 21.6 min.

2.3. Non-radioactive ^{nat}Ga-labeling of CDP1

Non-radioactive natural Gallium(III)chloride (^{nat}Ga; i.e. Gallium has two natural stable isotopes, namely, ^{69}Ga (60 %) and ^{71}Ga (40 %)) was utilized to label the CDP1 as previously described [35]. Therefore, 1.0 mg of CDP1 was dissolved in 828 µl of water; 167 µl 1.9 M sodium acetate and 5.0 µl of 0.7 M $^{nat}GaCl_3$. The solution was allowed to react for 15 min at room temperature.

Quantitative labeling of ^{nat}Ga-CDP1 was confirmed by Q-TOF LC-MS (Bruker Daltonics, Bremen, Germany).

2.4. LC-MS method for quantification of ^{nat}Ga-CDP1

Quantification of ^{nat}Ga-CDP1 was carried out on a Maxis LC-MS (Bruker Daltonics, Bremen, Germany) coupled with an Agilent 1100 HPLC equipped with a YMC Triart C18 column (3.0 mm x 150 mm). Mobile phase A was water with 0.1% formic acid (FA) and mobile phase B was acetonitrile with 0.1% FA, the HPLC parameters were as follows: the flow rate was 0.3 mL/min with a linear gradient from 5% to 95% phase B over a period of 15 min, hold 2 min at 95% phase B and finally re-equilibration at 5% phase B for 2 min. The mass spectrometer was used in positive ion mode, with a nebulizer pressure of 1.5 bar, dry gas flow rate of 8.0 L/min, drying temperature of 180 °C and capillary voltage of 5500V. The retention time of ^{nat}Ga-CDP1 was 10.1 min.

2.5. Uptake of ^{nat}Ga-CDP1 by S.aureus, E.coli and M. smegmatis

To determine the uptake of ^{nat}Ga-CDP1 by *S.aureus*, *E.coli* and *M.smegmatis*, 10^5 bacterial cells from each bacterial strain were incubated with ^{nat}Ga-CDP1 at a final concentration of 20 µg/ml. Uptake rates were determined at 4 and 37 ºC temperatures. Samples were collected at 0, 1, 2 and 3 hr time points post inoculation. Samples were then centrifuged at 15000 rpm for 10 min at 4 °C (Hermle, GmBH, Germany, Rotor 221, 23) and the supernatants were collected. The supernatants were treated with equal amounts of ice cold acetonitrile and vortexed for 30 sec followed by a 2 hr cooling step at -20 °C. The samples were centrifuged at 15000 rpm for 10 min at 4 °C and passed through C_{18} SPE cartridge (Waters, Milford, MA, USA) preconditioned with 100 % acetonitrile. All the samples were diluted in the same manner and the recovered amounts of the Ga-CDP1 in the media was determined by the optimized LC-MS method described in the previous section.

2.6. Uptake of ^{nat}Ga-CDP1 by hepatocellular carcinoma (HepG2) cells

HepG2 cells were obtained from Highveld Biologicals (Johannesburg, South Africa). Cells were cultured in Eagle's minimum essential media (Lonza Biowhittaker, Basel, Switzerland) supplemented with 10% foetal calf serum, 1% L-Glutamine and 1% pen/strep-fungizone (Sigma-Aldrich, St Louis, USA); in a humidified incubator at 37 ºC with 5% CO_2. Cells were then seeded in 6-well culture plates (200,000 cells/well) and allowed to adhere overnight prior to treatment. The peptide was administered once the cells had reached approximately 80% confluency. Cells were treated with 20 µg/ml of the compound in triplicate at 4 °C and 37 ºC temperatures. The cell culture supernatant was aspirated at 0, 1, 2 and 3 hr time points and the samples collected for both incubating temperatures. Samples were then centrifuged at 15,000 rpm (Hermle, GmBH,

Germany; Rotor 221, 23) for 10 min at 4 °C and the supernatants were collected. The collected supernatants were treated with an equal amount of ice cold acetonitrile and vortexed followed by a 2 hr cooling step at -20 °C. Finally, the samples were centrifuged at 15,000 rpm for 10 min at 4 °C and passed through C_{18} SPE cartridge preconditioned with 100 % acetonitrile. All samples were diluted in the same manner and the recovered amount of the ^{nat}Ga-CDP1 in the media was determined by LC-MS.

2.7. ^{68}Ge/^{68}Ga-Generator elution and ^{68}Ga-radiolabeling

Gallium-68 (^{68}Ga: 89 %; EC β^+ max. 1.9 MeV, half-life: 68 min) was yielded from an 1850 MBq-loaded, tin-dioxide-based ^{68}Ge/^{68}Ga generator (iThemba LABS, Somerset West, South Africa). The eluate fractionation and the radiolabeling was conducted by adapting a previously described method [21]. Briefly, the ^{68}Ge/^{68}Ga-generator provided radioactivity concentrated in 2 ml 0.6 M HCL which was buffered with 2.5 M sodium acetate trihydrate to yield a selected pH range of 3.5-4.0 where gallium is in its reactive state, the $[Ga(OH_2)_6)^{3+}]$ ion, which allows rapid complexation to the chelator molecule. CDP1 was dissolved in Millipore water to achieve a peptide stock concentration of 1 µg/µl necessary to develop the radiolabeling protocol. A 0.5 ml aliquot of buffered $^{68}Ga^{3+}$ (122 - 150 MBq) was mixed with 10-20 nmol CDP1, NODAGA (positive control) and LL37 (negative control) and was incubated at room temperature for at least 5 min followed by HPLC/UV analyses. ^{68}Ga-labeled c(RGDyK)-isothiocyanabenzyl-1,4,7-triazaclononane-1,4,7-triatetic acid (NOTA-RGD), an imaging agent for integrin receptor expression in cancer, was radiolabeled as previously described and employed as a radiolabeling performance reference (to reflect any variability in the generator eluate quality) [36].

2.8. Identification of the ^{68}Ga-CDP1 using UV/radio-HPLC analysis

For determination of the % RCP a reverse-phase HPLC column (Zorbax SB C18, 4.6 × 250 mm × 5 µm; Agilent Technologies, CA, USA) using a 5-95% A-B gradient (over 15 min) at a flow rate of 1 mL/min, was employed. Solvent A consisted of 0.1 % aqueous trifluoroacetic acid (TFA); solvent B utilized 0.1 % TFA dissolved in acetonitrile. The HPLC apparatus (Agilent 1200 series HPLC instrument, Agilent Technologies Inc., Wilmington DE, USA) contained a radioactive detector (Gina Star, Raytest, Straubenhardt, Germany) following radioactivity (counts per second) combined with a diode array detector following UV absorbance at 214, 220 and 240 nm. For determination of the radiolabeling efficiency (%LE) HPLC analysis was supported by control measures using radio-ITLC employing a silica-gel based solid phase and 0.1 M sodium citrate as mobile phase (free ^{68}Ga [R*f*=0.8] and ^{68}Ga-CDP1 [R*f*=0.2]). Both methods were utilized to detect ^{68}Ga-CDP1 and differentiate it from uncomplexed ^{68}Ga, potential radiolabeled by-products (^{68}Ga-NODAGA precursor), and any deteriorated peptide or

fractionated LL37-NODAGA where possible. The retention times for ^{68}Ga, NODAGA, CDP1 and NOTA were established and used for identification.

2.9. Biostatistics

If not indicated otherwise, results are expressed as mean ± standard deviation of mean (SD). Paired and unpaired Student-t tests were performed to indicate significance to compare different parameters and P values ≤ 0.05 were considered significant.

3. Results and Discussion

3.1. Synthesis of CDP1 and ^{nat}Ga-conjugation

The peptide LL37 was successfully synthesized with the coupling reagents DIC/OxymaPure in DMF using automatic microwave synthesis except for the coupling of 20th Ile residue in solid phase in which manual coupling in THF was necessary. The resultant product gave the desired m/z of 4493 using MALDI-TOF MS. The peptide functionalization with NODAGA was achieved in solid-phase using DIC/OxymaPure in THF at room temperature for 16 hrs to give the desired m/z of 4849 (Scheme 1). ^{nat}Ga was complexed to the CDP1 using sub-millimolar concentrations of $^{nat}Ga^{3+}$ as previously reported [35]. The complexation was confirmed by HRMS for ^{nat}Ga-CDP1.

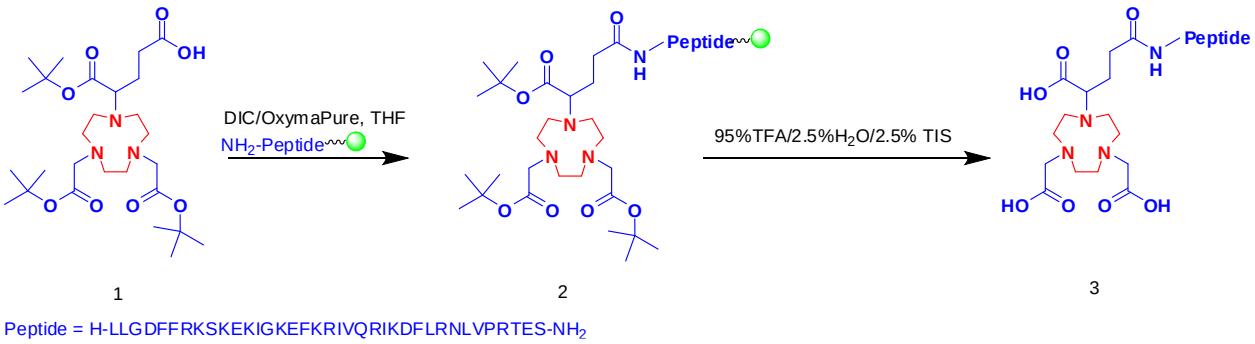

Scheme 1. Synthesis of CDP1

3.2. Bacterial and Hepatocellular uptake of the ^{nat}Ga-CDP1

The results of the bacterial and hepatocellular uptake of the ^{nat}Ga-CDP1 are presented in Figures 1A and 1B. The uptake was studied at two temperatures (4 °C and 37 °C). At lower temperature (4 °C), the bacterial cell growth will be slower. Slightly lower uptake of the conjugate ^{nat}Ga-CDP1 at 4 °C was observed compared to 37 °C. The conjugated peptide was also examined for its antimicrobial activity, which showed no bacteriostatic effects to *S. aureus, E. coli and M. smegmatis* at the concentrations applied in this study.

At both temperatures, the amount of ^{nat}Ga-CDP1 determined in the supernatant of the HepG2 cells was >99% after 3 hr of incubation when normalized with the 0 hr time point (**Fig. 1A**). This

result reveals that there was <1% uptake of the compound by the HepG2 cells regardless of the incubation temperature. In the same time, bacterial cells consumed 50-120 times more Ga-CDP1 as compared to HepG2 cells. This experiment reveals that the compound has negligible affinity towards the mammalian cells.

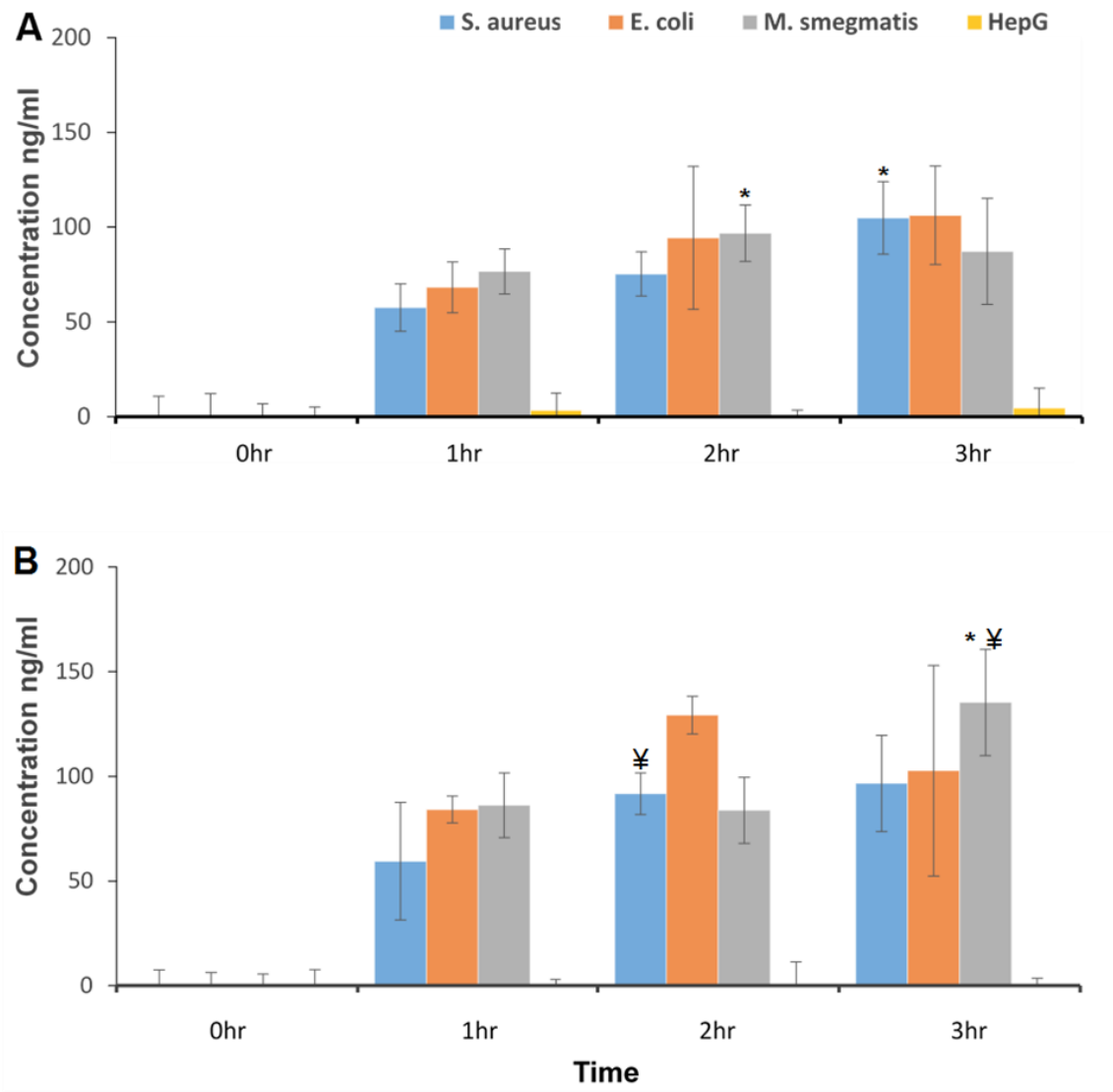

Figure 1. Comparison of ^{nat}Ga-CDP1 uptake by cellular (*HepG2*) and bacterial cells at (**A**) 4 °C and (**B**) 37 °C. Mean results ± SD (n=3) is presented. *) Paired 1-tailed *Student-t* test on the comparison of consecutive incubation times returned P<0.05. ¥) Paired 1-tailed *Student-t* test comparing cells incubated at 4°C to 37°C returned P<0.05.

3.2.1. Uptake of ^{nat}Ga-CDP1 by S.aureus

The ^{nat}Ga-CDP1 uptake by the gram positive candidate, *S.aureus*, was determined immediately and compared after 1, 2 and 3 incubation periods at 4 °C and 37 °C. At 4 °C the concentration of the compound was found to be 78% in the supernatant after 3 hr. This result showed that 22%

^{nat}Ga-CDP1 was taken up by *S. aureus*. Likewise, at 37 °C the concentration of the conjugated peptide taken up was 20% after 3 hr. All of the data were found to be within the allowed error limit of analytical method development guideline [37]. This bacterial uptake result suggests selectivity of the peptide towards gram positive *S. aureus* over HepG2 cells.

3.1.2. Uptake of ^{nat}Ga-CDP1 by E. coli

The uptake of ^{nat}Ga-CDP1 by *E. coli* was also determined at the time points described in the previous section. The results revealed that 22% and 21% of the compound was accumulating in *E. coli* cells at 4 °C and 37 °C after 3 hrs of incubation, respectively. This positive uptake of ^{nat}Ga-CDP1 by *E. coli* cells opens the opportunity to explore the efficacy of this peptide to be used as a PET radiotracer for infection diagnosis against gram-negative bacteria.

3.2.3. Uptake of ^{nat}Ga-CDP1 by M. smegmatis

Acid fast *M. smegmatis* represents mycobacteria for this uptake study because it is non-pathogenic and it has fast replicating time when compared to other members of this family. This bacteria shares a similar cell wall structure and more than 2000 homologous genes with *M. tuberculosis* [38]. Normalization of the data at the 0 hr with the 3 hr incubation time points for the compound showed 18% and 28% uptake by this bacterial cell at 4 °C and 37 °C, respectively. These results indicate potential affinity of ^{nat}Ga-CDP1 towards *Mycobacterium sp.* and should be further explored.

The *in vitro* results may allow translating the outcome for potential *in vivo* applications. The high degree of differentiation between bacterial and mammalian cell uptake may be reflected by the high targeting ability of ^{nat}Ga-CDP1, which may lead to potential detection of bacteria. The results show no significant difference in the uptake behavior between the bacterial strains evaluated, suggesting no bacterial selectivity of ^{nat}Ga-CDP1 towards bacterial identification.

3.3. ^{68}Ge/^{68}Ga-Generator elution and ^{68}Ga-radiolabeling

In ^{68}Ge/^{68}Ga-Generator elution, the fractionation method yielded 78 ± 5 % and 91± 4 % (360-560 MBq) of the total elutable ^{68}Ga-activity in 1 and 2 ml, respectively. NODAGA and CDP1 were labeled successfully within 5 min at room temperature with a percentage radiochemical purity (% RCP) of > 88 % adapting conditions from a former study radiolabeling NOTA-UBI. [21] ^{68}Ga-CDP1 was stable in its formulation throughout the 60 min period tested. To the best of our knowledge, this is the first (documented approach presenting) report showing the successful ^{68}Ga-radiolabeling of this bioconjugate. The results suggest an optimization of the radiolabeling parameters (pH, CDP1 molarity and purification of the generator eluate) which was

not considered within the scope of this study. As a reference peptide NOTA-RGD was radiolabeled successfully achieving >82 % radiolabeling efficiency (%LE).

3.4 Identification ^{68}Ga-CDP1

The chromatographic method was capable of confirming successful radiolabeling (peak integration) of ^{68}Ga-CDP1 (Figure 2). The retention times of 11.5-12 min allowed significant differentiation from the unbound buffered ^{68}Ga (2.3-3.5 min). Separately radiolabeled ^{68}Ga-NODAGA just used as a control was detected at retention times of 4- 4.2 min, but no notable ^{68}Ga-activity peak was detected during HPLC analyses of any ^{68}Ga-CDP1 samples at that retention time.

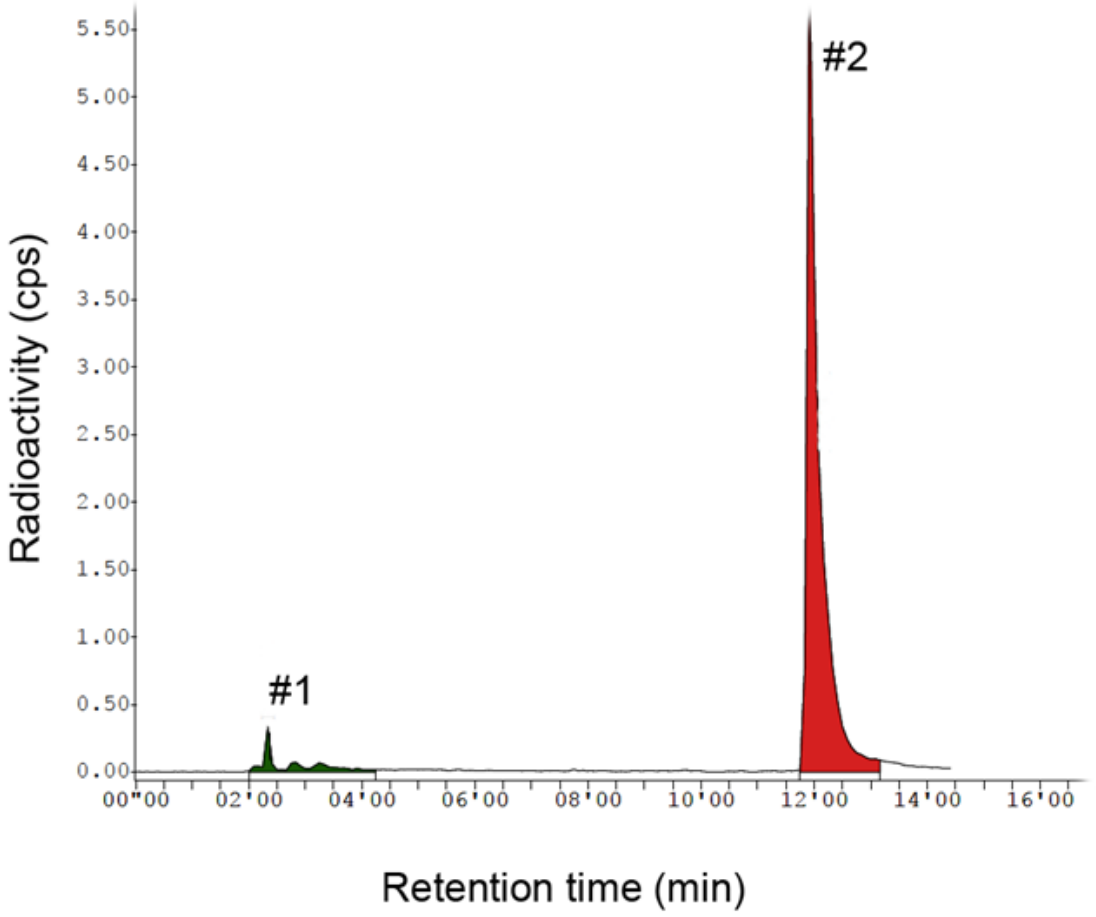

Figure 2. Representative radio-HPLC chromatogram showing successful differentiation of free ^{68}Ga (#1: 2.3-3.5 min retention) and ^{68}Ga-CDP1 (#2: 11.5-12 min retention). Quantification following radio-peak integration resulted in a 91% RCP for ^{68}Ga-CDP1.

The reference radiolabeled peptide (^{68}Ga-NOTA-RGD) confirmed ^{68}Ga-labeling performance of the CDP1 system (elution of ^{68}Ga-NOTA-RGD was faster on the RP-HPLC column - 7.45 min),

which was expected due to the increased polar character of NOTA-RGD compared to CDP1. The % LE for NOTA-RGD was well within the expected range, which indicates that the generator eluate quality was not a compromising parameter to yield the highest possible radiolabeling efficiency and yield. All retention times corresponded well with their respective UV peak maxima (wavelength ranged 212-260 nm). Following incubation with ^{68}Ga, unfunctionalized LL-37 was detected at 10.50 min (UV 214 and 220 nm) showing no radioactivity peak at this retention time using radio-HPLC.

It should be noted that the use of NODAGA allows for radiolabeling at room temperature, which can be beneficial for radiolabeling heat-vulnerable peptides [39]. Based on this identification of radiolabeled ^{68}Ga-CDP1, further refinements can be carried out to optimize the radiolabeling technique aiming for both, quantitative complexation and thermodynamic stability of ^{68}Ga to CDP1.

4. Conclusion

In this proof of concept study, we reported the functionalization of LL37 with NODAGA and its usability as a PET radiotracer for potential infection imaging using gallium. ^{nat}Ga-CDP1 showed significant affinity towards bacterial cells; it also has a low association with HepG2 cells, affording specific bacterial uptake. In conclusion, this complex can potentially be used as a candidate for preclinical studies in infection imaging.

Acknowledgement

The authors would like to thank the Nuclear Technologies in Medicine and the Biosciences Initiative (NTeMBI), a national technology platform developed and managed by the South African Nuclear Energy Corporation (Necsa). The authors would also like to thank National Research Foundation (NRF), South African Medical Research Council (SAMRC) and Aspen Pharmacare for their support.

Conflict of Interest

There is no conflict of interest.

Funding Sources

Funded by the Department of Science and Technology, University of KwaZulu Natal, National Research Foundation and Aspen Pharmacare

Reference

[1] M. Namavari, G. Gowrishankar, A. Hoehne, E. Jouannot, S. Gambhir, Synthesis of [18F]-labelled Maltose Derivatives as PET Tracers for Imaging Bacterial Infection, Mol. Imaging Biol., 17 (2015) 168-176.

[2] Z. Wang, X. Ning, Clinical diagnosis of bacterial infection via FDG-PET imaging, Can Chem Trans, 1 (2013) 85-104.

[3] S. Gratz, H.J.J.M. Rennen, O.C. Boerman, W.J.G. Oyen, F.H.M. Corstens, Rapid Imaging of Experimental Colitis with 99mTc-Interleukin-8 in Rabbits, J. Nucl. Med., 42 (2001) 917-923.

[4] A. Lupetti, M.M. Welling, E.K.J. Pauwels, P.H. Nibbering, Radiolabelled antimicrobial peptides for infection detection, Lancet Infect. Dis., 3 (2003) 223-229.

[5] A. Signore, A. Annovazzi, F. Corsetti, G. Capriotti, M. Chianelli, F. Winter, F. Scopinaro, Biological Imaging for the Diagnosis of Inflammatory Conditions, BioDrugs, 16 (2002) 241-259.

[6] S. Winklhofer, S. Kollias, Incidental MRI finding of a pons tuberculoma in a patient with so-far-undiagnosed multisystemic tuberculosis infection, Clin. Imaging, 36 (2012) 623-625.

[7] J.K. Kirchner, R.; Stein, A.; Kirchner, E. M., Mesenteric ossification in CT indicates sclerosing peritonitis in chronic bacterial infection and pancreatitis, Rontgenpraxis, 55 (2003) 99-102.

[8] T. Ebenhan, O. Gheysens, H.G. Kruger, J.R. Zeevaart, M.M. Sathekge, Antimicrobial peptides: their role as infection-selective tracers for molecular imaging, BioMed Res. Int., 2014 (2014) 867381.

[9] W. Becker, J. Meller, The role of nuclear medicine in infection and inflammation, Lancet Infect. Dis., 1 (2001) 326-333.

[10] C.J. Palestro, C. Love, G.G. Tronco, M.B. Tomas, Role of Radionuclide Imaging in the Diagnosis of Postoperative Infection, Radiographics, 20 (2000) 1649-1660.

[11] A.M. Peters, Nuclear medicine imaging in infection and inflammation, J. R. Coll. Physicians Lond, 32 (1998) 512-519.

[12] B.B. Mokaleng, T. Ebenhan, S. Ramesh, T. Govender, H.G. Kruger, R. Parboosing, P.P. Hazari, A.K. Mishra, B. Marjanovic-Painter, J.R. Zeevaart, M.M. Sathekge, Synthesis, ^{68}Ga-Radiolabeling, and Preliminary In Vivo Assessment of a Depsipeptide-Derived Compound as a Potential PET/CT Infection Imaging Agent, BioMed Res. Int., 2015 (2015) 284354.

[13] S. Auletta, F. Galli, C. Lauri, D. Martinelli, I. Santino, A. Signore, Imaging bacteria with radiolabelled quinolones, cephalosporins and siderophores for imaging infection: a systematic review, Clin Transl Imaging, 4 (2016) 229-252.

[14] E.A. Weinstein, A.A. Ordonez, V.P. DeMarco, A.M. Murawski, S. Pokkali, E.M. MacDonald, M. Klunk, R.C. Mease, M.G. Pomper, S.K. Jain, Imaging Enterobacteriaceae infection in vivo with 18F-fluorodeoxysorbitol positron emission tomography, Sci. Transl. Med., 6 (2014) 259ra146-259ra146.

[15] G. Gowrishankar, M. Namavari, E.B. Jouannot, A. Hoehne, R. Reeves, J. Hardy, S.S. Gambhir, Investigation of 6-[18F]-Fluoromaltose as a Novel PET Tracer for Imaging Bacterial Infection, PLoS ONE, 9 (2014) e107951.

[16] X. Ning, W. Seo, S. Lee, K. Takemiya, M. Rafi, X. Feng, D. Weiss, X. Wang, L. Williams, V.M. Camp, PET Imaging of Bacterial Infections with Fluorine-18-Labeled Maltohexaose, Angew. Chem., Int. Ed. Engl., 53 (2014) 14096-14101.

[17] M. Revest, S. Patrat-Delon, A. Devillers, P. Tattevin, C. Michelet, Contribution of 18fluoro-deoxyglucose PET/CT for the diagnosis of infectious diseases, Med Mal Infect, 44 (2014) 251-260.

[18] A. Signore, A.W.J.M. Glaudemans, The molecular imaging approach to image infections and inflammation by nuclear medicine techniques, Ann. Nucl. Med., 25 (2011) 681-700.

[19] C.L. A. Signore, and F. Galli, Radiolabelled probes targeting infection and inflammation for personalized medicine, Curr. Pharm. Des., 20 (2014) 2338-2345.

[20] F. Guilhelmelli, N. Vilela, P. Albuquerque, L.d.S. Derengowski, I. Silva-Pereira, C.M. Kyaw, Antibiotic development challenges: the various mechanisms of action of antimicrobial peptides and of bacterial resistance, Front. Microbiol., 4 (2013) 353.

[21] T. Ebenhan, N. Chadwick, M.M. Sathekge, P. Govender, T. Govender, H.G. Kruger, B. Marjanovic-Painter, J.R. Zeevaart, Peptide synthesis, characterization and ^{68}Ga-radiolabeling of NOTA-conjugated ubiquicidin fragments for prospective infection imaging with PET/CT, Nucl. Med. Biol., 41 (2014) 390-400.

[22] M.M. Welling, P.S. Hiemstra, M.T. van den Barselaar, A. Paulusma-Annema, P.H. Nibbering, E. Pauwels, W. Calame, Antibacterial activity of human neutrophil defensins in experimental infections in mice is accompanied by increased leukocyte accumulation, J. Clin. Invest., 102 (1998) 1583.

[23] M. Rusckowski, T. Qu, J. Pullman, R. Marcel, A.C. Ley, R.C. Ladner, D.J. Hnatowich, 99mTc-Neutrophil Elastase Inhibitor in Monkeys, J. Nucl. Med., 41 (2000) 363-374.

[24] M. Liberatore, A. Pala, S. Scaccianoce, C. Anagnostou, U. Di Tondo, E. Calandri, P. D'Elia, M.D. Gross, D. Rubello, Microbial Targeting of 99mTc-Labeled Recombinant Human β-Defensin-3 in an Animal Model of Infection: A Feasibility Pilot Study, J. Nucl. Med., 50 (2009) 823-826.

[25] M.M. Welling, A. Paulusma-Annema, H.S. Balter, E.K. Pauwels, P.H. Nibbering, Technetium-99m labelled antimicrobial peptides discriminate between bacterial infections and sterile inflammations, Eur. J. Nucl. Med., 27 (2000) 292-301.

[26] J.W. Larrick, M. Hirata, R.F. Balint, J. Lee, J. Zhong, S.C. Wright, Human CAP18: a novel antimicrobial lipopolysaccharide-binding protein, Infect. Immun., 63 (1995) 1291-1297.

[27] M. Frohm Nilsson, B. Sandstedt, O. Sørensen, G. Weber, N. Borregaard, M. Ståhle-Bäckdahl, The Human Cationic Antimicrobial Protein (hCAP18), a Peptide Antibiotic, Is Widely Expressed in Human Squamous Epithelia and Colocalizes with Interleukin-6, Infect. Immun., 67 (1999) 2561-2566.

[28] D.A. Devine, Antimicrobial peptides in defence of the oral and respiratory tracts, Mol. Immunol., 40 (2003) 431-443.

[29] M.J. Nell, G.S. Tjabringa, A.R. Wafelman, R. Verrijk, P.S. Hiemstra, J.W. Drijfhout, J.J. Grote, Development of novel LL-37 derived antimicrobial peptides with LPS and LTA neutralizing and antimicrobial activities for therapeutic application, Peptides, 27 (2006) 649-660.

[30] K. Gill, B.K. Mohanti, A.K. Singh, B. Mishra, S. Dey, The over expression of cathelicidin peptide LL37 in head and neck squamous cell carcinoma: the peptide marker for the prognosis of cancer, Cancer Biomark., 10 (2011) 125-134.

[31] R. Koczulla, G. von Degenfeld, C. Kupatt, F. Krötz, S. Zahler, T. Gloe, K. Issbrücker, P. Unterberger, M. Zaiou, C. Lebherz, An angiogenic role for the human peptide antibiotic LL-37/hCAP-18, J. Clin. Invest., 111 (2003) 1665-1672.

[32] D. Yang, Q. Chen, A.P. Schmidt, G.M. Anderson, J.M. Wang, J. Wooters, J.J. Oppenheim, O. Chertov, LL-37, the neutrophil granule–and epithelial cell–derived cathelicidin, utilizes formyl peptide receptor–like 1 (FPRL1) as a receptor to chemoattract human peripheral blood neutrophils, monocytes, and T cells, J. Exp. Med., 192 (2000) 1069-1074.

[33] J. Dutta, S. Ramesh, S.M. Radebe, A.M. Somboro, G. Beatriz, H.G. Kruger, S.Y. Essack, F. Albericio, T. Govender, Optimized Microwave Assisted Synthesis of LL37, a Cathelicidin Human Antimicrobial Peptide, Int. J. Pept. Res. Ther., 21 (2015) 13-20.

[34] S.C. Ghosh, K.L. Pinkston, H. Robinson, B.R. Harvey, N. Wilganowski, K. Gore, E.M. Sevick-Muraca, A. Azhdarinia, Comparison of DOTA and NODAGA as chelators for 64Cu-labeled immunoconjugates, Nucl. Med. Biol., 42 (2015) 177-183.

[35] J. Dutta, P.K. Chinthakindi, P.I. Arvidsson, G. Beatriz, H.G. Kruger, T. Govender, T. Naicker, F. Albericio, A Facile Synthesis of NODASA-Functionalized Peptide, Synlett, 27 (2016) 1685-1688.

[36] J.M. Jeong, M.K. Hong, Y.S. Chang, Y.S. Lee, Y.J. Kim, G.J. Cheon, D.S. Lee, J.K. Chung, M.C. Lee, Preparation of a promising angiogenesis PET imaging agent: 68Ga-labeled c(RGDyK)-isothiocyanatobenzyl-1,4,7-triazacyclononane-1,4,7-triacetic acid and feasibility studies in mice, J. Nucl. Med., 49 (2008) 830-836.

[37] C.f.M.P.f.H. Use, Guideline on bioanalytical method validation, European Medicines Agency, (2011).

[38] G.M. King, Uptake of Carbon Monoxide and Hydrogen at Environmentally Relevant Concentrations by Mycobacteria†, Appl. Environ. Microbiol., 69 (2003) 7266-7272.

[39] W. Beaino, C.J. Anderson, PET imaging of very late antigen-4 in melanoma: comparison of 68Ga- and 64Cu-labeled NODAGA and CB-TE1A1P-LLP2A conjugates, J. Nucl. Med., 55 (2014) 1856-1863.

Supplementary information:

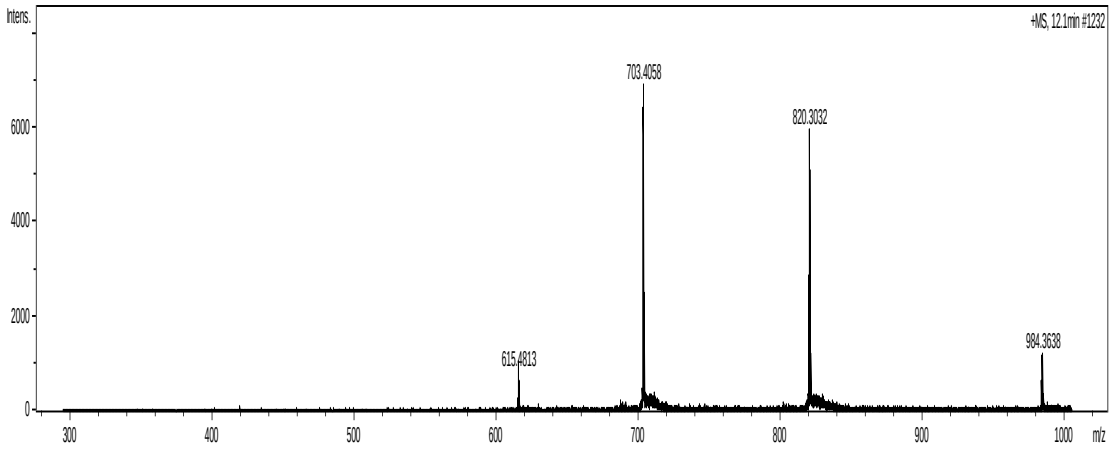

Supplementary figure 1. Product ion spectra of ^{nat}Ga-NODAGA-LL37 showing 703,41 m/z, which was used for the quantitation of the analyte in bacterial and mammalian cells.

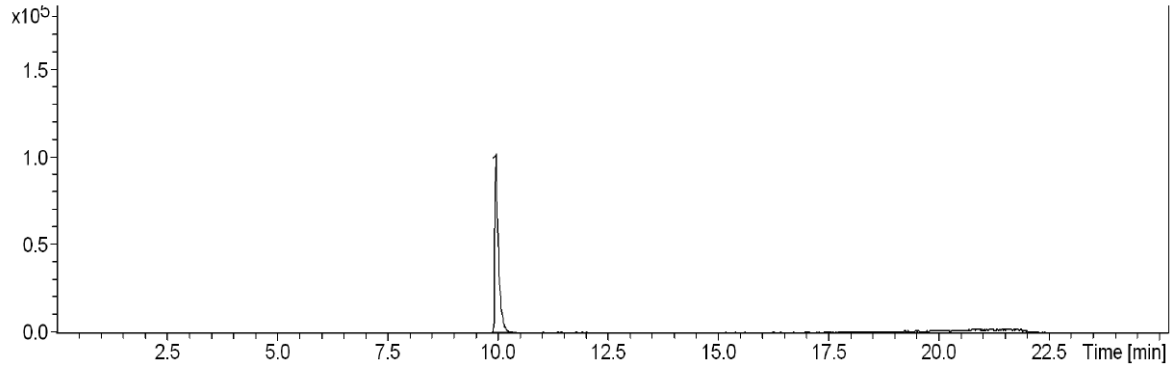

Supplementary figure 2. Typical chromatogram for ^{nat}Ga-NODAGA-LL37, showing its retention at 10.1 min using a YMC Triart C18 column (150mm x 3.0mm; 3µm i.d.).

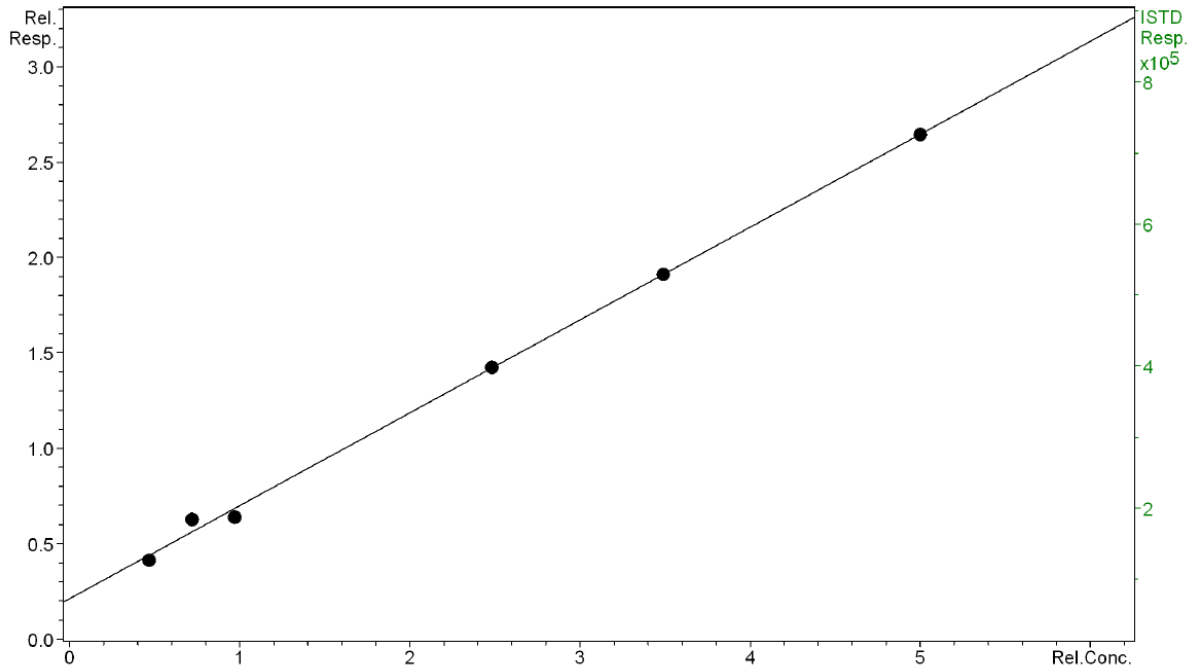

Supplementary figure 3. Calibration curve, created using QuantAnalysis (Bruker Daltonics, Bremen, Germany), used for the quantitation of ^{nat}Ga-NODAGA-LL37.

Chapter 6

Summary

The first part of the thesis reviews the synthetic approaches for existing radiotracers for the purpose of bacterial imaging. Essentially, these radiotracers have been divided into two categories in the review 1) commercially available tracers and 2) novel imaging probes for bacterial infections. Commercially available tracers that are FDA approved are mostly based on leukocytes. This category can be further classified as i) radiolabeled leukocytes (^{111}In-oxine-leukocyte, ^{99m}Tc-HMPAO-leukocute and ^{99m}Tc-Stannous Colloid), ii) radiolabeled anti-granulocyte antibodies (^{99m}Tc-Besilesomab and ^{99m}Tc-Sulesomab) and iii) unspecific biomolecules such as 2-deoxy-2-(^{18}F)fluoro-D-glucose (^{18}F-FDG) and $^{67/68}$Ga-citrate. These available radiotracers cover a vast range of modules that include (but not limited to) spatial localization of infection for gram-positive and gram negative bacteria, infection in soft tissues, endocarditis, neurological infections, fever of unknown origin, diabetic foot, inflammatory bowel disease, prosthetic graft infection, abdominal sepsis, osteomyelitis, pyrexia of unknown origin, appendicitis and acute myocarditis. On the other hand, the novel imaging radiotracers for the bacterial imaging are categorized based on their source of origin. Potential origin of these tracers are antimicrobial peptides, antibiotics, vitamins, aptamers, puromycin, glycopyranose derivatives and siderophores. Majority of these compounds are labelled with radioisotopes such as ^{68}Ga, ^{99m}Tc, ^{125}I, ^{18}F, ^{111}In and ^{11}C. The most commonly employed reducing agent for successful conjugation/coupling of the radioisotope to the tracer molecule is found to be $SnCl_2$. Moreover, various modalities used for the detection of the radio signals includes scintigraphy, SPECT and PET. These novel tracers were successfully evaluated for imaging infections caused by microorganisms such as *Staphylococcus aureus*, *Escherichia coli*, *Candida albicans*, *Aspergillus fumigatus*, *Klebsiella pneumonia* and *Mycobacterium tuberculosis*. However, despite extensive studies in the area of radiopharmaceutics development, only a handful of them cross the barrier of clinical trial to reach commercial levels. In recent years, numerous radiotracers for bacterial imaging have been developed; these molecules demonstrated promise in small animals; but never reached the clinical stage. From the angle of nuclear imaging, PET/CT and PET/MRI are the most useful methods as it can be applied to whole body imaging with great sensitivity and promising spatial resolution. This extended the horizon for the development of more promising radiopharmaceutics for bacterial imaging. To be a successful PET tracer, its radio synthesis is expected to be simple, preferably a single step radiolabelling with radion active atoms such as ^{18}F or ^{68}G. From the perspective of radiochemistry ^{68}Ga-UBI and ^{68}Ga-Biotin are some of the

potential candidates of radiopharmaceutics, which may be used successfully for bacterial imaging in near future.

In radiopharmaceutics bifunctional chelators (BFC) are utilized for the development of radiotracers. These molecules act as bridge between the tracer moiety and the radioisotope. The functional group present in the BFCs are used to covalently couple it to the tracking molecules such as peptides, antibodies and nucleotides. Moreover, the pharmacokinetic properties such as bio distribution and renal excretion are greatly affected by the characteristics of radiometal-chelator complex. This makes the selection procedure of the BFCs crucial for the success of a radiotracer. The next part of the thesis focused on the synthetic approach of BFC, where a facile method for on and off resin synthesis of a 1,4,7-triazacyclononane-*N′*,*N′*,*N′′*-tri acetic acid (NOTA) derivative 1,4,7-triazacyclononane-1-succinic acid-4,7-diacetic acid (NODASA) functionalized peptide (YGGF) was established. NODASA can successfully be used to chelate radioisotopes ^{64}Cu and ^{68}Ga, which make it as a potential BFC in the field of PET tracer development. A short sequence of peptide YGGF was synthesized on rinkamide MBHA resin with coupling reagent HBTU/DIPEA; this was used as a model peptide for the entire synthesis. A failed attempt was encountered with the NODASA synthesis when coupling 4-(benzyloxy)-3-bromo-4-oxobutanoic acid to the model peptide on resin followed by the addition of 1,4,7-triazacyclononane; that resulted in a HBr elimination reaction. Furthermore, monomethyl fumarate was coupled with the peptide followed by addition of 1,4,7-triazacyclononane, which resulted in another unsuccessful attempt. However, a successful seven-step synthesis was initiated with a Michael addition reaction between monomethyl fumarate and 1,4,7-triazacyclononane (94% yield); and terminated with a product of NODASA-YGGF giving an isolated yield of 84%. NODASA-YGGF was also efficiently conjugated with cold gallium. Additionally, a 500 fold excess of EDTA was used to evaluate the stability of the gallium complexation, ensuring no significant trans chelation even after 240 min. These results confirm the potential of a synthetic route for constructing PET imaging agents. This synthetic approach can be attempted on other peptides of interest and provide a cheap alternative to the commercially available NODASA.

LL37 is a cationic antimicrobial peptide originating from humans. This peptide comprises of 37 amino acids ($^{\mathbf{1}}$LLGDFFRKS$^{\mathbf{10}}$KEKIGKEFKR$^{\mathbf{20}}$IVQRIKDFLR$^{\mathbf{30}}$NLVPRTE$^{\mathbf{37}}$S) and has potential toward therapeutic applications because of its close association with the human immune system. Moreover, this peptide is also involved in different biological processes such as cytokine production, chemotaxis, release of histamine, angiogenesis and cell migration. In the third section of this thesis we described the solid phase synthesis of this vital peptide. A range of coupling

reagents along with a combination of solvents were evaluated for optimisation. The synthesis of LL37 was not satisfactory when it was attempted with HBTU and HATU in DMF, despite the use of double couplings in certain amino acid residues such as Ser, Arg, Val, Leu and Ile under microwave conditions. However, MALDI results for the above synthesis represented a decrease trend of coupling efficiencies after the 20th amino acid, which represents the ^{20}Ile to ^{21}Val coupling. Further, to identify the difficult amino acid coupling combinations of the sequence, a segment extension approach was performed using HATU/DIPEA. This again confirmed that the 16-20 amino acid residues were critical coupling combinations. After the difficulties with certain segments were determined, the region 21–37 were synthesized using HATU/DIPEA in the synthesizer under microwave conditions. However, the subsequent amino acid residues (16-20) were coupled manually to the progressing sequence at ambient temperature using DIC/OxymaPure in THF. This coupling reagent combination is stable for longer times in comparison with HATU and HBTU. This synthesis gave promising results proving that ^{20}Ile to ^{21}Val coupling difficulties can be overcome by the DIC/OxymaPure in THF. Finally, DIC/OxymaPure in THF was utilized for synthesis of the segment 20-37 of the peptide under microwave conditions followed by manual coupling of the ^{20}Ile at ambient temperature. Rest of the sequence was again extended in the synthesizer using the same combination of coupling reagents giving 52% of the crude product. The synthesized peptide was also verified for antimicrobial activity against Gram positive and Gram negative bacteria which was comparable to previously reported MICs.

The naturally occurring antimicrobial peptides are the rational biomarkers for the development of the possible vector for PET tracers; due to the fact that they show low toxicity, high target specificity and non-immunogenicity to the recipient. Moreover, these biomolecules are easy to scale up in the laboratory environment, which may also affect the cost of production. Based on these facts, in the last section of the thesis, LL37 was successfully coupled with the bifunctional chelator NODAGA using DIC/OxymaPure in THF at room temperature for 16 hr. This NODAGA-LL37 was successfully complexed with ^{nat}Ga. Moreover, radiolabelling of NODAGA-LL37 with ^{68}Ga was obtained within 5 min at room temperature. Furthermore, ^{nat}Ga-NODAGA-LL37 was evaluated against gram positive *S. aureus*, gram negative *E. coli* and acid fast bacteria *M. smegmatis* along with mammalian hepatic originated HepG2 cells *in vitro*. The results showed bacterial specificity of the compound rather than affinity towards mammalian cells making it a potential radiotracer for infection imaging. However, this was a proof of concept study that needs to be further evaluated in animal models.